2022

The Burning Bush: Linking LiDAR-derived Shrub Architecture to Flammability

Michelle S. Bester
michelle.bester@mail.wvu.edu

The Burning Bush:
Linking LiDAR-derived Shrub Architecture to Flammability

Michelle S. Bester

Dissertation submitted
to the Eberly College of Art and Sciences
at West Virginia University

in partial fulfillment of the requirements for the degree of

Doctor of Philosophy in

Geography

Brenden McNeil, Ph.D., WVU, Chair
Nicholas Skowronski, Ph.D., Forest Service, Co-chair
Jamison Conley, Ph.D., WVU
Aaron Maxwell, Ph.D., WVU
Timothy Warner, Ph.D.,WVU

Department of Geology and Geography

Morgantown, West Virginia

December 2022

Keywords: Remote Sensing, LiDAR, Fire Ecology, Quantitative Structure Models, Fire Fuels, 3D Modelling, Machine Learning

ABSTRACT

The Burning Bush: Linking LiDAR-derived Shrub Architecture to Flammability

Michelle S. Bester

Light detection and ranging (LiDAR) and terrestrial laser scanning (TLS) sensors are powerful tools for characterizing vegetation structure and for constructing three-dimensional (3D) models of trees, also known as quantitative structural models (QSM). 3D models and structural traits derived from them provide valuable information for biodiversity conservation, forest management, and fire behavior modeling. However, vegetation studies and 3D modeling methodologies often only focus on the forest canopy, with little attention given to understory vegetation. In particular, 3D structural information of shrubs is limited or not included in fire behavior models. Yet, understory vegetation is an important component of forested ecosystems, and has an essential role in determining fire behavior.

In this dissertation, I explored the use of TLS data and quantitative structure models to model shrub architecture in three related studies. In the first study, I present a semi-automated methodology for reconstructing architecturally different shrubs from TLS LiDAR. By investigating shrubs with different architectures and point cloud densities, I showed that occlusion, shrub complexity, and shape greatly affect the accuracy of shrub models.

In my second study, I assessed the 3D architectural drivers of understory flammability by evaluating the use of architectural metrics derived from the TLS point cloud and 3D reconstructions of the shrubs. I focused on eight species common in the understory of the fire-prone longleaf pine forest ecosystem of the state of Florida, USA. I found a general tendency for each species to be associated with a unique combination of flammability and architectural traits. Novel shrub architectural traits were found to be complementary to the direct use of TLS data and improved flammability predictions.

The inherent complexity of shrub architecture and uncertainty in the TLS point cloud make scaling up from an individual shrub to a plot level a challenging task. Therefore, in my third study, I explored the effects of lidar uncertainty on vegetation parameter prediction accuracy. I developed a practical workflow to create synthetic forest stands with varying densities, which were subsequently scanned with simulated terrestrial lidar. This provided data sets quantitatively

similar to those created by real-world LiDAR measurements, but with the advantage of exact knowledge of the forest plot parameters, The results showed that the lidar scan location had a large effect on prediction accuracy. Furthermore, occlusion is strongly related to the sampling density and plot complexity.

The results of this study illustrate the potential of non-destructive lidar approaches for quantifying shrub architectural traits. TLS, empirical quantitative structural models, and synthetic models provide valuable insights into shrub structure and fire behavior.

ACKNOWLEDGEMENTS

I would like to thank my advisors, Dr. Brenden McNeil and Dr. Nicholas Skowronski, for their enthusiasm for the project, invaluable advice and continuous support throughout my PhD. I would also like to thank my committee members, Dr. Timothy Warner, Dr. Aaron Maxwell, and Dr. Jamison Conley. A special thanks to Tim and Aaron for their mentorship, unwavering support, and guidance throughout the most challenging stages of this dissertation. Recognition also goes to my lab, tech, and field assistants. I appreciate all your hard work.

I am also grateful to the Strategic Environmental Research and Development Program (SERDP) 3D Fuel Characterization for Evaluating Physics-based Fire Behavior, Fire Effects, and Smoke Models on US Department of Defense Military Lands [RC19-1064] for funding this research. I also appreciate the opportunity to work with the 3D Fuels SERDP project members, especially Susan Prichard; thank you for your helpful contributions and support.

I would like to express my gratitude to my husband, Fritz Petersen. Without your tremendous understanding, love, and motivation over the past few years, it would have been impossible for me to complete my PhD. My appreciation also goes out to my twin sisters and grandparents, Manie and Nora Boshoff, for their encouragement and confidence in me. I also appreciate the support I received from the rest of my family and friends.

Finally and quite importantly, I would like to dedicate this work to my mom, Anneline Bester, who was a great role model and inspiration, but sadly never got to see me finish this. I know you would have been proud of me. Love you forever my momps.

TABLE OF CONTENTS

INTRODUCTION

Understory vegetation is essential for overstory succession, nutrient cycling, and wildlife habitat, thus forming a vital component of many forested ecosystems (Kutnar et al., 2019; Young & Koerner, 2022; G. Zhou et al., 2022; Zinnert et al., 2013). Moreover, their structural characteristics affect wildland fire behavior and act as ladder fuels which, if left unchecked, could lead to stand-replacing fires (Burger & Bond, 2015; Weiser et al., 2021). Therefore, quantifying these structures and understanding understory dynamics can provide valuable information for biodiversity conservation, forest management, and fire behavior. Unfortunately, understories are often not as extensively studied, as research has tended to focus on overstory architecture, composition, and interactions with fire (Hernandez-Santin et al., 2019; X. Su et al., 2019).

Remote sensing offers an innovative approach for acquiring vegetation information without having to be in physical contact with the object. Since it can provide information consistently and cost-effectively that is less laborious than traditional approaches, it has become an indispensable tool for many forestry applications and ecology, including fire ecology research (Clawges et al., 2008; Jensen, 2013; Meng et al., 2018). In particular, Light detection and ranging (LiDAR) has been used since the early 2000s to characterize ecosystem structural features and can reconstruct the vertical and horizontal vegetation arrangement for an area of interest based on three-dimensional (3D) measurements taken by the sensor (Åkerblom et al., 2017; Atkins et al., 2018; Calders et al., 2018; Coops et al., 2021). Terrestrial Laser Scanning (TLS) is a stationary ground-level LiDAR system that captures detailed 3D point cloud representations of vegetation structure, especially within the understory. In recent advancements, TLS data have been used to reconstruct trees as 3D models.

Quantitative structure models (QSM) is one such 3D modeling approach. Modeling hierarchical collections of geometric primitive structures from the TLS data, these models provide 'real' depictions of tree structures (Burt et al., 2018; Malhi et al., 2018; Martin-Ducup et al., 2020; Raumonen et al., 2013). Since QSMs can isolate and model the woody structure of trees, it is possible to calculate biomass estimations, height and volume calculations, obtain the physical branch structure, branch sizes as well derive other ecological properties (Bournez, Landes, Saudreau, Kastendeuch, & Najjar, 2017; Pasi Raumonen et al., 2013). Although QSM reconstruction has successfully been implemented and optimized for trees, I found minimal research pertaining to understory vegetation architecture, such as shrubs.

Therefore, in the first chapter of this dissertation, we investigated the potential of using QSMs to model shrub architectural traits. In this chapter, we present a semi-automated methodology for reconstructing woody shrubs from TLS LiDAR by adapting current QSM methods optimized for trees. To assess the accuracy of this methodology, we used ten architecturally different shrubs and evaluated the shrub reconstructions from the point clouds. As this was a feasibility test, we acquired the shrubs from a nursery and manually removed the leaves to minimize the occlusion of the woody architecture. To determine how occlusion would impact the accuracy of the models, we used two different point cloud resolutions. Furthermore, by investigating shrubs with different architectures, it was possible to understand how shrub complexity and shape may influence the modeling process. The results of this chapter highlighted the potential for incorporating QSMs of understory shrubs into ecological applications, especially fire behavior.

In the context of fire behavior, the architecture of species, such as the spatial arrangement and branching patterns, affect flammability (Morandini et al., 2019; Santacruz-García et al., 2019). According to studies by Pausas et al. (2017) and Schwilk & Kerr (2002), understory shrubs with dense branching patterns of smaller twigs have a higher chance of undergoing pyrolysis and can be characterized as flammability-enhancing traits. Conversely, loose branching with open canopies reduces the plants' flammability. Characterizing how vegetation architectural traits influence flammability may provide insight into wildland fire behavior, including the intensity, severity, and spread patterns in species coexistence and plant succession (Gale et al., 2021; Loudermilk et al., 2022). Although researchers have investigated architectural traits, they again primarily focus on the overstory or are often limited to small-scale (leaves, plant components, etc.) or large fuel bed scales. Moreover, most plant flammability research occurs in a laboratory setting (Santacruz-García et al., 2019; Tachajapong et al., 2008; Tumino et al., 2019) and fuel characterization is typically represented by two-dimensional components (surface area, mass, bulk density, etc.). Even though these measurements provide valuable information for fire modeling and behavior analysis, they tend to oversimplify understory fuels and do not capture the architectural variability or other 3D functional traits (Bright et al., 2016; Rowell et al., 2020).

Chapter two of this dissertation aids in closing these knowledge gaps by exploring the link between 3D metrics derived from TLS and QSM and flammability components. To ensure this research is relevant, we decided on a study area within a fire-prone area with a diverse understory. Pine forest ecosystems within the southeastern coastal plain met these criteria. Pine

forest ecosystems depend on frequent fire; without it, the forest structure changes, and essential habitat of economic, social, and environmental importance disappears. As such, prescribed burning and fire management has become integral to managing coastal plain ecosystems (Bailey et al., 2007; Noss, 2018; Peet et al., 2018). Therefore, it is important to understand fire components and their interaction with the understory ecosystems. Particularly knowledge about fuel types, flammability, and vegetation characteristics in the understory.

To achieve this, our study was divided into three sections. First, we characterize understory shrubs using TLS- and QSM- architectural metrics. Although previous studies have used TLS to characterize the architecture of vegetation, we included additional novel metrics related to the topological architecture of shrubs. Additionally, we focus on less extensively studied understory vegetation. This allowed us to identify similarities and highlight species differences in the vertical architectural structure, including shrub branch ramification, branching angle, woody volume etc. The second portion of this chapter's research focused on experimentally analyzing shrub flammability in the field. Here we burn and record flammability components relating to combustibility, sustainability, and consumability. In the last section of this chapter, we tie the first two sections together by evaluating the TLS and QSM architectural metrics to predict the variability of shrub flammability. The results of this chapter high highlight the importance of incorporating topological vegetation architecture in fire behavior studies.

In chapters one and two, we note that the inherent complexity of vegetation architecture and wildland fuels at different spatial and temporal scales makes it challenging to accurately measure combustible fuels. Moreover, all lidar-based measurements of physical objects are subject to some uncertainty (Disney et al., 2018; Raumonen et al., 2013; Riley & Thompson, 2016). This could be due to errors in the sensor position from incorrect interaction with GPS, interference from the atmosphere, or sensor calibration. Errors can also occur due to the density of trees, leaves, and branches as well as terrain variables (Andersen et al., 2005; Moorthy et al., 2011). Moreover, lidar-based estimations' quality is influenced by the number of acquisition stations with different angles within the area of interest. For example, lidar pulses that reach the uppermost part of the canopy have a larger footprint, depending on the beam divergence of the instrument (Disney et al., 2018). Higher the number of stations set up in the plot or stand, provide more point cloud data lowering the number of omissions of vegetation structure. In addition, weather conditions such as wind or precipitation induce artifacts (noise) in the point cloud data (Bournez et al., 2017). Finally, the processing procedure from raw point clouds to lidar-estimated models further creates uncertainties.

This includes georeferencing, co-registration, merging, segmentation, sampling, and point cloud classification (Alonso-Benito, Arroyo, Arbelo, & Hernández-Leal, 2016; Calders et al., 2018).

Therefore in chapter three, I wanted to explore the effects of lidar uncertainty on vegetation parameter prediction accuracy. For this research, we use scripting (coding) to present a semi-automated methodology to mimic LiDAR sampling characteristics and run controlled sampling tests over synthetic forest plots. This provides data sets quantitatively similar to those created by real-world LiDAR measurements but with the advantage that we have exact knowledge of the forest plot parameters. By comparing the outputs of LiDAR-derived metrics with the 'known' properties of the stand, we can directly and accurately measure the success of prediction algorithms (Wang et al., 2013). We evaluate three machine learning prediction algorithms and measure uncertainty based on scan density and forest complexity.

In summary, this dissertation contains three stand-alone manuscripts written for journal submission. There are slight differences in formatting in each of the three chapters due to target journal requirements. These manuscripts seek to fill the knowledge gap for accurately characterizing the architectural diversity and complexity of understory fuels using non-destructive approaches. Quantifying links between architectural traits of understory vegetation and flammability and investigating the uncertainties that arise.

References

Åkerblom, M., Raumonen, P., Mäkipää, R., & Kaasalainen, M. (2017). Automatic tree species recognition with quantitative structure models. *Remote Sensing of Environment*, *191*, 1–12. https://doi.org/10.1016/j.rse.2016.12.002

Atkins, J. W., Bohrer, G., Fahey, R. T., Hardiman, B. S., Morin, T. H., Stovall, A. E. L., Zimmerman, N., & Gough, C. M. (2018). Quantifying vegetation and canopy structural complexity from terrestrial LiDAR data using the forestr r package. *Methods in Ecology and Evolution*, *9*(10), 2057–2066. https://doi.org/10.1111/2041-210X.13061

Bailey, A. D., Mickler, R., & Frost, C. (2007). *Presettlement fire regime and vegetation mapping in southeastern coastal plain forest ecosystems*. *46*.

Burger, N., & Bond, W. J. (2015). Flammability traits of Cape shrubland species with different post-fire recruitment strategies. *South African Journal of Botany*, *101*, 40–48. https://doi.org/10.1016/j.sajb.2015.05.026

Burt, A., Disney, M., & Calders, K. (2018). Extracting individual trees from lidar point clouds using treeseg. *Methods in Ecology and Evolution*, *0*(0). https://doi.org/10.1111/2041-210X.13121

Calders, K., Origo, N., Burt, A., Disney, M., Nightingale, J., Raumonen, P., Åkerblom, M., Malhi, Y., & Lewis, P. (2018). Realistic Forest Stand Reconstruction from Terrestrial LiDAR for Radiative Transfer Modelling. *Remote Sensing*, *10*(6), 933. https://doi.org/10.3390/rs10060933

Clawges, R., Vierling, K., Vierling, L., & Rowell, E. (2008). The use of airborne lidar to assess avian species diversity, density, and occurrence in a pine/aspen forest. *Remote Sensing of Environment*, *112*(5), 2064–2073. https://doi.org/10.1016/j.rse.2007.08.023

Coops, N. C., Tompalski, P., Goodbody, T. R., Queinnec, M., Luther, J. E., Bolton, D. K., White, J. C., Wulder, M. A., van Lier, O. R., & Hermosilla, T. (2021). Modelling lidar-derived estimates of forest attributes over space and time: A review of approaches and future trends. *Remote Sensing of Environment*, *260*, 112477.

Disney, M. I., Boni Vicari, M., Burt, A., Calders, K., Lewis, S. L., Raumonen, P., & Wilkes, P. (2018). Weighing trees with lasers: Advances, challenges and opportunities. *Interface Focus*, *8*(2). https://doi.org/10.1098/rsfs.2017.0048

Gale, M. G., Cary, G. J., Van Dijk, A. I. J. M., & Yebra, M. (2021). Forest fire fuel through the lens of remote sensing: Review of approaches, challenges and future directions in the remote sensing of biotic determinants of fire behaviour. *Remote Sensing of Environment*, *255*, 112282. https://doi.org/10.1016/j.rse.2020.112282

Hernandez-Santin, L., Rudge, M. L., Bartolo, R. E., & Erskine, P. D. (2019). Identifying Species and Monitoring Understorey from UAS-Derived Data: A Literature Review and Future Directions. *Drones*, *3*(1), 9. https://doi.org/10.3390/drones3010009

Jensen, J. R. (2013). *Remote Sensing of the Environment: An Earth Resource Perspective*. Pearson.

Kutnar, L., Nagel, T. A., & Kermavnar, J. (2019). Effects of Disturbance on Understory Vegetation across Slovenian Forest Ecosystems. *Forests*, *10*(11), Article 11. https://doi.org/10.3390/f10111048

Loudermilk, E. L., O'Brien, J. J., Goodrick, S. L., Linn, R. R., Skowronski, N. S., & Hiers, J. K. (2022). Vegetation's influence on fire behavior goes beyond just being fuel. *Fire Ecology*, *18*(1), 9. https://doi.org/10.1186/s42408-022-00132-9

Malhi, Y., Jackson, T., Patrick Bentley, L., Lau, A., Shenkin, A., Herold, M., Calders, K., Bartholomeus, H., & Disney, M. I. (2018). New perspectives on the ecology of tree structure and tree

communities through terrestrial laser scanning. *Interface Focus*, *8*(2). https://doi.org/10.1098/rsfs.2017.0052

Martin-Ducup, O., Ploton, P., Barbier, N., Momo Takoudjou, S., Mofack II, G., Kamdem, N. G., Fourcaud, T., Sonké, B., Couteron, P., & Pélissier, R. (2020). Terrestrial laser scanning reveals convergence of tree architecture with increasingly dominant crown canopy position. *Functional Ecology*, *34*(12), 2442–2452. https://doi.org/10.1111/1365-2435.13678

Meng, R., Wu, J., Zhao, F., Cook, B. D., Hanavan, R. P., & Serbin, S. P. (2018). Measuring short-term post-fire forest recovery across a burn severity gradient in a mixed pine-oak forest using multi-sensor remote sensing techniques. *Remote Sensing of Environment*, *210*, 282–296. https://doi.org/10.1016/j.rse.2018.03.019

Morandini, F., Santoni, P. A., Tramoni, J. B., & Mell, W. E. (2019). Experimental investigation of flammability and numerical study of combustion of shrub of rockrose under severe drought conditions. *Fire Safety Journal*, *108*, 102836. https://doi.org/10.1016/j.firesaf.2019.102836

Noss, R. F. (2018). *Fire Ecology of Florida and the Southeastern Coastal Plain*. University Press of Florida. http://ebookcentral.proquest.com/lib/wvu/detail.action?docID=5394340

Peet, R. K., Platt, W. J., & Costanza, J. K. (2018). Fire-Maintained Pine Savannas and Woodlands of the Southeastern United States Coastal Plain. In A. M. Barton & W. S. Keeton (Eds.), *Ecology and Recovery of Eastern Old-Growth Forests* (pp. 39–62). Island Press/Center for Resource Economics. https://doi.org/10.5822/978-1-61091-891-6_3

Raumonen, P., Kaasalainen, M., Åkerblom, M., Kaasalainen, S., Kaartinen, H., Vastaranta, M., Holopainen, M., Disney, M., & Lewis, P. (2013). Fast Automatic Precision Tree Models from Terrestrial Laser Scanner Data. *Remote Sensing*, *5*(2), 491–520. https://doi.org/10.3390/rs5020491

Riley, K., & Thompson, M. (2016). An Uncertainty Analysis of Wildfire Modeling. In K. Riley, P. Webley, & M. Thompson (Eds.), *Geophysical Monograph Series* (pp. 191–213). John Wiley & Sons, Inc. http://doi.wiley.com/10.1002/9781119028116.ch13

Santacruz-García, A. C., Bravo, S., Corro, F. del, & Ojeda, F. (2019). A comparative assessment of plant flammability through a functional approach: The case of woody species from Argentine Chaco region. *Austral Ecology*, *44*(8), 1416–1429. https://doi.org/10.1111/aec.12815

Su, X., Wang, M., Huang, Z., Fu, S., & Chen, H. Y. (2019). Forest Understorey Vegetation: Colonization and the Availability and Heterogeneity of Resources. *Forests*, *10*(11), 944.

Tachajapong, W., Lozano, J., Mahalingam, S., Zhou, X., & Weise, D. R. (2008). An investigation of crown fuel bulk density effects on the dynamics of crown fire initiation in shrublands. *Combustion Science and Technology*, *180*(4), 593–615.

Tumino, B. J., Duff, T. J., Goodger, J. Q., & Cawson, J. G. (2019). Plant traits linked to field-scale flammability metrics in prescribed burns in Eucalyptus forest. *PloS One*, *14*(8). https://doi.org/10.1371/journal.pone.0221403

Wang, L., Birt, A. G., Lafon, C. W., Cairns, D. M., Coulson, R. N., Tchakerian, M. D., Xi, W., Popescu, S. C., & Guldin, J. M. (2013). Computer-based synthetic data to assess the tree delineation algorithm from airborne LiDAR survey. *GeoInformatica*, *17*(1), 35–61. https://doi.org/10.1007/s10707-011-0148-1

Weiser, F., Sauer, A., Gettueva, D., Field, R., Irl, S. D. H., Vetaas, O., Chiarucci, A., Hoffmann, S., Fernández-Palacios, J. M., Otto, R., Jentsch, A., Provenzale, A., & Beierkuhnlein, C. (2021). Impacts of Forest Fire on Understory Species Diversity in Canary Pine Ecosystems on the Island of La Palma. *Forests*, *12*(12), Article 12. https://doi.org/10.3390/f12121638

Young, A. L., & Koerner, S. E. (2022). Understory dynamics in North Carolina longleaf pine savannas: Biodiversity, dominance, and biomass. *Journal of Vegetation Science*, *33*(2), e13126. https://doi.org/10.1111/jvs.13126

Zhou, G., Lucas-Borja, M. E., Eisenhauer, N., Eldridge, D. J., Liu, S., & Delgado-Baquerizo, M. (2022). Understorey biodiversity supports multiple ecosystem services in mature Mediterranean forests. *Soil Biology and Biochemistry*, *172*, 108774. https://doi.org/10.1016/j.soilbio.2022.108774

Zinnert, J. C., Shiflett, S. A., Vick, J. K., & Young, D. R. (2013). Plant functional traits of a shrub invader relative to sympatric native shrubs. *Ecosphere*, *4*(10), 1–11.

RESEARCH QUESTIONS AND OBJECTIVES

This dissertation research aims to measure understory shrub architectural traits using a LiDAR-derived methodology. Then using these measurements to predict vegetation parameters and find a link between them and shrub flammability.

We will achieve this by answering the following research questions:

Chapter 1 Research Question:

Can we accurately reconstruct the 3D architecture of woody shrubs using QSMs derived from TLS LiDAR?

Chapter 2 Research Questions:

As measured from QSM and point cloud representations derived from TLS LiDAR, how many, and which architectural traits best discriminate representative understory species of the longleaf/slash pine forest ecosystems?

How do these species vary in their flammability, especially along the flammability components of combustibility, sustainability, and consumability?

Is the architecture of longleaf/slash pine forest understory species adapted to flammability?

Chapter 3 Research Question:

Is there a significant difference in occlusion between single and multiple TLS scan locations?

With known forest parameters, are there differences in prediction accuracies using machine learning algorithms?

PROJECT SIGNIFICANCE

This research will expand our knowledge on how mechanisms of vegetation architecture affect the flammability of understory species. Further intellectual merit was achieved by the development of QSM representations specifically for understory species. Using TLS combined with QSM opens up new approaches for studying vegetation structure, provides 3D fuel information that can be incorporated into fire models, and links the architectural traits to flammability. The field burn experiments of complete individual plants and not just components (leaves, shoots) within the southeastern coastal plain can be incorporated into existing fire models as little information about understory fuels in this area is available. The 3D models and the flammability characteristics could also prompt the development of new fire behavior models that include 3D fire information.

The datasets used in chapter two of this study fall within a more extensive dataset collection. Thus, the is an opportunity to investigate the methodology at larger scales and evaluate plot-level flammability characteristics. The semi-automated methodologies proposed in this research, both for the development of 3D models of understory species and synthetic forest plot generation, could provide researchers with an established framework that can be implemented in multiple fields of study. Other studies have already sought 3D models of understory architecture to investigate the influence of vegetation disturbance and wind flow and other fire behavior modeling. Sythetic data and computer algorithms provide an environment where multiple experiments can be tested with controlled settings. Similarly, multiple experiments can be run on the simulated LiDAR investigating different sensor or plot characteristics.

My research has broader impacts as it forms part of a larger 3D fuel characterization for physics-based fire behavior, fire effects, and smoke models on US Department of Defense military lands which will integrate state-of-the-art modeling and analysis to provide foundational methods and tools for both managers and scientists. Finally, the methods and results from this dissertation are not limited to fire ecology but can be implemented in other 3D modeling, forestry, and ecology applications.

1. CHAPTER ONE

Lidar-Based Quantitative Structure Modeling Of Architecturally Different Shrubs

Michelle Bester [1]*, Brenden McNeil [1] and Nicholas S. Skowronski [2,]

[1] Department of Geology and Geography, West Virginia University, Morgantown, WV, 26505, USA

[2] USDA Forest Service, Northern Research Station, 180 Canfield Street, Morgantown, WV 26505, USA

* Corresponding author

Abstract:

Accurate characterization of shrub architecture is important for understanding how architectural traits affect ecosystem dynamics and processes. 3D modeling methodologies, including Terrestrial Laser Scanning (TLS), have demonstrated their potential to capture plant architecture; however, few studies have evaluated these methods for woody shrubs. Therefore, in this study, we investigate the accuracy of shrub architectural traits of derived from Quantitative Structure models (QSMs), developed using TLS data. We used TreeQSM, to model the shrub architecture of ten architecturally different shrubs at two-point cloud density levels. As a reference, we manually measured the shrub's architectural parameters and compared them to the QSM-derived parameters. The QSMs derived from both the low-density point clouds (QSM_L), and the high-density point clouds (QSM_H), showed a high agreement with reference shrub height measurements, with R^2 values of 0.98 and 0.99, respectively. QSM_H correctly modeled an average of 80% of branches, while QSM_L correctly modeled 56% of the branches. The accuracy of the models was similar across growth forms, but was strongly affected by architectural complexity and branch diameter size. The results of this study illustrate the potential of non-destructive lidar approaches for quantifying shrub architectural traits.

Keywords: Terrestrial light detection and ranging; Quantitative Structure Models (QSM); architectural traits; woody shrubs

1.1 Introduction

Shrubs comprise a significant portion of biodiversity in many biomes in North America and worldwide (Kutnar et al., 2019; Li et al., 2020). They account for a large portion of the vegetation in tundra, tropical savannas, Mediterranean and arid regions. Shrubs are also abundant in the understory of forests and woodlands (Götmark et al., 2016; Prévosto et al., 2020; Zhou et al., 2020). Thus, their diversity, abundance, and architectural forms have broad implications for many ecosystem functions.

Studies indicate that the architecture and spatial arrangements of shrubs influence the ability of wildlife species to persist. Indeed, changes in architecture, complexity, and density can affect wildlife species range dynamics, composition, and abundance (Rodomsky-Bish, 2016; Zhou et al., 2020; Zuliani et al., 2021). In many ecosystems, shrubs serve as ecosystem engineers that modify the physical environment and influence various levels of biological organization (Cushman et al., 2010, Kleinhesselink et al., 2014). They can alter environmental conditions, influence nutrient cycling, create fertile sites that facilitate succession, and support seedling regeneration and growth (Hillman et al., 2019; Morsdorf et al., 2010). The architecture and vertical stratification of shrubs also has direct and indirect influences on fire behavior (Morandini et al., 2019; Rowell et al., 2020). For example, dense branching patterns of smaller twigs have a higher chance of undergoing pyrolysis, and the spatial arrangement of shrubs influences wind flow and turbulence across plots (Pausas et al., 2017; Rowell et al., 2020; Schwilk & Kerr, 2002). Therefore, quantifying shrub architecture can provide important metrics for understanding and assessing ecosystem dynamics and processes. Additionally, information on shrub architecture can contribute to the sustainable management of forests and woodlands, as shrubs influence forest hydrology, productivity, and other ecosystem services (Moore et al., 2008; Moskal & Zheng, 2012). In particular, detailed shrub measurements and 3-dimensional (3-D) representations enable measurement of important parameters and inputs to ecological and fire models.

LiDAR (Light Detection and Ranging) is an active remote sensing technology that has been established as a valuable tool with 3D mapping abilities that allows the non-destructive assessment of woody vegetation architecture and traits (Andersen et al., 2005; Atkins et al., 2018; Beland et al., 2019; Disney, 2018; Disney, 2019; Skowronski et al., 2011). LiDAR is usually acquired from a moving platform above the vegetation. In contrast, with Terrestrial Laser Scanning (TLS), the instrument is usually stationary, fixed on a survey tripod close to the target. Scans are sometimes acquired from multiple vantage points around the target, and combined to increase coverage and minimize occlusions (Beland et al., 2019; Bournez et al., 2017; Putman et al., 2018).

TLS provides a detailed 3D point cloud representation of the vertical and horizontal distribution of vegetation architecture, with particularly rich information regarding the understory. For example, Tansey et al._(2009) assessed the feasibility of using TLS-based methods to estimate tree variables such as diameter at breast height (DBH) in a woodland environment, and found that the TLS measurements compared well (RSME 0.019m) with field measurements. More recently, Pokswinski et al. (2021) reviewed the effectiveness of TLS data for extracting fuels, forestry, and vegetation variables. Furthermore, structural parameters derived from the analysis of the point cloud coupled with 3D modeling techniques can be utilized in many forestry and ecology applications (Huang et al., 2011a; Shi et al., 2018; Torresan et al., 2018).

Quantitative Structure Modelling (QSM) is one of the 3D modeling approaches developed to reconstruct architecture from LiDAR point clouds. QSM utilizes a cylinder-fitting procedure through either a segmentation-based or skeleton-based method. *TreeQSM* utilizes a segmentation approach to partition the point cloud from the LiDAR scans into small surface patches (https://github.com/InverseTampere/TreeQSM). The model building occurs by covering the point cloud with the small surface patches using a building-block approach. Once complete, the model is segmented into branches, and reconstructed with appropriately sized cylinders fitted to each segment (Åkerblom et al., 2015; Raumonen et al., 2013). The output files from *TreeQSM* provide structural attributes computed from the QSM.

TreeQSM has been recognized as an established tool for reconstructing and assessing structural parameters of individual trees (Arseniou et al., 2021; Calders et al., 2015; Fan et al., 2020; Lau et al., 2018; Raumonen et al., 2013; Reich et al., 2021). For example, Calders et al. (2015) used a slightly modified version of the Raumonen et al. (2013) methodology to extract single trees from TLS data and create QSMs for 65 trees in a eucalypt open forest in Victoria, Australia. These authors estimated aboveground biomass from the QSM models, and found a high agreement with the values obtained from destructive sampling, with a concordance correlation coefficient (CCC) of 0.98. Furthermore, Åkerblom et al. (2017) successfully used *TreeQSM* to model trees and automatically recognize various tree species.

Most QSM methods derived from LiDAR and TLS have thus far focused on the 3D reconstruction of different tree varieties, with little attention given to understory vegetation, such as shrubs. Therefore, our objective for this paper is to evaluate the possibility of reconstructing shrubs from TLS data using a QSM approach, and to determine if either TLS point density or shrub shape and complexity influence the accuracy of the QSMs. To achieve this, we first reconstruct shrubs of varying architectural characteristics and complexities, using the TLS data and the *TreeQSM* approach. Thereafter, we validate and test the fidelity of the QSMs by comparing them to the original point cloud and the manual measurements. We

conclude with an evaluation of the potential of QSM approaches for identifying invasive species and the extraction of essential architectural information.

1.2 Materials and Methods

1.2.1 Shrub Selection and Plant Trait Measurements

The shrubs selected to investigate the QSM reconstructions came from a plant nursery in Pittsburgh, PA, USA. We based our selections to ensure a wide variety of geometrical and architectural traits, choosing ten shrubs with different heights, complexities, branching patterns, and crown shapes.

To prepare our shrubs for scanning and measurement, we carefully picked off all leaves from branches exposing the architectural form of each shrub. By only having the woody structure we can determine how well the QSM can delineate the shrub architecture, without it being occluded by leaves. We then manually measured the aboveground height of the leaf-off shrubs to the closest centimeter (cm). Additionally, we recorded the DBB (diameter before branching) of the main stem(s) and the diameter of shrub branches to the nearest millimeter using a digital Vernier Caliper.

We determined branching patterns and branch order using centrifugal ordering, where each branch was given a unique BranchID. We adapted our BranchID methodology from Borchert & Slade's, (1981) botanical method and by Lau's et al. (2018) branch coding strategy. The first branch order started at the main stem(s) and followed a dendroidal pattern. A new branch order was assigned every time a branch furcated into approximately equal parts. We color-coded up to six branch orders of each shrub using the same color scheme and created a unique BranchID for each measured branch. Additionally, we recorded the orientation of every branch with respect to the first-order branch. The BranchIDs were paired with the QSM results for accuracy assessment. Figure 1 illustrates the branching order strategy and unique BranchID label assigned to the measured branches.

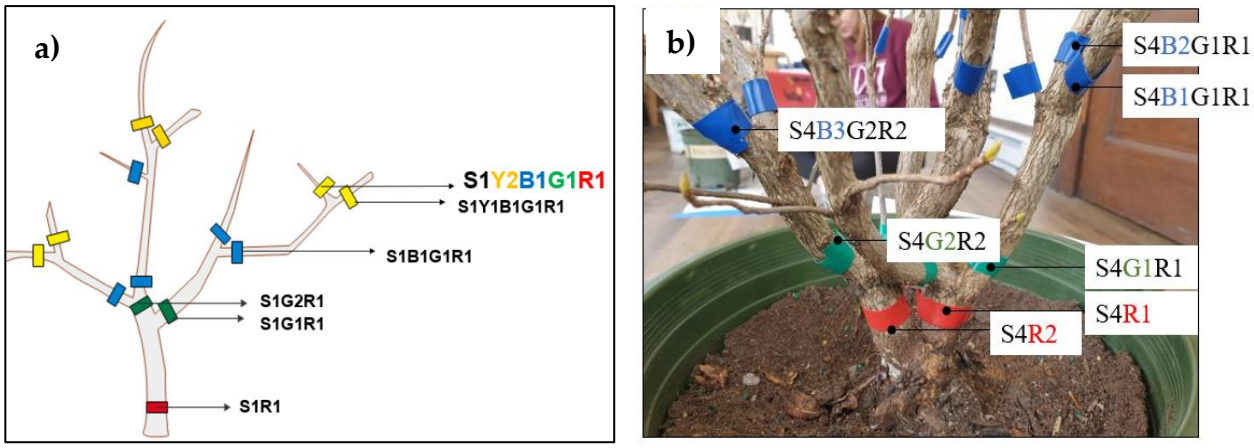

Figure 1. **(a)** Diagram of branching order strategy, where 'S' represents the shrub number. First branching order red (R), second branching order (G), third branching order blue (B), fourth branching order yellow (Y), fifth branching order white (W), and sixth branching order colored red again, but represented by (RR). The numbers behind the branching order letter represent the number of branches within that specific order. **(b)** Example of unique branch ID's for a few branches from shrub 4.

We defined the complexity of each shrub as the sum of three architectural traits: degree of ramification, the average bifurcation ratio, and the number of branches in the shrub relative to the total branches of all shrubs. Each of these measures is described in more detail below.

We calculated the degree of ramification (*Rd*) as the rate of change of the branch cross-sectional area (assumed to be circular) from the maximum crown width (*cw*) to the stem before branching (Eq 1). *Rd* provides a measure of the density of the shrub branches, and is adapted from the approach of Harris and Pannell, (2010) and Roddy et al., (2019). Higher values are associated with denser branching and a more compact architecture (Pérez-Harguindeguy et al., 2013; Walter et al., 2021).

$$Rd = \frac{Branch\ cross\ sectional\ area\ at\ \max cw - Branch\ cross\ sectional\ area\ at\ BO_f}{Distance\ between\ BO_f\ and\ cw} \quad (1)$$

Where *BO* is the branching order and the subscript *f* indicates the first branching order.

We measured the overall bifurcation ratio (López-López et al., 2017; Orozco-Aguilar et al., 2019) of one representative stem per shrub (*OBR*) using (Eq. 2)

$$OBR = \sum_{x=l+1}^{h} \frac{NBO_x}{NBO_{x-1}} \quad (2)$$

Where NBO_x represents the shrub's number of branches for branch order x, and l represents the lowest branch order (1), and h the highest branch order for that particular shrub.

The shrub's branch proportion (B_t) is the number of branches of an individual shrub expressed as a percentage of the total number of branches of all the shrubs (Eqn 3)

$$B_{t,i} = Ntot_i / \sum_{y=1}^{10} Ntot_y \quad (3)$$

Where $Ntot$ is the total number of branches for a particular shrub, subscript y is an index for the shrub number, and subscript i is the shrub of interest.

Finally, to characterize the shrub's complexity, we combined Rd, OBR, and B_t, to generate a composite value. This variable was then normalized to produce a final metric, S_c, with a range between 0 and 1, where higher values are associated with more complex shrubs (Eq. 3) (Borchert & Slade, 1981; S. Zhang et al., 2021; Zheng et al., 2021a).

$$Sraw_i = Rd_i + B_{t,i} + OBR_i \quad (4)$$

$$S_{c,i} = \frac{Sraw_i - Sraw_{min}}{Sraw_{max} - Sraw_{min}} \quad (5)$$

Where $Sraw$ is the complexity raw sum before normalization, subscript i is an index representing the shrub number (i = 1, 2, 3… 10), and subscripts min and max indicate the shrubs with the maximum and minimum values of $Sraw$.

1.2.2 TLS data acquisition

We used a FARO® Focus S350 terrestrial laser scanner to acquire leaf-off scans of our shrubs (FARO Technologies, Inc., www.faro.com). This scanner is compact, lightweight, and specifically designed for indoor and outdoor applications. The instrument's performance specifications include: field of view of 300° vertical and 360° horizontal, wavelength of 1550 nm, beam divergence of 0.3 mrad (1/e), and ranging error of approximately 1 mm. In addition, the scanner has an integrated camera, which acquires high-resolution RGB images that can be co-registered post-scanning.

We collected scans between January and March 2021 at an indoor location, which eliminated the effect of wind or other disturbances. Eight 145 mm diameter spherical targets were placed at different heights in the scanned region, and used for co-registration of the scans (Figure 2). We performed scans from four different viewpoints around the shrub, and at two different resolutions, resulting in eight scans (four low-resolution and four high-resolution scans). For the

high-resolution scans, the laser scanner acquisition time for each scan was approximately 18 minutes with the following parameter settings: ½ resolution; 3x quality; scan size of 20480 x 8533; 174 Million points (MPts), and a point distance of 3.1 mm/10 m. The point distance interval specifies the maximum distance at which the scanner can accurately measure points with the selected settings. These settings were based on guidelines from best practice information for FARO scanning (FARO® Knowledge Base, 2021). For the low-resolution scans, we used the "Indoor…10 m" predefined factory scan settings with the following optimized parameters: scan duration of approximately 5 minutes, 3x quality, and scan size of 5156 x 2134 with a resolution of 11 MPts.

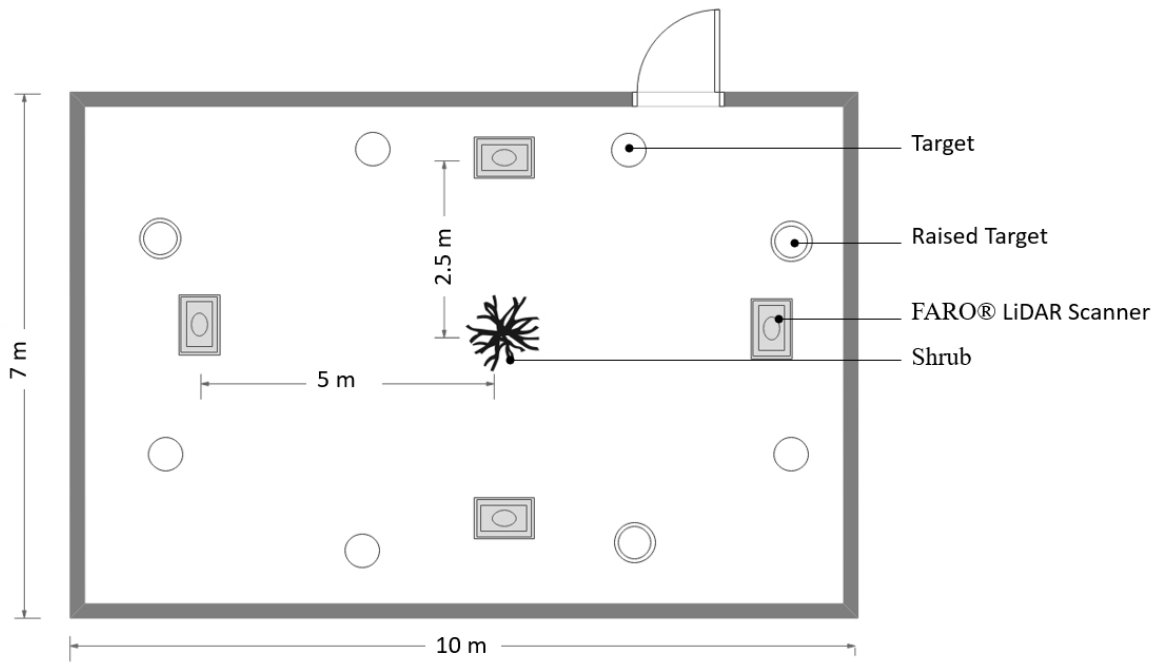

Figure 2. Top view of indoor scan location layout, showing TLS scanner (grey rectangles), shrub, and spherical target locations (represented by circles; double circles indicate elevated target locations).

To describe the overall shrub form, we implemented a 3D convex hull onto the shrub point cloud with the Qhull algorithm (Barber, 2020). The convex hull was then enclosed within a mesh representing shapes associated with three common growth form categories (Figure 3): columnar (growing upright), rounded (globose), vase-like (inverted conical) (Lenard, 2008; Lio & Dewi, 2018; Yan et al., 2019). Finally, we labeled the shrub according to the mesh growth form category that most closely described the convex hull shape; if there was no acceptable fit, the growth form category was labeled as irregular (no apparent shape)

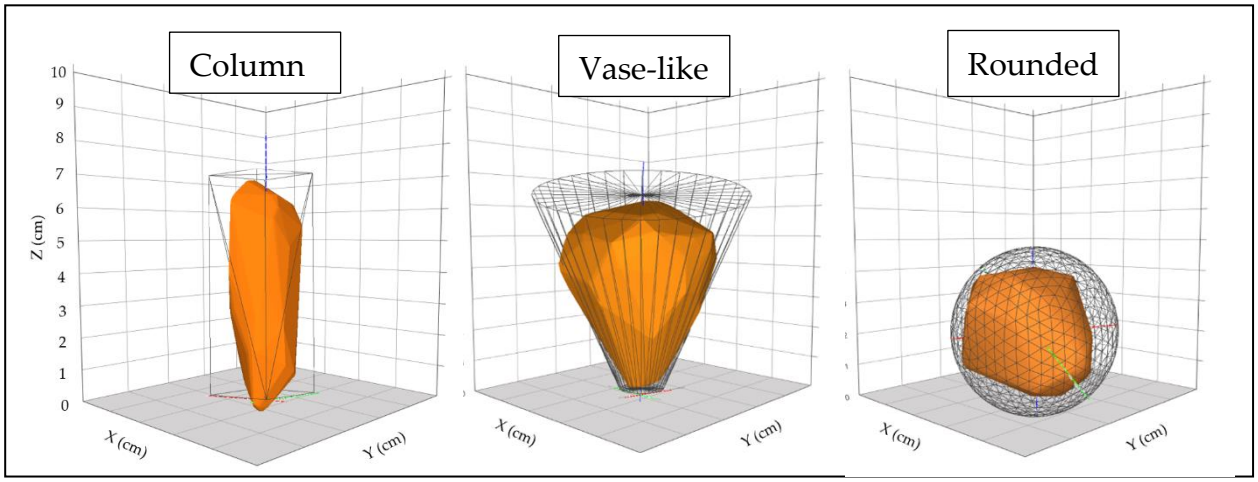

Figure 3. Examples of shrub form categories described by applying a 3D convex hull to the point cloud and enclosing that shape with mesh based on common growth form shapes.

1.2.3 Quantitative Structure Modelling (QSM)

The purpose of the shrub reconstruction is to reflect the architecture of the shrub, including its 3D geometry and topology. Our reconstruction procedure consisted of a multi-step process. First, we extracted the point cloud and converted it into a useable modeling format. We employed the following steps for each shrub to achieve this:

- Co-register the four individual point cloud scans at each of the two resolutions (low and high) using FARO® Scene software (FARO® SCENE software).
- Create a bounding box around the individual shrub.
- Extract and export the point clouds within these bounding boxes to .las format for further analysis in CloudCompare v 2.12 Software (http://cloudcompare.org/).
- Separately export the high and low-resolution point clouds for each shrub.
- Remove features unrelated to the aboveground portion of the shrub (e.g., planter, targets) from the point cloud.
- Apply noise and Statistical Outlier Removal (SOR) filters to remove artifacts and the final .las files.

We then applied the *TreeQSM* algorithm to the cleaned individual shrub point clouds to generate QSM representations of the high- (hereafter referred to as QSM_H) and low-resolution (hereafter referred to as QSM_L) datasets. *TreeQSM* is open-source code developed by Pasi

Raumonen and available via Github (https://github.com/InverseTampere/TreeQSM). The algorithm is a semi-automatic script run within MATLAB software (*MATLAB*, 2018).

The main *TreeQSM* input parameter is the surface patch diameter *d*, used for the first uniform-size cover, and the minimum and maximum values for the second cover. Following previous works and the "Optimization of input parameters" section in the *TreeQSM* manual (Calders et al., 2015; Raumonen, 2020), we fitted a range of values between 0.001 to 0.5 for parameter *d* for each shrub. Then, using visual inspection, we selected a single optimal *d* value for the entire collection of shrubs. Since *TreeQSM* is optimized for trees, it uses meters as a unit; to suit this study's needs, we adjusted the units to millimeters.

The *TreeQSM* approach includes a random function, resulting in a slight variation each time the model is run, even when the parameters remain unchanged (Calders et al., 2015). Therefore, we ran the model twelve times for each shrub, and at each resolution, in order to characterize the distribution of results generated.

1.2.4 Accuracy Assessment

First, we performed a brief qualitative assessment based on a visual inspection of the models to identify gross errors, incompleteness, and overall visual accuracy. We kept the six most representative models for every shrub for further analysis. We characterized the model robustness by the mean standard error and range of the *TreeQSM* iterations.

We manually performed branch-to-branch pairing of the *TreeQSM* models and our manual shrub measurements using our color-coded unique ID system and orientation measurements (Figure 2). To speed up this process, for each shrub, we manually paired one QSM with the manual measurements, and then used mesh boolean intersection algorithms (Badillo & Parfenov, 2022; Magalhães et al., 2017) to pair the remaining iterations. Mesh intersection algorithms have the capability to find overlapps between 3D objects . In addition, we employed mesh boolean difference algorithms to locate branches not in the first manually paired QSM in order to assign additional branches where needed (Zhou et al., 2016). Following the approach of Lau et al. (2018) and Wang et al. (2020), branches without a corresponding QSM branch were excluded from accuracy assessment matrices (except for the branch detection analysis).

We also compared the six QSM iterations of each shrub with the associated point cloud. First, we extracted a subset of points from the TLS point cloud at various height bins and randomly selected a subset. Next, we extracted the corresponding cylinder slices from the six associated QSM models. Using the cloud-to-mesh algorithm in CloudCompare, we generated a summary measure of the distance between the TLS reference points and the corresponding mesh in the QSM, based on the Hausdorff distance calculation (Figure 4) (Kumazaki & Kunii, 2020; Mohammadi et al., 2021; Wu et al., 2021).

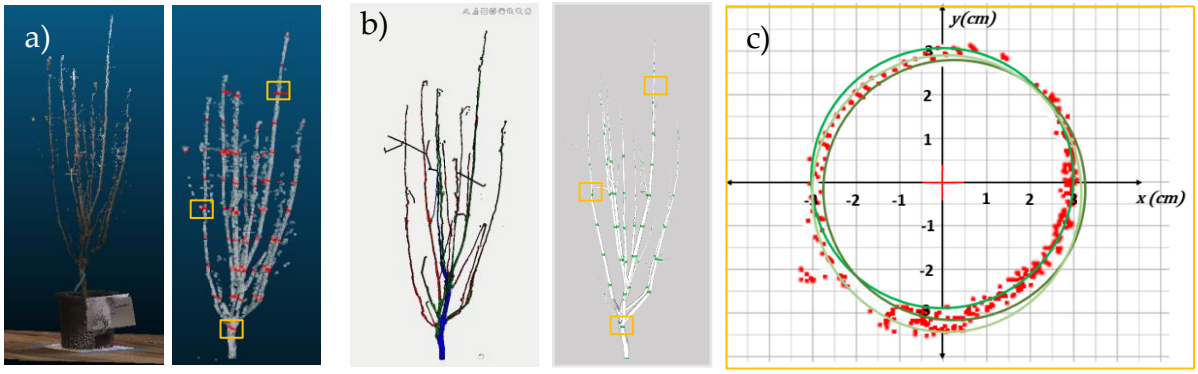

Figure 4. Example of accuracy validation of TLS-QSM for Shrub 1 **(a)** Point cloud query point extraction from height bins. **(b)** QSM query cylinder slice extraction **(c)** Example of the first section for Hausdorff distance calculation where red indicates point cloud and greens various QSM iteration slices.

Destructive sampling measurements are the only true way to validate plant properties (Disney et al., 2018). To evaluate the performance of the QSM_L and QSM_H models, we used linear regression analysis to compare the average of the six QSM models to the associated manual measurement. We calculated the Mean Absolute Error (MAE) and the root-mean-squared error (RMSE), along with the coefficient of determination (R^2). For branch detection, we calculated the average total number of branches as a percentage of the reference measurements (Atkins et al., 2018; Calders et al., 2015; Disney et al., 2018; Kumazaki & Kunii, 2020; Lau et al., 2018). Additionally, we computed the absolute and relative error of the QSM branch diameters by diameter class, to explore how accuracy varies as a function of branch size. Moreover, to explore the effect of architectural traits on modeling accuracy, we also summarized the diameters by shrub form and complexity.

1.3 Results

1.3.1 Manual Measurements and Qualitative Evaluation

The diameters of the shrubs ranged from 1 to 32 mm, and the shrub heights ranged from 36 to 121 cm (Table 1). The ten shrubs had a total of 1347 branches, and a branching order that ranged from two to six. The categorization of the ten shrubs using the convex hull and the best-fit mesh identified three examples of each shrub form (columnar, vase-like, rounded), and one shrub, *Vaccinium Corymbosum,* was classified as irregular as it did not fit any of the three standard growth forms. The normalized complexity measure, S_c, calculated from equation 5, indicated that

shrub 4, *Rhododendron Klondyke*, had the lowest complexity due to low *Rb*, *OBR*, and N_{BO}. Its branches are arranged in an open architecture, with fewer branch orders and less bifurcation. Conversely, shrub 9, *Ilex x Meserveae* had the highest complexity due to its densely packed branches, higher branch count, and higher ramification. Higher ramification suggests that the branch cross-sectional area at the crown width was greater than the branch cross-sectional area before branching (Table 1, Figure 5).

Table 1. Summary of shrubs characteristics and calculated traits

Shrub ID	Shrub Common Name *(Scientific Name)*	Height (cm)	Branch Diameter Range (mm)	Shrub Form	BO_h	S_c
1	Winterberry Holly *(Ilex Verticillate)*	121	1-29	Columnar	5	0.27
2	Highbush Blueberry *(Vaccinium Corymbosum)*	54	2-7	Irregular	4	0.14
3	Alder-leaved Buckthorn *(Rhamnus Alnifolia)*	64	2-15	Vase-like	6	0.92
4	Azalea *(Rhododendron Klondyke)*	95	4-27	Vase-like	3	0.00
5	Lodense Privet *(Ligustrum vulgare)*	43	3-8	Columnar	4	0.53
6	'Rosebud' Azalea *(Rhododendron Rosebud)*	36	2-5	Rounded	2	0.06
7	Southern Arrowwood *(Viburnum Dentatum)*	57	0.5-32	Rounded	6	0.32
8	Barberry 'Concorde' *(Berberis Thunbergii)*	40	3-10	Rounded	3	0.2
9	Meserve Holly *(Ilex x Meserveae)*	62	3-24	Vase-like	6	1.00
10	Sky Pencil *(Ilex Crenata)*	71	3-15	Columnar	4	0.32

A qualitative inspection of Figure 5 shows that the main architecture of the shrubs was generally well represented by the *TreeQSM* models, with only a small percentage of branches occluded or modeled incorrectly. The reduction of the point density did not notably alter the overall representation of the architecture. However, branch connectivity was less consistently well-modelled, particularly for the lower resolution point clouds, which had more occluded and inaccurately modeled branches than the high resolution point clouds. Shrub models with lower complexity generally had higher levels of completeness and correct placement of branches. Furthermore, the denser and more architecturally complex shrubs models included artifacts not in the original point cloud.

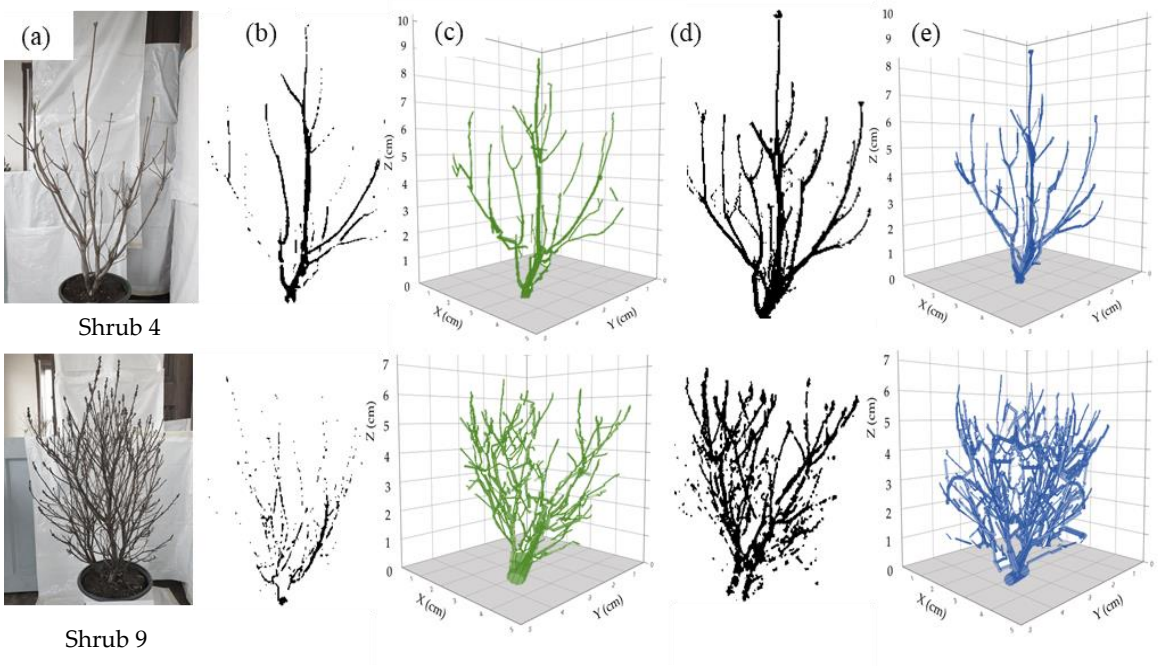

Figure 5. Examples of shrub representation as point clouds and QSM models. Top row: shrub 4, the shrub with the lowest complexity (S_c). Bottom row: shrub 9, the shrub with the highest complexity. (a) photo of shrub (b) low-resolution TLS point cloud. (c) Reconstructed QSM_L using *TreeQSM*. (d) High-resolution TLS point cloud and (e) reconstructed QSM_H using *TreeQSM*

1.3.2 Shrub height and branch detection

Both QSM_L and QSM_H calculated shrub heights showed a good linear fit with the measured shrub heights. QSM_L had an R2 of 0.98, an RMSE of 5.18 cm, and an MAE of 4.43 cm. Except for shrub 3, there were only slight variations between iterations. The QSM_H had a marginally higher R2 of 0.99, and lower RMSE and MAE of 3.20 cm and 2.40 cm, respectively. Although the derived heights plotted close to the 1:1 line, the TreeQSM data consistently underestimated the shrub heights.

The average number of branches correctly detected and modeled by QSM_H(correct) was nearly 80%, whereas QSM_L(correct) only successfully detected 56% of branches across the six repetitions of the ten shrubs (Table 3). QSM_H(correct) and QSM_L(correct) refers to branches that are located and paired correctly with the manually measured branches. The QSM_H(correct) standard deviation was also notably smaller than the QSM_L(correct) branch

detection standard deviation, indicating less variability when detecting and reconstructing branches in the high resolution data. When all the identified branches are included in the total branch count, including the incorrectly labeled branches (e.g., QSM_H(error_included)), not surprisingly, the total number of branches increased, and these increased number of branch estimates are closer to the measured number (Table 3). The erroneously modeled branches inflated branch detection percentages by nearly 11% and 26% for QSM_H and QSM_L, respectively.

Table 3. Percentage of manually measured branches detected by QSM_H and QSM_L

Model	Reference Branch Count	Average QSM branch Count	Average Std. dev	% branches detected
QSM_H(Correct)	1347	1059.33	12.98	**78.64**
QSM_L(Correct)	1347	748.50	21.46	**55.57**
QSM_H(error_included)	1347	1203.00	10.50	89.31
QSM_L(error_included)	1347	1098.00	18.60	81.51

1.3.3 Branch Diameter

For the QSM_L, the prediction of branch diameter had an R^2 was 0.94 with RMSE of 0.79 mm and MAE of 0.61 mm. The regression results for the QSM_H had a slightly lower R^2 of 0.91 and higher RMSE and MAE than the QSM_L. However, the slope of the QSM_H linear fitting line was closer to the 1:1 line than that of QSM_L. Both sets of models underestimated branch diameter. The standard errors of the models indicate that the QSM_L models had extensive ranges of modeled values for the same branch. Moreover, the variability of the modeled values increased for smaller branch diameters.

Plots of the predicted versus measured branch diameters indicate that the model performance differed for 0-5 mm and >5 mm branch diameters, and therefore separate regression analyses were carried out for these two diameter intervals. For diameters smaller than 5mm, the *TreeQSM* models generally overestimated the branches, with both the QSM_L and QSM_H models exhibiting relatively low R^2 values of 0.44 and 0.37, respectively, and high standard errors. In contrast, branch diameters larger than 5 mm were predicted much more accurately. The regression slope of QSM_L is 0.93 (green line, Figure 6a) and of QSM_H is 0.99 (blue line, Figure 6b), which is very close to the 1:1 diagonal line.

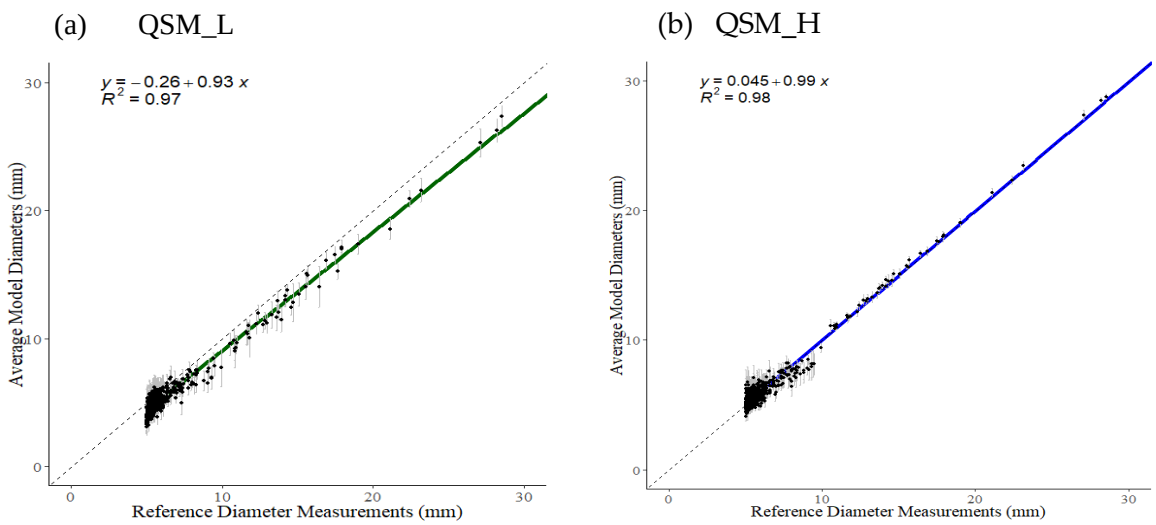

Figure 6. Linear regression of modeled vs measured bush branch diameter for branches > 5 mm in diameter for QSM_L (a) and QSM_H (b)

For QSM_L, 13% of detected branches were overestimated (0.6 mm thicker on average) and diameters larger than 5 mm were underestimated by 9% (1.12 mm thinner on average, Figure 7a). Notwithstanding that the QSM_H had a higher branch count, it performed better for branch diameter classes larger than 5 mm, with an average percentage error of only 2.6% (Figure 7b). For branches larger than 10 mm, the QSM_H diameters were only slightly overestimated. Furthermore, the range in diameter predictions for any one branch was generally smaller for QSM_H than for QSM_L. However, the main difference between the two model methods was that QSM_L predominantly underestimated diameters, whereas QSM_H predominately overestimated diameters. Comparing the two QSM point densities, we found that of the 750 branches detected by QSM_L, there was an average relative error of 10%, and of 1347 branches detected by QSM_H, there was a slightly smaller average relative error of 8%. Both methods generally overestimated the smallest diameter class.

(a) L_QSM

Diameter Class (mm)	Mean Abs. Error	Std. Dev	Relative Error (%)	Branch Count
0-5	0.46	0.60	13.15	433
5-10	-0.42	0.33	-12.50	288
10-15	-1.17	0.43	-10.07	15
15-20	-1.12	0.46	-6.08	7
20+	-1.77	0.43	-7.02	7

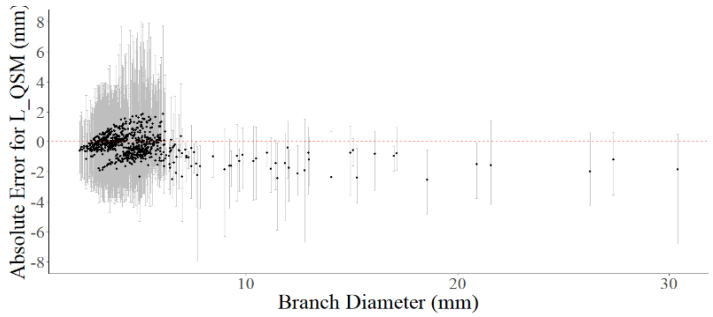

(b) H_QSM

Diameter Class (mm)	Mean Abs. Error	Std. Dev	Relative Error (%)	Branch Count
0-5	0.92	0.60	27.20	887
5-10	-0.42	0.33	-7.16	417
10-15	0.19	0.16	1.6	25
15-20	0.13	0.14	0.80	11
20+	0.23	0.08	0.89	7

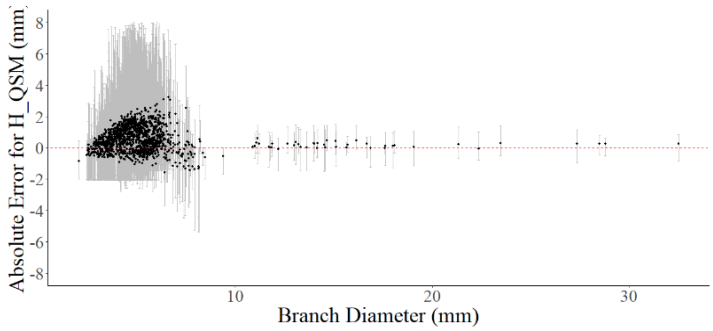

Figure 7. Table of average absolute and average relative error of shrub branches by diameter class with the corresponding graph for L_QSM (a) and H_QSM (b). The dashed red line indicates zero error. The error bar represents the range of modeled diameters, and the small circles are average error. Negative values indicate underestimation, and positive values show overestimation.

1.3.4 Influence of Architectural Traits on Model Accuracy

The final objective of this study was to determine whether architectural traits influence the accuracy of the models. We classified shrubs into one of four categories of shrub complexity (S_c): Low= $S_c \leq 0.25$, Medium = S_c between 0.25 and 0.5, High = S_c larger than 0.5 and less than 0.75 and very high = $S_c \geq 0.75$. As the shrub's complexity increases, the percentage of branches detected decreases for both modeling methods. However, this change in accuracy for the QSM_L method is greater than for the QSM_H method (Table 4, Figure 8a). Overall, the QSM_H maintains a high level of accuracy, above 75%, which remains relatively constant as the shrub complexity increases. We found that the QSM_L method accurately detected branches in low-complexity shrubs (72.69%); however, the accuracy of branches detected for highly complex shrubs fell to 56.47%. For example, of the 117 branches of medium complex shrubs, 81 branches were undetected by QSM_H, while for the most complex shrubs with 685 branches, QSM_H did not detect approximately 150 branches.

For shrub form, the rounded crown-shaped shrubs had more branches detected with both QSM_H and QSM_L methods, 83% and 68%, respectively. Similarly, the columnar-shaped shrubs had the least number of branches detected in both QSM methods (Table 4, Figure 8b). The maximum difference in branch detection between the various shrubs forms was approximately 12% for QSM_H and 16% for QSM_L.

Table 4. Percentage of manually measured branches detected as a percentage by shrub complexity and shrub form for QSM_H and QSM_L (shaded)

Model	Reference Branch Count	Average QSM branch Count	Average Std. dev	% branches detected
Shrub Complexity				
QSM_H(Low)	119	100.67	2.44	84.59
QSM_L(Low)	119	86.50	4.09	72.69
QSM_H(Medium)	177	138.17	5.42	78.06
QSM_L(Medium)	177	105.17	9.83	59.42
QSM_H(High)	366	285.00	14.56	77.87
QSM_L(High)	366	196.67	31.22	60.14
QSM_H(V.High)	685	535.50	38.54	78.18
QSM_L(V.High)	685	386.83	55.21	56.47
Shub Form				
QSM_H(Columnar)	316	225.00	10.71	71.20
QSM_L(Columnar)	277	144.17	20.13	52.05
QSM_H(Vase-like)	733	581.33	26.03	79.31
QSM_L(Vase-like)	733	416.83	37.24	56.87
QSM_H(Rounded)	239	198.67	5.13	83.12
QSM_L(Rounded)	210	143.83	12.37	68.49

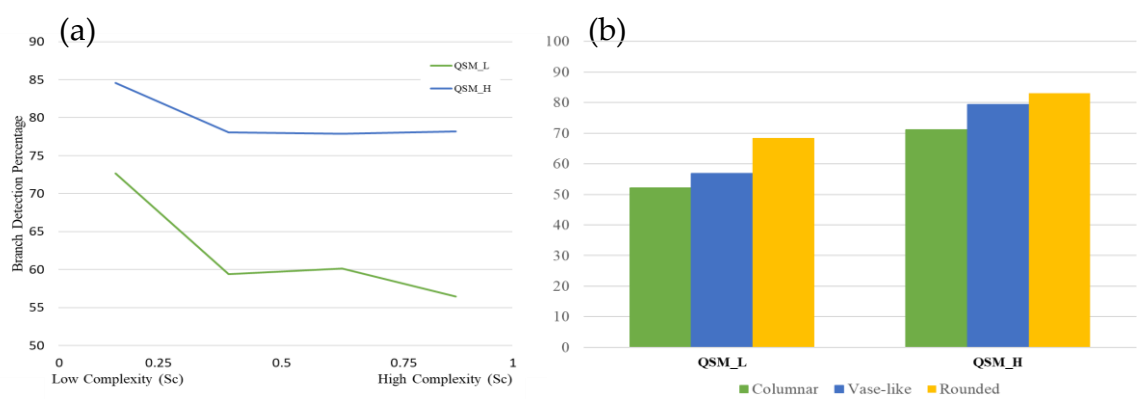

Figure 8. (a) Percentage of branches detected by QSM_L (green) and QSM_H (blue) for increasing degrees of complexity.* *Axis started at 50% to highlight differences.* (b) Percentage of branches detected for QSM_L and QSM_H grouped by shrub form.

Additionally, to gain insight into how shrub architecture influenced modeling, we evaluated branch diameter accuracy for varying shrub complexities and by shrub form. We performed regression analysis on the QSM_H method to observe whether there was a significant difference between the accuracy of diameters. We observed a gradual decline in R^2 as the S_c value increased, ranging from 0.97 for the least complex group to 0.84 for highly complex shrubs (Table 5). Furthermore, we noted that the shape form R^2 stayed relatively consistent (0.9-0.92) regardless of shrub form. Only shrub 2, which we could not categorize into a common growth form, had a lower R^2 of 0.63.

Table 4. Coefficient of determination results comparing manually measured diameters to modeled diameters for QSM_H by complexity and by shrub form

Shrub Complexity	**Branch diameter prediction vs. model R^2**	**Shrub Form**	**Branch diameter prediction vs. model R^2**
Low	0.97	Columnar	0.90
Medium	0.94	Rounded	0.92
High	0.87	Vase-like	0.92
Very high	0.84	Irregular	0.63

1.4 **Discussion**

1.4.1 Accuracy of shrub traits

The qualitative evaluation of the QSM models indicates that while the models successfully captured the overall shrub form, incorrectly modeled or occluded branches were more common with the low density TLS data. In general, the quality of TLS data varies with the type of TLS instrument used and also its characteristics, scan setup and layout, co-registration and the processing of the point cloud (Disney et al., 2018; D. Wang et al., 2020). We kept the model input parameters (patch diameter and ball radius) consistent for all the shrubs over the multiple model runs for each shrub, after having optimized them based on initial experiments with the shrubs. It is important to note that changing these parameters would likely change the resulting QSM models. Furthermore, the parameters we chose may not be suitable for all shrubs, and therefore should be modified for each new study, prior to collecting data. The *TreeQSM* user's manual Raumonen (2020) provides detailed information on the optimization procedure.

Spurious branches were occasionally included in the models. Lau et al., (2018) also found their models sensitive to incorrectly added cylinders. These errors were often due to artifacts or empty areas in the point clouds due to occlusion. Paynter et al. (2018) found inconsistencies in the TLS scan information, and even with multiple scans occlusion still occurred. For our study, both low and high point cloud resolutions had high R^2 values for predicting shrub height, although the margin of error for height estimations for QSM_L shrubs was larger. Wagers et al. (2021), with their research focusing on small (<5 m) spruce trees, also found a strong relationship between measured and modeled QSM heights. However, previous work on tree QSMs by Torresan et al. (2018) reported underestimations for tree heights under 10 m, and other studies on larger trees did not obtain accurate height estimations (Huang et al., 2011b; Krooks et al., 2014; Liang & Hyyppä, 2013; Srinivasan et al., 2015). We suspect that these low accuracies can be attributed to TLS beam divergence and uncertainties in treetop visibility, as other trees often obscure the treetops.

The large standard errors of the model repetitions highlighted the variability in diameter predictions when run on the same input data. Standard error was notably higher for smaller diameter branches, even for the QSM_H models. We suspect these errors are due to partial and noisy branch reconstructions from TLS occlusion and a less dense point cloud, making the diameter estimates unreliable, especially for smaller diameters. Previous QSM studies achieved similar results (Calders et al., 2015; Fan et al., 2020; Hackenberg et al., 2015). For example, Lau et al., (2018) evaluated tropical trees and identified limitations for accurately estimating branch diameters smaller than 20 cm. Even more recently, Demol et al., (2022) and Wilkes et al., (2021) found that the accuracy of QSM branch diameter estimates was much lower for smaller diameters.

The absolute and relative error by diameter class gives insight regarding which diameters are estimated accurately and where the QSM may need improvement. The QSM_L had a relatively high percentage of errors for all diameter classes, whereas the primary source in the QSM_H resulted from the '0-5 mm' diameter class. Both methods overestimated the smallest diameter class. These results are comparable to Demol et al.'s (2022) research on small branches of *Fraxinus excelsior* trees. They noted that branches with diameters smaller than 5 cm accounted for more than 80% of the overestimation of all branches. Similarly, Wilkes et al.'s (2021) branch architecture comparison results showed smaller branches were overestimated. According to Calders et al. (2015) and Torresan et al. (2018), overestimation is possibly related to TLS data

input quality and QSM reconstruction error. We consider that in our study, overestimation is likely due to cylinder overfitting in the QSM reconstruction process and the distance between points in the sparse point cloud.

1.4.2 Influence of shrub characteristics on QSM accuracy

We found that shrub architectural form and complexity have a notable effect on model accuracy metrics such as the percentage of branches detected. As suspected, accuracy decreased as complexity increased for QSM_L. We observed a gradual decline in R^2 as the shrubs' complexity (S_c) value increased. However, for the QSM_H method, the percentage of branches detected for low complexity shrubs initially declined (approximately 10%), then stabilized at 75% as shrub complexity increased. Although the portion of branches detected remains relatively constant, we noted that the count of branches that were not detected nevertheless increased as shrub complexity increased. The decrease in branch detection is conceivably due to intricate branching patterns causing occlusion of the internal architecture of the shrub as well as small twigs not captured by the TLS point cloud. Our research highlights a strong relationship between the TLS input data and the *TreeQSM* results, confirming the results of previous work (Lau et al., 2018; Raumonen et al., 2013; Zheng et al., 2021b).

The experimental results also indicate that shrub growth form significantly affects modeling accuracy (p-value < 0.05). Previous studies have shown that TLS data can be used to classify the plant architectural form. However, we did find similar studies on how architectural form influences accuracy (Jiang et al., 2019; Tomșa et al., 2021). In summary, the modeling algorithms provide realistic results for less complex shrubs like *Rhododendron Klondyke*. However, the reconstruction is less accurate for architectures that are more complex.

1.5 **Conclusions**

Our study assessed the accuracy of TLS data in reconstructing various shrub species' architectural traits. In this study, we tested high (QSM_H) and low (QSM_L) lidar density point-cloud data to model ten architecturally different shrubs. We demonstrated that with the *TreeQSM* algorithm, we could reconstruct the overall architecture of the shrubs using QSM_L and QSM_H methods. The derived heights from both approaches produced a high coefficient of determination. However, the QSM_H method could detect branches with better accuracy than the QSM_L method. In addition, our analysis showed accurate reconstruction for larger diameters (> 5 mm), while more work is needed for modeling smaller diameters. Furthermore,

the complexity of the shrub (i.e., more branches, more compact, higher bifurcation, smaller diameter branches, etc.) affect the accuracy of the 3-D architectural model.

In general, we noted trade-offs between TLS point-cloud density, the complexity of the shrub, model input parameters, and processing time. For example, the more detailed the input data, the longer the preparation and processing time; however, this does produce more precise results. Therefore, the desired resolution of the 3-D models, and the complexity of the shrubs scanned, should be considered in designing the experimental setup to generate the appropriate point cloud density. Other trade-offs may include TLS technology available, project budget and timeline, as well as project significance.

Further research into optimizing QSM algorithms for understory vegetation is still needed, especially for complex architectures. Future work should include fine-tuning input parameters and evaluating other parameters, such as volume estimations. A key focus of future research should also include improving QSM modeling to account for and better resolve uncertainties from TLS occlusion. We also need to test the feasibility of leaf modeling and models derived from in-situ TLS data. In addition, future studies could include scaling up from single shrub level to multiple shrub or plot level studies. Despite these future research needs, the methodology used in this study already demonstrates the generally high accuracy of shrub models generated using existing TLS instrumentation. QSM shrub reconstructions are non-destructive, versatile representations of plant architecture. Many fields, including forestry, agriculture, ecology, silviculture, and fire behavior, would benefit from these detailed 3D shrub models.

References

Andersen, H.-E., McGaughey, R. J., & Reutebuch, S. E. (2005). Estimating forest canopy fuel parameters using LIDAR data. *Remote Sensing of Environment*, *94*(4), 441–449. https://doi.org/10.1016/j.rse.2004.10.013

Arseniou, G., MacFarlane, D. W., & Seidel, D. (2021). Woody Surface Area Measurements with Terrestrial Laser Scanning Relate to the Anatomical and Structural Complexity of Urban Trees. *Remote Sensing*, *13*(16), 3153.

Atkins, J. W., Bohrer, G., Fahey, R. T., Hardiman, B. S., Morin, T. H., Stovall, A. E. L., Zimmerman, N., & Gough, C. M. (2018). Quantifying vegetation and canopy structural complexity

from terrestrial LiDAR data using the forestr r package. *Methods in Ecology and Evolution*, *9*(10), 2057–2066. https://doi.org/10.1111/2041-210X.13061

Barber, C. B. (2020). *Qhull manual*. http://www.qhull.org/html/index.htm#authors

Beland, M., Parker, G., Sparrow, B., Harding, D., Chasmer, L., Phinn, S., Antonarakis, A., & Strahler, A. (2019). On promoting the use of lidar systems in forest ecosystem research. *Forest Ecology and Management*, *450*, 117484. https://doi.org/10.1016/j.foreco.2019.117484

Borchert, R., & Slade, N. A. (1981). Bifurcation ratios and the adaptive geometry of trees. *Botanical Gazette*, *142*(3), 394–401.

Calders, K., Newnham, G., Burt, A., Murphy, S., Raumonen, P., Herold, M., Culvenor, D., Avitabile, V., Disney, M., Armston, J., & Kaasalainen, M. (2015). Nondestructive estimates of above-ground biomass using terrestrial laser scanning. *Methods in Ecology and Evolution*, *6*(2), 198–208. https://doi.org/10.1111/2041-210X.12301

Demol, M., Wilkes, P., Raumonen, P., Krishna Moorthy, S., Calders, K., Gielen, B., & Verbeeck, H. (2022). Volumetric overestimation of small branches in 3D reconstructions of *Fraxinus excelsior*. *Silva Fennica*, *56*(1). https://doi.org/10.14214/sf.10550

Disney, M. I., Boni Vicari, M., Burt, A., Calders, K., Lewis, S. L., Raumonen, P., & Wilkes, P. (2018). Weighing trees with lasers: Advances, challenges and opportunities. *Interface Focus*, *8*(2). https://doi.org/10.1098/rsfs.2017.0048

Fan, G., Nan, L., Chen, F., Dong, Y., Wang, Z., Li, H., & Chen, D. (2020). A New Quantitative Approach to Tree Attributes Estimation Based on LiDAR Point Clouds. *Remote Sensing*, *12*(11), Article 11. https://doi.org/10.3390/rs12111779

FARO® Knowledge Base. (2021, January 20). *Laser Scanner Best Practices*. FARO® Knowledge Base. https://knowledge.faro.com/Hardware/3D_Scanners/Focus/Laser_Scanner_Best_Practices

Hackenberg, J., Wassenberg, M., Spiecker, H., & Sun, D. (2015). Non Destructive Method for Biomass Prediction Combining TLS Derived Tree Volume and Wood Density. *Forests*, *6*(4), Article 4. https://doi.org/10.3390/f6041274

Harris, M. S., & Pannell, J. R. (2010). Canopy seed storage is associated with sexual dimorphism in the woody dioecious genus Leucadendron. *Journal of Ecology*, *98*(2), 509–515. https://doi.org/10.1111/j.1365-2745.2009.01623.x

Hillman, S., Wallace, L., Reinke, K., Hally, B., Jones, S., & Saldias, D. S. (2019). A Method for Validating the Structural Completeness of Understory Vegetation Models Captured with 3D Remote Sensing. *Remote Sensing*, *11*(18), Article 18. https://doi.org/10.3390/rs11182118

Huang, H., Li, Z., Gong, P., Cheng, X., Clinton, N., Cao, C., Ni, W., & Wang, L. (2011a, March). *Automated Methods for Measuring DBH and Tree Heights with a Commercial Scanning Lidar* [Text]. https://doi.org/info:doi/10.14358/PERS.77.3.219

Huang, H., Li, Z., Gong, P., Cheng, X., Clinton, N., Cao, C., Ni, W., & Wang, L. (2011b). Automated Methods for Measuring DBH and Tree Heights with a Commercial Scanning Lidar. *Photogrammetric Engineering & Remote Sensing*, *77*(3), 219–227. https://doi.org/10.14358/PERS.77.3.219

Jiang, Y., Li, C., Takeda, F., Kramer, E. A., Ashrafi, H., & Hunter, J. (2019). 3D point cloud data to quantitatively characterize size and shape of shrub crops. *Horticulture Research*, *6*, 43. https://doi.org/10.1038/s41438-019-0123-9

Krooks, A., Kaasalainen, S., Kankare, V., Joensuu, M., Raumonen, P., & Kaasalainen, M. (2014). Predicting tree structure from tree height using terrestrial laser scanning and quantitative structure models. *Silva Fenn*, *48*, 1125.

Kumazaki, R., & Kunii, Y. (2020). Application of 3d Tree Modeling Using Point Cloud Data by Terrestrial Laser Scanner. *The International Archives of Photogrammetry, Remote Sensing and Spatial Information Sciences*, *43*, 995–1000.

Kutnar, L., Nagel, T. A., & Kermavnar, J. (2019). Effects of Disturbance on Understory Vegetation across Slovenian Forest Ecosystems. *Forests*, *10*(11), Article 11. https://doi.org/10.3390/f10111048

Lau, A., Bentley, L. P., Martius, C., Shenkin, A., Bartholomeus, H., Raumonen, P., Malhi, Y., Jackson, T., & Herold, M. (2018). Quantifying branch architecture of tropical trees using terrestrial LiDAR and 3D modelling. *Trees*, *32*(5), 1219–1231. https://doi.org/10.1007/s00468-018-1704-1

Lenard, E. (2008). Habits of trees and shrubs in landscape design. *Architecture Civil Engineering Environment*, *4*, 13–20.

Li, L., Chen, J., Mu, X., Li, W., Yan, G., Xie, D., & Zhang, W. (2020). Quantifying Understory and Overstory Vegetation Cover Using UAV-Based RGB Imagery in Forest Plantation. *Remote Sensing*, *12*(2), Article 2. https://doi.org/10.3390/rs12020298

Liang, X., & Hyyppä, J. (2013). Automatic Stem Mapping by Merging Several Terrestrial Laser Scans at the Feature and Decision Levels. *Sensors*, *13*(2), 1614–1634. https://doi.org/10.3390/s130201614

Lio, F. X. S., & Dewi, M. P. S. (2018). Karst vegetation in the natural habitat of sandalwood (Santalum album) at various altitude places in Timor Island, Indonesia. *Biodiversitas Journal of Biological Diversity*, *19*(5), 1703–1713. https://doi.org/10.13057/biodiv/d190516

López-López, S. F., Martínez-Trinidad, T., Benavides-Meza, H., Garcia-Nieto, M., & de los Santos-Posadas, H. M. (2017). Non-destructive method for above-ground biomass estimation of Fraxinus uhdei (Wenz.) Lingelsh in an urban forest. *Urban Forestry & Urban Greening*, *24*, 62–70. https://doi.org/10.1016/j.ufug.2017.03.025

MATLAB. (2018). *MATLAB 9.7.0.1190202 (R2019b)*. The MathWorks Inc.

Mohammadi, M., Rashidi, M., Mousavi, V., Karami, A., Yu, Y., & Samali, B. (2021). Quality Evaluation of Digital Twins Generated Based on UAV Photogrammetry and TLS: Bridge Case Study. *Remote Sensing*, *13*(17), Article 17. https://doi.org/10.3390/rs13173499

Moore, P. T. M. T., Miegroet, H. V. M. V., & Nicholas, N. S. N. S. (2008). Relative role of understory and overstory in carbon and nitrogen cycling in a southern Appalachian spruce–fir forestAES Publication 7863. Utah Agricultural Experiment Station, Utah State University, Logan, Utah. *Canadian Journal of Forest Research*. https://doi.org/10.1139/X07-115

Morsdorf, F., Mårell, A., Koetz, B., Cassagne, N., Pimont, F., Rigolot, E., & Allgöwer, B. (2010). Discrimination of vegetation strata in a multi-layered Mediterranean forest ecosystem using height and intensity information derived from airborne laser scanning. *Remote Sensing of Environment*, *114*(7), 1403–1415. https://doi.org/10.1016/j.rse.2010.01.023

Moskal, L. M., & Zheng, G. (2012). Retrieving Forest Inventory Variables with Terrestrial Laser Scanning (TLS) in Urban Heterogeneous Forest. *Remote Sensing*, *4*(1), Article 1. https://doi.org/10.3390/rs4010001

Orozco-Aguilar, L., Livesley, S. J., Brack, C., & Johnstone, D. (2019). Standing volume yield, canopy structure and allometric relationships of dominant urban trees in Melbourne, Australia. *Urban Forestry & Urban Greening*, *43*, 126363. https://doi.org/10.1016/j.ufug.2019.06.006

Paynter, I., Genest, D., Saenz, E., Peri, F., Li, Z., Strahler, A., & Schaaf, C. (2018). Quality Assessment of Terrestrial Laser Scanner Ecosystem Observations Using Pulse Trajectories. *IEEE Transactions on Geoscience and Remote Sensing*, *56*(11), 6324–6333. https://doi.org/10.1109/TGRS.2018.2836947

Pérez-Harguindeguy, N., Díaz, S., Garnier, E., Lavorel, S., Poorter, H., Jaureguiberry, P., Bret-Harte, M. S., Cornwell, W. K., Craine, J. M., Gurvich, D. E., Urcelay, C., Veneklaas, E. J., Reich, P. B.,

Poorter, L., Wright, I. J., Ray, P., Enrico, L., Pausas, J. G., de Vos, A. C., … Cornelissen, J. H. C. (2013). New handbook for standardised measurement of plant functional traits worldwide. *Australian Journal of Botany*, *61*(3), 167. https://doi.org/10.1071/BT12225

Pokswinski, S., Gallagher, M. R., Skowronski, N. S., Loudermilk, E. L., Hawley, C., Wallace, D., Everland, A., Wallace, J., & Hiers, J. K. (2021). A simplified and affordable approach to forest monitoring using single terrestrial laser scans and transect sampling. *MethodsX*, *8*, 101484. https://doi.org/10.1016/j.mex.2021.101484

Raumonen, P. (2020). *InverseTampere/TreeQSM Manual* (2.4.0) [MATLAB]. https://github.com/InverseTampere/TreeQSM

Raumonen, P., Kaasalainen, M., Åkerblom, M., Kaasalainen, S., Kaartinen, H., Vastaranta, M., Holopainen, M., Disney, M., & Lewis, P. (2013). Fast Automatic Precision Tree Models from Terrestrial Laser Scanner Data. *Remote Sensing*, *5*(2), 491–520. https://doi.org/10.3390/rs5020491

Reich, K. F., Kunz, M., & von Oheimb, G. (2021). A new index of forest structural heterogeneity using tree architectural attributes measured by terrestrial laser scanning. *Ecological Indicators*, *133*, 108412. https://doi.org/10.1016/j.ecolind.2021.108412

Roddy, A. B., van Blerk, J. J., Midgley, J. J., & West, A. G. (2019). Ramification has little impact on shoot hydraulic efficiency in the sexually dimorphic genus Leucadendron (Proteaceae). *PeerJ*, *7*, e6835. https://doi.org/10.7717/peerj.6835

Shi, Y., Skidmore, A. K., Wang, T., Holzwarth, S., Heiden, U., Pinnel, N., Zhu, X., & Heurich, M. (2018). Tree species classification using plant functional traits from LiDAR and hyperspectral data. *International Journal of Applied Earth Observation and Geoinformation*, *73*, 207–219. https://doi.org/10.1016/j.jag.2018.06.018

Skowronski, N. S., Clark, K. L., Duveneck, M., & Hom, J. (2011). Three-dimensional canopy fuel loading predicted using upward and downward sensing LiDAR systems. *Remote Sensing of Environment*, *115*(2), 703–714. https://doi.org/10.1016/j.rse.2010.10.012

Srinivasan, S., Popescu, S. C., Eriksson, M., Sheridan, R. D., & Ku, N.-W. (2015). Terrestrial Laser Scanning as an Effective Tool to Retrieve Tree Level Height, Crown Width, and Stem Diameter. *Remote Sensing*, *7*(2), 1877–1896. https://doi.org/10.3390/rs70201877

Tomșa, V. R., Curtu, A. L., & Niță, M. D. (2021). Tree Shape Variability in a Mixed Oak Forest Using Terrestrial Laser Technology: Implications for Mating System Analysis. *Forests*, *12*(2), Article 2. https://doi.org/10.3390/f12020253

Torresan, C., Chiavetta, U., & Hackenberg, J. (2018). Applying quantitative structure models to plot-based terrestrial laser data to assess dendrometric parameters in dense mixed forests. *Forest Systems*, *27*(1), 004. https://doi.org/10.5424/fs/2018271-12658

Wagers, S., Castilla, G., Filiatrault, M., & Sanchez-Azofeifa, G. A. (2021). Using TLS-Measured Tree Attributes to Estimate Aboveground Biomass in Small Black Spruce Trees. *Forests*, *12*(11), Article 11. https://doi.org/10.3390/f12111521

Walter, J. A., Stovall, A. E. L., & Atkins, J. W. (2021). Vegetation structural complexity and biodiversity in the Great Smoky Mountains. *Ecosphere*, *12*(3), e03390. https://doi.org/10.1002/ecs2.3390

Wang, D., Momo Takoudjou, S., & Casella, E. (2020). LeWoS: A universal leaf-wood classification method to facilitate the 3D modelling of large tropical trees using terrestrial LiDAR. *Methods in Ecology and Evolution*, *11*(3), 376–389. https://doi.org/10.1111/2041-210X.13342

Wilkes, P., Shenkin, A., Disney, M., Malhi, Y., Bentley, L. P., & Vicari, M. B. (2021). Terrestrial laser scanning to reconstruct branch architecture from harvested branches. *Methods in Ecology and Evolution*, *12*(12), 2487–2500. https://doi.org/10.1111/2041-210X.13709

Wu, B., Zheng, G., Chen, Y., & Yu, D. (2021). Assessing inclination angles of tree branches from terrestrial laser scan data using a skeleton extraction method. *International Journal of Applied Earth Observation and Geoinformation*, *104*, 102589. https://doi.org/10.1016/j.jag.2021.102589

Yan, Z., Liu, R., Cheng, L., Zhou, X., Ruan, X., & Xiao, Y. (2019). A concave hull methodology for calculating the crown volume of individual trees based on vehicle-borne LiDAR data. *Remote Sensing*, *11*(6), 623.

Yang, P., & Qian, X. (2009). Direct boolean intersection between acquired and designed geometry. *Computer-Aided Design*, *41*(2), 81–94. https://doi.org/10.1016/j.cad.2008.12.006

Zhang, S., Liu, G., Cui, Q., Huang, Z., Ye, X., & Cornelissen, J. H. C. (2021). New field wind manipulation methodology reveals adaptive responses of steppe plants to increased and reduced wind speed. *Plant Methods*, *17*(1), 5. https://doi.org/10.1186/s13007-020-00705-2

Zheng, J., Tarin, M. W. K., Jiang, D., Li, M., Zhang, M., Chen, L., He, T., Hong, X., & Zheng, Y. (2021a). Various distances and orientations influenced the branching traits of Dendrocalamus minor var. Amoenus in Dongshan Island, China. *Global Ecology and Conservation*, *26*, e01468. https://doi.org/10.1016/j.gecco.2021.e01468

Zheng, J., Tarin, M. W. K., Jiang, D., Li, M., Zhang, M., Chen, L., He, T., Hong, X., & Zheng, Y. (2021b). Various distances and orientations influenced the branching traits of Dendrocalamus minor

var. Amoenus in Dongshan Island, China. *Global Ecology and Conservation*, *26*, e01468. https://doi.org/10.1016/j.gecco.2021.e01468

Zhou, Q., Grinspun, E., Zorin, D., & Jacobson, A. (2016). Mesh arrangements for solid geometry. *ACM Transactions on Graphics*, *35*(4), 39:1-39:15. https://doi.org/10.1145/2897824.2925901

2. CHAPTER TWO

Linking LiDAR-Measured Architectural Traits to Flammability of Understory Shrubs

Michelle Bester [1]*, Brenden McNeil [1] and Nicholas S. Skowronski [2,]

[1] Department of Geology and Geography, West Virginia University, Morgantown, WV, 26505, USA

[2] USDA Forest Service, Northern Research Station, 180 Canfield Street, Morgantown, WV 26505, USA

* Corresponding author

Abstract: Three-dimensional (3D) architectural plant traits are associated with plant flammability and influence fire behavior. Understanding vegetation flammability, especially in the understory, is essential for minimizing fire-related risks. However, fuel-related studies often focus on canopy fuels with little attention given to understory vegetation. In this study, we assessed the 3D architectural drivers of understory flammability by evaluating the use of architectural metrics derived from the TLS point cloud and 3D reconstructions of the shrubs. The study area was located in a fire-prone longleaf pine forest ecosystem using eight species based on their representativeness in the understory. We found that the same shrubs species were clustered together, and each species was associated with a unique combination of flammability and architectural traits. The final correlation results suggest that higher crown depth-to-height (CD:H) and lower crown width-to-height (CW:H) ratios are less flammable. In contrast, shrubs with lower CD:H and larger CW:H are generally more flammable. These results demonstrate the potential of using QSM to provide metrics that are complementary to TLS data, potentially improve flammability predictions, and increase our understanding of the linkages between flammability and architectural traits. Furthermore, this study represents the first effort comparing flammability obtained through TLS-derived architectural trait analysis, including novel shrub topology metrics.

Keywords: Terrestrial light detection and ranging; Quantitative Structure Models (QSM); architectural traits metrics; flammability; fire behavior

2.1 Introduction

Fire has played an essential role for centuries in the natural structure of ecosystems throughout North America and the world. It helps maintain biodiversity by creating a mosaic of diverse habitats for flora and fauna, specifically by clearing out invasive species, affecting species competition, and recycling nutrients back into the soil (Chiodi et al., 2019; Gale et al., 2021; Pausas & Bond, 2020). Importantly, fire also assists in removing fuels, which, left unchecked, can cause more devastating wildfires (Linn et al., 2002; Primer, 2016; Warner et al., 2020). Each year, more than 50,000 wildfires are reported in the United States (NICC, 2021). Although large western forest fires draw considerable attention, the southeastern coastal plain accounts for nearly 40% of fire occurrences annually (NICC, 2021). Additionally, prescribed fires for forest management and agriculture occur more frequently in this region than elsewhere in the country (Lear & Harlow, 2002; Melvin, 2021).

With a long history of frequent low-intensity fires and regular lightning strikes, the southeastern coastal plane has favored dominance by fire-adapted pine forest ecosystems with incendiary-type understory vegetation (Noss, 2018; Peet et al., 2018). In this type of fire regime, understory fuels comprise a major portion of plant diversity, act as ladder fuels and significantly influence fire behavior processes and patterns (Bailey et al., 2007; Bright et al., 2016; Gale et al., 2021). Therefore, understanding vegetation flammability, especially in the understory, is essential for minimizing fire-related risks. In addition, characterizing how these fuels influence flammability may provide insight into wildland fire behavior, including intensity, severity, and spread as well as species coexistence patterns and plant succession (Halpern & Antos, 2022; Schwilk, 2003; Skowronski et al., 2020; Varner et al., 2015; Wyse et al., 2016).

Current flammability studies vary in approaches and methods. Most research on plant flammability occurs in laboratory settings, focusing either on small (leaves, plant components, litter, etc.) or large fuel bed scales (Ganteaume et al., 2014; Morandini et al., 2019; Tumino et al., 2019). Moreover, investigations of individual plants only consider a small number of traits and even fewer architectural traits (Morandini et al., 2019; Schwilk, 2003; Tachajapong et al., 2008). Due to logistics, plant dimensions, and difficulties in taking controlled measurements, limited results are available on full-scale plants and their burning characteristics under field conditions (Pausas & Moreira, 2012; Skowronski et al., 2020; White & Zipperer, 2010).

Furthermore, fuel characterization is typically represented by two-dimensional components (surface area, mass, bulk density, etc.). These measurements provide valuable information for fire modeling and behavior analysis. However, they tend to oversimplify the understory fuels and do not capture the architectural variability or other three-dimensional (3D) functional traits (Bright et al., 2016; Rowell et al., 2020). Studies have shown that 3D plant functional traits influence fire dynamics and are associated with flammability (García et al., 2017; Loudermilk et al., 2022; Skowronski et al., 2020). For example, more architecturally complex plants with dense branching patterns of smaller twigs and dead material with low moisture content have a higher chance of igniting, rapidly combusting, and spreading to adjacent fuels (Dent et al., 2019; Peet et al., 2018; Santacruz-García et al., 2019). Additionally, 3D understory architecture variations affect turbulent fluxes of energy and airflow, which can either aid combustion by supplying the fire with additional oxygen or act as barriers creating higher wind drag to impede fire intensity and spread (Banerjee et al., 2019; Parsons et al., 2017; Skowronski et al., 2020). Plant architecture also influences vegetation moisture content, affecting fire ignition and spread in low-intensity fires (Loudermilk et al., 2022).

Remote sensing technologies, particularly Light Detection and Ranging (LiDAR), have opened up opportunities for understory fuel characterization. LiDAR produces a 3D point cloud, which provides information regarding the vertical and horizontal distribution of vegetation (Åkerblom et al., 2017; Calders et al., 2018). Terrestrial Laser Scanning (TLS), or ground-based LiDAR, provides a below canopy perspective of the understory, allowing for higher resolution point clouds and better architectural approximations than airborne LiDAR (Atkins et al., 2018; Moorthy et al., 2011; Rowell et al., 2016). Numerous studies have shown the potential of using TLS data to measure plant functional traits, including height estimation, diameter at breast height (DBH), canopy structure and shape, and to distinguish foliage from woody plant material (Lau et al., 2018; Shi et al., 2018; Skowronski et al., 2007; Su et al., 2018).

Recently, quantitative analysis advancements have enabled derivation of 3D models from TLS data. These models, known as quantitative structure models (QSM), create object-based depictions of plant topology and geometry from the point clouds (Burt et al., 2018; M. Disney, 2019; Raumonen et al., 2013). QSMs isolate and model the woody structure of trees, making it possible to estimate architectural properties. For example, Bayer et al. (2013) showed that QSMs have the potential to predict branch angles, branch length, and branch bending. Lau et al. (2018) further demonstrated the use of QSM algorithms to reconstruct the woody structure of tropical

rainforest trees. The QSM model accurately calculated branching orders, tree volume, and length and diameter of specific branches. Numerous other studies also successfully used QSM to approximate ecological properties (Åkerblom et al., 2015; Bournez et al., 2017; Raumonen et al., 2013; Calders et al., 2018; Disney, 2019; Du et al., 2019; Martin-Ducup et al., 2020). However, QSM algorithms have predominantly focused on 3D tree reconstruction for forestry and ecology applications, with little attention given to understory vegetation or using derived traits for fire behavior analysis.

The main objective of our study was to evaluate the use of TLS and QSM data to characterize understory fuels for fire behavior analysis. We addressed this by (1) measuring TLS- and QSM-derived architectural traits on dominant understory species, (2) experimentally analyzing flammability of these species and (3) evaluating the use TLS and QSM architectural metrics for predicting variability in shrub flammability.

2.2 **Methods**

2.2.1 Study Area

We conducted our research in the Middle Aucilla Conservation Area (MACA) within the Aucilla Wildlife Management Area (AWMA), approximately 7 miles south of the town of Lamont, Florida (Figure 1a). Using a stratified sampling approach, we located and set up twenty-five 5m by 5m plots within MACA. We then randomly selected 12 of these plots for this study, while the others were utilized for a different 3D fuel characterization study (Figure 1b).

The study site was representative of mesic flatwoods, the most common natural community type remaining in the southeastern Coastal Plain (FWC, 2016; Noss, 2018). Our study site had relatively flat terrain and low-lying elevation (lower than 14 m above mean sea level). The area is dominated by either slash (*Pinus elliottii var. densa*) or longleaf pine (*Pinus palustris*) overstory with dense short shrub understory with a few scattered sections of ferns and grasses (Figure 1c). Characteristic understory species include saw palmetto (*Serenoa repens*), gallberry (*Ilex glabra*), tarflower (*Bejaria racemosa*), Darrow's blueberry (*Vaccinium darrowii*), and dwarf live oak (*Quercus minima*). These flatwoods essential to the biota of this region, providing habitat for numerous wildlife species, including rare species such as the red-cockaded woodpecker, flatwoods salamander, Florida black bear, and gopher tortoise.

Frequent low-intensity fires (2-5 years) are the leading environmental factor maintaining these ecosystems. As a result, most animal and plant life inhabiting these communities have adapted to periodic fires or depend on them for their existence. Although some periodic fires occur under natural conditions, the Florida Fish and Wildlife Conservation Commission (FWC), in collaboration with other agencies, employs prescribed management practices in the AWMA. Using prescribed fires ensures that historic natural communities are maintained in this area by limiting the build-up of mid-story fuels and controlling hardwood encroachment.

Our research area was representative of a four to five-year fire return interval. Additionally, we selected our timeframe based on when environmental conditions were most conducive to fires. As such, our fieldwork took place during May 2021, which is historically one of the driest months for the state. On average for the months of May and June, the Wildland Fire Danger Index (FDI), a continuous reference scale for estimating the likelihood of fire ignitions, ranges from moderate to very high probability of wildland fires.

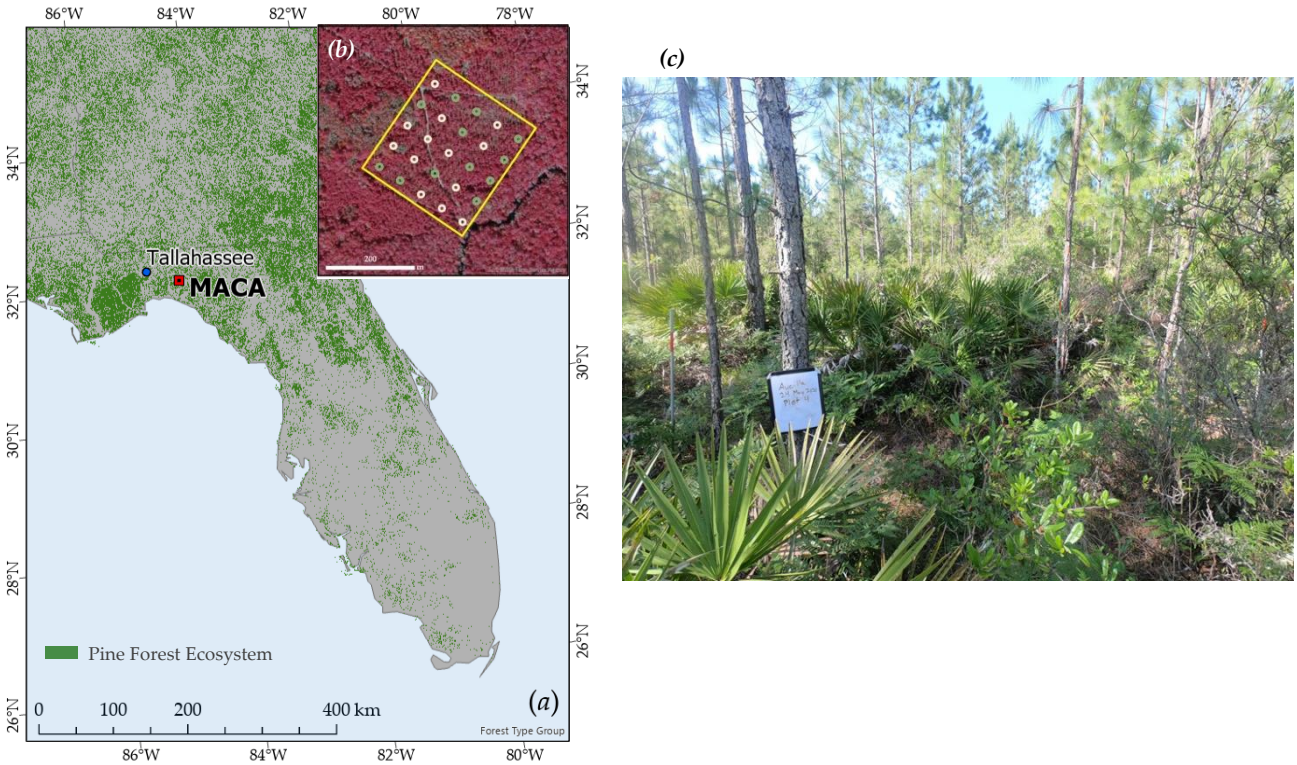

Figure 1. *(a)* Middle Aucilla Conservation Area study site within Florida, USA. *(b)* Approximate locations of the 25 stratified study plots with green circles representing the 12 randomly selected plots used in this study. *(c)* Representative photo of typical vegetation within the study area.

2.2.2 *Sampling and TLS Collection*

For this study, we selected the eight most dominant shrub species across the 12 plots. We sampled ten replica plants of each of the eight species (Table 1). To facilitate comparisons between the species and the burn experiments, we constrained our sampling of the ten plants, keeping heights per species similar. First, we chose and flagged our species samples in all the plots. Although not used in this study (for future scaling up studies), we acquired TLS data at two scales before conducting the in-field measurements. At the study site scale, the entire area was scanned systematically every 50 m, and at the plot level, each plot was scanned from four viewpoints on the plot's boundary.

Field measurements included above-ground height, height to first branch(s), crown widths (North-South and East-West), number of stems, and dead branch/stem count. We also recorded the spatial arrangement of the selected shrub indicating whether the shrub was isolated or growing within a cluster of other shrubs. Thereafter, we carefully uprooted the flagged species, preserving the shrub architecture as much as possible, and moved them to an indoor location in pots that retained the root system and surrounding soil. Where species grew in clusters, we uprooted surrounding species to include in burn experiments (section 2.3). We harvested the shrubs samples in increments over multiple days to ensure plants represented 'in-field' conditions during the acquisition of measurements, scanning, and subsequently, for selected shrubs, burning.

Table 1. List of eight dominant shrub species collected with mean height (cm) and standard deviation (Std dev.) across the ten replicas.

Scientific Name	Common Name	USDA Abbreviation	Mean height of replicas (cm)	Std dev.
Vaccinium darrowii	Darrow's Blueberry	VADA	95	10.60
Vaccinium stamineum	Deerberry	VAST	139	16.82
Vaccinium arboreum	Farkleberry	VAAR	148	5.73
Ilex coriacea	Gallberry	ILCO	161	14.54
Ilex glabra	Inkberry	ILGL	142	5.89
Quercus minima	Dwarf Live Oak	QUMI2	82	3.24
Serenoa repens	Saw Palmetto	SERE2	121	6.77
Cyrilla racemiflora	Swamp Titi	CYRA	162	22.87

After harvesting the samples, we moved them to an indoor location to minimize the effects of wind and other disturbances. We carefully set up between 2 to 8 shrubs (depending on the sizes) in a circular pattern at our 6m x 5m site. We recorded branch orders using

centrifugal ordering and diameter before branching (DBB). Using a unique branch identification methodology, we also recorded ten random branch diameters for each shrub. More information on the branch identification methodology is provided in the previous paper (Manuscript 1). Next, we placed eight 145mm diameter spherical targets at different heights around the room and collected LiDAR scans using a FARO® Focus S350 TLS (FARO Technologies, Inc., www.faro.com). The scanner uses a phase-based scanning technique, in which the returned signal is compared to the wave pattern of the emitted laser beam; and the displacement is determined via the phase shift (FARO® Knowledge Base, 2021). The advantage of using phase-based scanners is a higher accuracy and resolution within the short distances measured. Since we place our shrubs within 10 m of the scanner, the FARO® Focus is an optimal choice for this study. The scanner has respectively a 300° vertical and 360° horizontal field of view. It uses a laser with a 1550 nm wavelength with a beam divergence of 0.3 mrad.

We performed eight scans from various positions around the room, with two scans from the center, one with a low scanner position (0.5 m) and one with a higher scan position (1.5 m). The acquisition time for each scan was approximately 18 minutes using 3x quality and ½ resolution settings. Each scan captures about 174 Million points (MPts), and has a range accuracy of 3.1 mm at a 10 m distance from the scan. In addition, the integrated camera captured high-resolution true color images that we used for co-registration post-scanning. We based our decision to use these specifications on previous studies' findings (Manuscript 1, Lingfors et al., 2017). We repeated the process of scanning in intervals until all shrubs were measured and scanned. Finally, we processed the raw LiDAR point cloud using FARO Scene software and saved the outputs as .laz files for further processing and analysis.

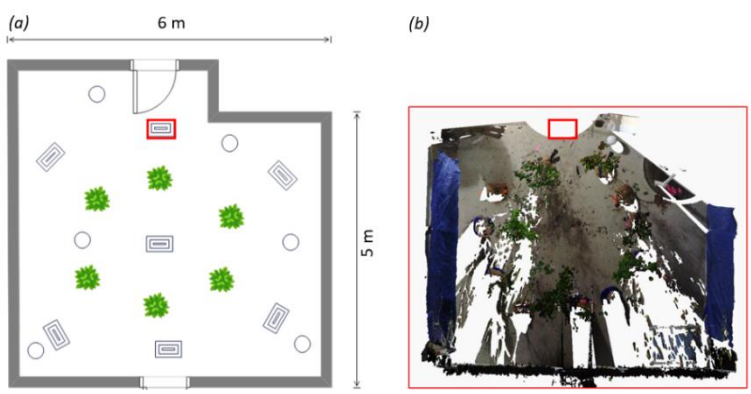

Figure 2. *(a)* Top view of indoor scan location layout, displaying TLS scanner (rectangles), target and approximate shrub locations. *(b)* Point cloud extract from one TLS scan position (red rectangle)

2.2.3 *Controlled Field burns and flammability trait measurements*

After we completed the scanning and measurements, we carefully relocated six replicas of each shrub species to Tall Timbers research station in Tallahassee, Florida, for controlled experimental field burns. Here we prepared 1 m by 3 m burn plots to replicate MACA field conditions as close as possible. To achieve this, we replanted the sampled shrub in front of a ruled metal rod towards the end of the burn plot. If the sampled shrub grew within a cluster in MACA, we also replanted those shrubs around our sampled shrub. After that, we layered pine needle litter within the burn plot. We placed mixed litter collected from around the specific shrub in MACA around the shrub. Finally, we set up an RGB camera at the base of the plot to record each experiment and a Forward Looking InfraRed (FLIR) A655sc fixed thermal infrared camera placed perpendicular to the sampled shrub to capture fuel temperatures throughout the experimental burns (Figure 3). The FLIR sensor has a spectral range of 7.5 – 14.0 μm and features a 640 x 480 pixel microbolometer that can detect temperatures up to 660 °C (FLIR A655sc, FLIR Systems, Inc., Wilsonville, Oregon, USA).

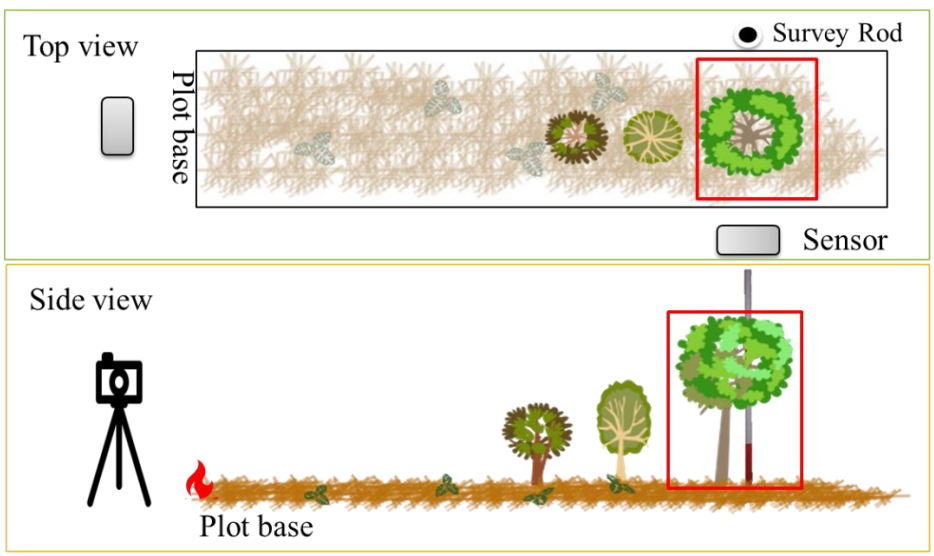

Figure 3. Top and side view of burn plot layout. The red rectangle depicts sampled shrub location.

With the assistance of fire science technicians, we ignited the plot along a line perpendicular to the wind with hand-held drip torches from the base edge. Burns occurred within 48 hours from the time when the shrubs were harvested in the field. The average daytime temperature during burns ranged between 25 and 28°C; relative humidity ranged from 48 to 52%, and wind speed was approximately 6 to 8m/s. After each burn, we cleared the burn plot of debris before setting up the next sampled shrub. If the fire did not completely consume the sampled shrub, we set up the LiDAR scanner and scanned the remaining shrub architecture. We used the scans for consumption percentage calculations. During each burn, we recorded various flammability traits. Table 2 outlines the different methods applied for measuring and calculating the various flammability traits from the TLS and QSM reconstructions. Similar flammability measurements have been employed by Morandini et al. 2019; Santacruz-García et al. 2019; Tumino et al. 2019; Wyse et al. 2016 and others.

Table 2. Description of shrub flammability trait measurements and calculations.

Traits	Abbreviation	Measurement method
Flaming duration (sec)	FD	Difference in seconds between time of ignition and end of flaming
Maximum flame height (cm)	F_{H_MAX}	Estimation of maximum height of flame during flaming from metal rod
Flame height ratio	F_H	The ratio of maximum flame height to shrub height
Peak temperature (°C)	T_{PEAK}	Peak temperature recorded during combustion (not including litter)
Peak Radiative Heat Flux ($W \cdot m^{-2}$)	RHF_{PEAK}	The peak radiative heat flux during the flaming duration (not including litter)
Consumption (%)	% Con	Difference in volume as a percentage calculated from lidar derived QSM of shrub before and after the burn.
Relative burn rate (cm^3 sec^{-1})	RBR	Shrub volume consumption difference divided by the flaming duration

2.2.4 Shrub trait measurements

We preprocessed the TLS data of the six shrubs used in our fire experimental burns for analysis using FARO Scene software. Thereafter, we clipped the individual shrub's point clouds and cleaned these data in CloudCompare software (Girardeau-Montaut, 2016). Using the processed point cloud data, we estimated the North-South and East-West crown width ($CW_{NS/EW}$) from the diameters fitted to the convex hull of the shrub crown. We used these data

to approximate the average crown width (Avg_CW) and crown area (CA) with an elliptical formula (Zhu et al., 2020). To characterize how much of the shrub consisted of foliage, we calculated the crown depth-to-shrub height ratio (CD:H), where crown depth is defined as the difference between maximum shrub height and height to first branching order as recorded manually (Martin-Ducup et al., 2020). We also computed the crown depth to average crown width (CD:CW) and average crown width to height (CW:H). Lastly, we calculated shrub-form metrics independent of shrub size by defining relative height bins of 0-20% (H_B1) of the maximum height (H_{Max}), 20-40% of HMax (H_B2), 40-60% (H_B3), 60-80% of H_{Max} (H_B4), and 80%-H_{Max} (H_B5). Within each relative height bin, we calculated the percentage of returns. Using the Z-values, we computed the descriptive statistics (mean, median, standard deviation (std. dev), skewness, and kurtosis) for the entire point cloud of each shrub.

In order to create QSM models for each shrub, we needed to separate the foliage from the woody points. We used the well-recognized LeWoS methodology Wang et al. (2020) developed to achieve this. LeWoS is adapted from previous work by Vicari et al. (2019); it is an automatic algorithm with some manual fine-tuning parameters that separate leaf and woody components from point cloud data. It utilizes recursive point cloud segmentation and regularization procedures and yields overall accuracies upward of 90%. For this study, we tested four feature similarity tuning thresholds (0.1, 0.125, 0.15, and 0.2) and selected the point cloud that visually best represented the woody portion of the shrub. We set these thresholds based on the results from Wang et al. (2018). Once separation was completed, we extracted only the woody points and reconstructed the individual shrubs using the QSM method developed by Raumonen et al. (2013) and further adapted for shrubs in a previous study (Manuscript 1), where we described the reconstruction process in detail. We further refined these models using the aRchi package in R (R Core Team, 2013) to compute topology metrics (Martin-Ducup et al., 2020). For improved visualization, we make use of the QSM add-in feature for Blender 3.1 open-source software (https://www.blender.org/). Figure 4 shows an example of the processing steps from point cloud to the final QSM.

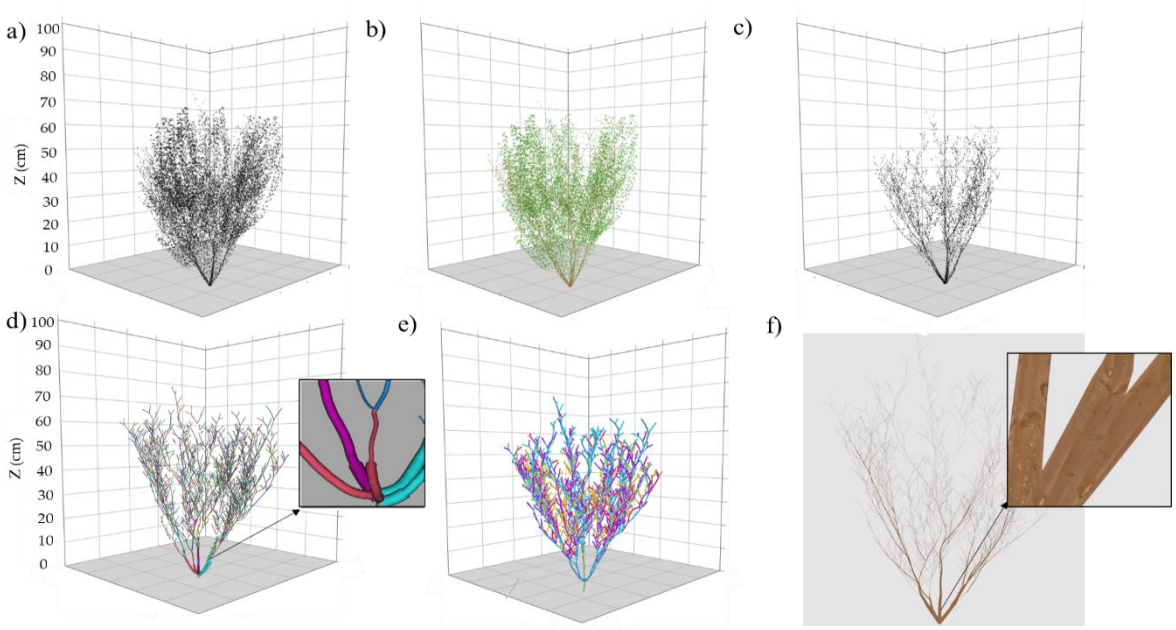

Figure 4. a) Cleaned and processed point cloud b) LeWoS leaf/wood separation algorithm. c) Filtered point cloud with only woody attributes. d) QSM model. e) Paths created with aRchi package (colored by branch order). f) Final visualization after enhancement using QSM add-on within Blender software.

We recorded the highest branching order (BO_H) of every shrub, total branch count (BC), and the shrub's average diameter of the first ($AvgD\_BO_F$) and last branch orders ($AvgD\_BO_H$). The first-order branching was defined as the first ramification from the shrub's main stem(s)/trunk. Then, we calculated the average branching angle (BA) per shrub using the mean zenithal angle of all segments (branches) except the main stem(s)/trunk. This metric indicates the growing orientation of branches, with higher branching angles associated with shrubs with on average a more horizontal-orientated branching pattern. Moreover, we calculated the fork rate (FR) as the mean number of ramifications per height bin calculated by modifying the aRchi 'ForkRate' function from open source code available from Github (https://github.com/umr-amap/aRchi/blob/main/R/ForkRate.R). A lower fork rate designates less complex branching patterns. In contrast, a higher fork rate would suggest a more complex branching habit (i.e., many branches), with branches often growing outward rather than upward. We also recorded the estimated woody volume from the QSMs. Table 3 summarizes the frequently utilized shrub traits along with the measurement descriptions.

Table 3. Description of shrub trait measurements from TLS and QSM.

Architectural Traits	Measurement
TLS	
Point cloud (All)	Mean, median, standard deviation, skewness, and kurtosis of z-values
Point cloud (relative height bins)	Percentage of point clouds within each of the five bins, where the bin is 20%,40%,60%,80% and 100% of the maximum height of the shrub
Crown depth to height ratio (CD:H)	Maximum shrub height divided by the height of foliage cover
Crown width to height ratio (CW:H)	Average crown width divided by the height of the shrub
Crown width to crown depth ratio (CW:CD)	Average crown width divided by the crown foliage cover height
Crown area (CA)	Ellipsoid area formula from estimated crown widths
QSM	
Fork rate (FR)	Average number of forks per relative height bin
Branch count (BC)	Total number of branches
Branch angle (BA)	Average zenithal angle of all branches (except the main stem(s))
Branch diameters	Average branching diameter of first and last branch order estimated from QSMs
Volume	Volume of woody portion of shrub obtained from QSM
Highest Branching Order	Recorded the highest ramification of shrub branches

Since the moisture content of vegetation significantly influences fire behavior and plant flammability (Banerjee et al., 2019; Castro et al., 2003; Grootemaat et al., 2015), we used the four remaining samples of each shrub species to obtain leaf moisture content. We systematically removed the leaves and weighed them to give us their fresh weight (g). Thereafter, they were stored in a Ziplock plastic bag until we could dry them in an oven for two days at 80 °C (Krix & Murray, 2018; Pérez-Harguindeguy et al., 2013), after which we re-measured the dried leaves and calculated fuel moisture content (*MC*) as a percentage (Eq.1).

$$MC = \frac{LW_{Fresh} - LW_{Dry}}{LW_{Dry}} \times 100 \qquad \text{(Eq.1)}$$

where LW_{Fresh} is the fresh weight of the shrub leaves in grams and LW_{Dry} is the weight of dried shrub leaves in grams. The average *MC* percentage from the four replicas of each shrub species was calculated and attributed to the burned shrubs species.

2.2.5 Statistical Data Analysis

We calculated the Pearson Correlation Coefficients between the TLS and QSM-derived traits to determine associations between shrub traits. Given the inherent multicollinearity of shrub characteristics, we computed principal component analysis (PCA) to explore correlation patterns between various shrub species. PCA is a traditional multivariate statistical method that rescales features to a common scale and is used to solve multicollinearity and reduce the number of predictive variables without losing a significant amount of information (Alam et al., 2019; Engber & Varner, 2012). We performed an initial PCA on all the architectural shrub traits. Then, we used the squared cosine to identify variables that were poorly represented by the PCA, removed them, and reran the PCA with the remaining variables. The squared cosine indicates the contribution of a component to the squared distance of the variable to the origin and is a measure of the importance of the given variable (Abdi & Williams, 2010).

We further used PCA as a preliminary analysis to determine flammability patterns among each species and to select influential flammability variables, explaining at least 70% of the variation. Following the PCA, we performed a partial least squares (PLS) analysis to find associations between the explanatory variables (shrub traits) and the most influential flammability variable(s) as determined by our PCA. The PLS was performed on the QSM-derived and TLS traits separately as well as in conjunction to evaluate which traits (QSM or TLS or combined) promote flammability and influence these metrics. Finally, we used the first PCA's of the flammability and architectural traits to compare species flammability by traits (García et al., 2017; Wyse et al., 2016). We used a combination of R software environment (R Core Team, 2013) and JMP® statistical software (*JMP Pro ® Statistical Software*, 2021) to run our analyses.

2.3 **Results**

2.3.1 Shrub Architectural Diversity

Using the squared cosines of our initial PCA results of all the architectural shrub traits, we found that height, standard deviation, skewness, percentage of points in all height bins (except 4), and the average diameter of the first branching order of the shrubs, had low $\cos^2$ values (≤ 0.25) for both of the first two principal components (Table 4). A low $\cos^2$ indicates that these variables are not well represented by the first two principal components, despite the fact they explained 53% of the variability.

Table 4. Squared cosines of all TLS and QSM architectural traits depicting the variable contribution for the first two components.

Trait Variable	Cos^2	
	PC 1 (30.98%)	PC 2 (21.88%)
Total Stems	**0.711**	0.132
Height	0.085	0.280
CD:H	0.044	**0.413**
Avg_CW	**0.517**	0.050
CA	**0.595**	0.057
CW:H	**0.652**	0.259
CW:CD	**0.326**	0.006
Mean	0.146	**0.666**
Median	0.098	**0.661**
Std. dev	0.006	0.200
Skewness	0.001	0.120
Kurtosis	0.166	**0.419**
%B1	**0.235**	0.205
%B2	0.232	**0.248**
%B3	0.000	0.154
%B4	**0.432**	0.178
%B5	0.102	0.173
BA	**0.774**	0.011
FR	0.214	**0.504**
BC	0.139	**0.406**
BO_H	**0.602**	0.007
Volume	0.379	0.001
$AvgD\_BO_F$	0.251	0.097
$AvgD\_BO_H$	**0.627**	0.030
MC	**0.408**	0.192

**Values in bold correspond to each trait variable for which the squared cosine is the largest of the principal components*

The rerun of the PCA without these variables represented 65% of the total variability within the first two biplot axes (Figure 5a). PC 1 (41.52%) is associated with shrubs that have larger branching angles and a higher number of branch orders on the positive side of the axis. On the negative horizontal axes, PC 1 is associated with shrubs with larger diameters for the last branching order, which have more stems and a wider crown (high CW:H). PC 2 (23.77%) primarily represents shrubs with higher fork rates and are taller on the positive side of the vertical axis, and shrubs with fuller crowns (high CD:H) on the opposing side of the axis. The architectural variable contributions (in percentages) to PC 1 and PC 2 are illustrated in Figure 5b. BA and total stem architectural traits had the highest contribution for PC 1, with 11.65% and 11.62%, respectively, while the mean (17.37%) and median (15.41%) had the highest contribution for PC 2.

Within the multivariate space delimited by PC 1 and PC 2, shrub species are denoted by unique colored points. From this biplot, we observed that individual members of each shrub species are generally clustered in close proximity. The *Serenoa repens* shrub replicas, which have a large number of stems and wider crown are clustered in the negative quadrant (Figure 5a, *q4*), *Cyrilla racemiflora*, *Vaccinium arboretum, Ilex coriacea* and *Ilex glabra* shrubs are primarily grouped in the positive quadrant (Figure 5a, *q2*), and *Quercus minima* shrubs towards the center of the PCA biplot.

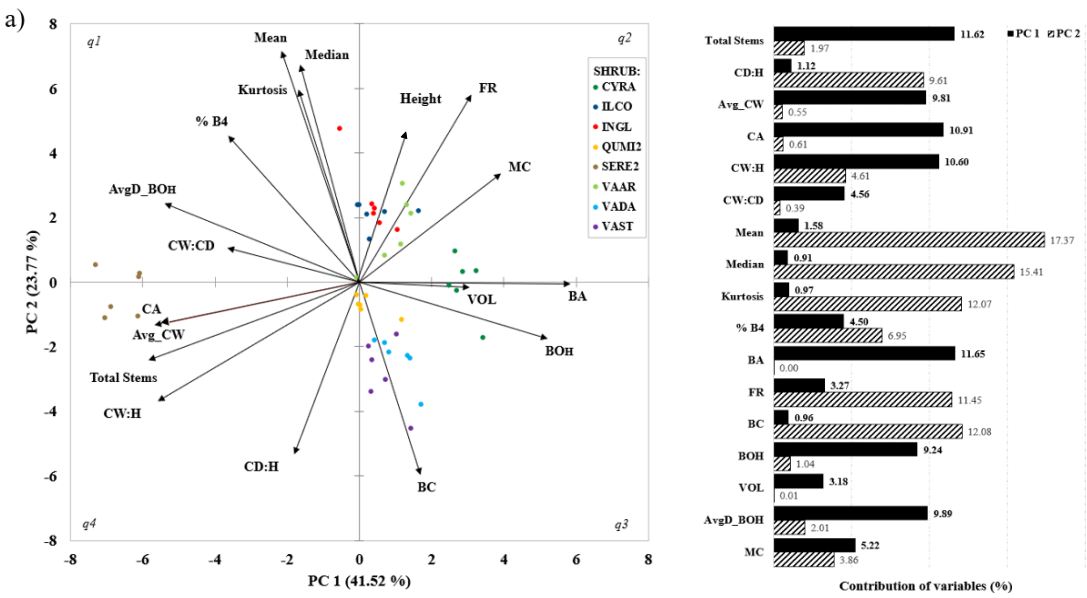

Figure 5. a) PCA of shrub architectural traits with points representing the shrub replicas' mean score, colored by shrub species. b) Variable percentage contribution to PC1 and PC2.

Pearson's correlation tests demonstrated significant ($p < 0.05$) interrelationships between trait variables, shown in bold in Table 5. All the shrub traits displayed some significant relationship with two or more other traits. The average crown width, crown area, average diameter of the last branching order, and CW:H ratio demonstrated a significantly strong positive ($r < 0.7$) relationship with the total number of stems. Conversely, the average branching angle of shrubs revealed a strong negative ($r < -0.7$) correlation with the total number of stems as well as the CW:H ratio. The average crown width also had a significantly strong positive correlation with CW:H and the average branch diameters of the last branching order. However, it only presented a moderate negative correlation with BO_H ($r = -0.64$; $p < 0.05$) and branching

angle (r = -0.66; p <0.05). The TLS-derived CW:CD ratio and percentage of returns in bin four (% B1) and QSM-derived branch count variables only had low to moderate correlations with other traits. We found that the CW:H ratio statistic showed a strong negative correlation with moisture content (r = -0.70; p <0.05), branching angle (r = -0.72; p <0.05) and fork rate (r = 0.71; p <0.05). Moreover, we noted that the height of the shrubs was not significantly (p >0.05) correlated to most of the other variables, whereas the branching angle and the average diameter of the last branching order were.

Table 5. Pearson's correlations among shrub architectural traits. Values in bold indicate a significant (p <0.05) correlation, green highlighted cells display strong positive correlations, and grey highlighted cells show strong negative correlations.

Variables	Total stems	Height	CD:H	Avg_CW	CA	CW:H	CW:CD	Mean	Median	Kurtosis	% B4	BA	FR	BC	BOH	VOL	AvgD_BOH
Height	-0.28																
CD:H	**0.53**	**-0.46**															
Avg_CW	**0.78**	0.11	0.18														
CA	**0.83**	0.04	0.25	**0.99**													
CW:H	**0.88**	**-0.48**	**0.46**	**0.81**	**0.84**												
CW:CD	**0.35**	-0.08	**-0.45**	**0.62**	**0.58**	**0.56**											
Mean	0.09	**0.51**	**-0.36**	0.23	0.22	-0.08	0.21										
Median	0.02	**0.41**	**-0.39**	0.14	0.13	-0.11	0.25	**0.93**									
Kurtosis	0.00	0.00	**-0.42**	0.00	0.01	-0.02	**0.34**	**0.54**	**0.52**								
% B4	**0.37**	-0.02	0.07	0.20	0.25	0.21	0.07	**0.61**	**0.44**	**0.55**							
BA	**-0.87**	0.19	**-0.39**	**-0.66**	**-0.73**	**-0.72**	**-0.32**	**-0.31**	-0.22	-0.15	**-0.58**						
FR	**-0.57**	**0.71**	**-0.57**	**-0.33**	**-0.37**	**-0.71**	-0.17	**0.41**	**0.36**	0.26	-0.06	**0.43**					
BC	-0.09	-0.01	0.15	0.11	0.04	0.08	-0.07	**-0.54**	**-0.46**	**-0.54**	**-0.65**	**0.36**	-0.28				
BOH	**-0.65**	-0.04	-0.18	**-0.64**	**-0.69**	**-0.54**	**-0.33**	**-0.39**	-0.28	-0.24	**-0.62**	**0.79**	0.18	**0.35**			
VOL	**-0.36**	**0.70**	-0.01	-0.07	-0.12	**-0.47**	**-0.43**	-0.03	-0.05	**-0.46**	**-0.42**	**0.40**	**0.50**	**0.38**	0.15		
AvgD_BOH	**0.70**	0.14	0.09	**0.74**	**0.78**	**0.57**	**0.45**	**0.49**	**0.35**	**0.30**	**0.58**	**-0.76**	-0.09	**-0.40**	**-0.86**	-0.15	
MC	**-0.63**	**0.61**	**-0.33**	**-0.39**	**-0.43**	**-0.70**	**-0.40**	0.13	0.08	-0.14	-0.15	**0.52**	**0.67**	-0.15	0.28	**0.66**	-0.15

2.3.2 Shrub flammability

The correlation circle for the PCA of the shrub flammability data (Figure 6a) demonstrated that peak temperature and peak radiative heat flux during the combustion of shrubs are positively correlated. Similarly, the FH:SH ratio and percentage consumption are

positively correlated, but both are negatively correlated with the highest branching order left on the shrub after we burned it. Furthermore, the first two components of the PCA explained most of the data's variation (79%). The first PC axis explained 61% of the variation and had an eigenvalue of 3.6. It was predominantly associated with consumption components (% consumption and BO_H_AB) and combustion components (T_{peak}, RHF_{peak}, and FH:SH). Whereas the second PC axis explained approximately 19% of the variation with nearly four times smaller eigenvalue of 1.1, it was mainly associated with the sustainability component we calculated as the relative burn rate (RBR).

Figure 6b illustrates large flammability differences among most species. By looking at PC 1, which explained the most variation, we see that *Ilex coriacea* and *Ilex glabra* species are clustered together and associated with highest branch orders left after the burn. The PCA results also indicate that *Vaccinium darrowii* and *Serenoa repens* had similar flammability characteristics and were associated with higher maximum temperatures, maximum radiative heat fluxes, flame height to shrub height ratios and greater consumption of the shrub by the fire.

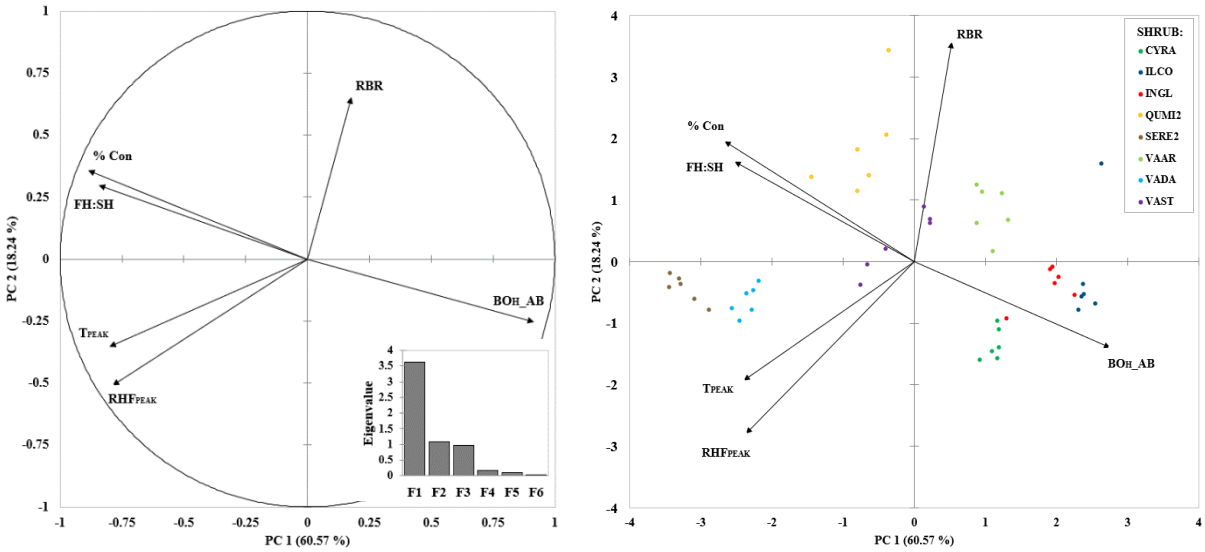

**Table 1 provides the shrub's scientific name with corresponding USDA abbreviations used in the figure.*

Figure 6. a) PCA correlation circle of flammability components and histogram of eigenvalues. b) PCA biplot of flammability variables with points representing the shrub replicas' mean score, colored by shrub species.

As mentioned before, % Con and FH:SH are correlated with each other and inversely correlated with BO_H_AB, and T_{PEAK} and RHF_{PEAK} are correlated with each other. However, T_{PEAK} and RHF_{PEAK} are approximately orthogonal to % Con and FH:SH and thus not likely correlated. As such, we further investigated T_{PEAK} and % Con as they had the highest variable contribution and loading factors in PC 1 that were unrelated.

Overall, we observed different responses between the shrub species during the experimental burns. *Serenoa repens* and *Vaccinium darrowii* had the highest measures for both flammability metrics and remained relatively consistent for shrub replicas of the same species (Figure 7). We found the most peak temperature variation among the same species in *Quercus minima* and *Vaccinium stamineum* shrubs, with maximum temperatures ranging from 309°C to 575°C and 239°C to 532°C, respectively (Figure 7a). *Ilex coriacea* and *Ilex glabra* shrubs had the lowest percentage of consumption and peak temperatures, with mean % Con of 14% and 39% and mean T_{PEAK} of 120°C and 132°C, respectively (Figure 7). Our experimental burn results also highlighted a stark difference between peak temperature and percentage consumption for *Cyrilla racemiflora* (High T_{PEAK}, Low % Con) and *Vaccinium arboreum* (Low T_{PEAK}, Higher % Con).

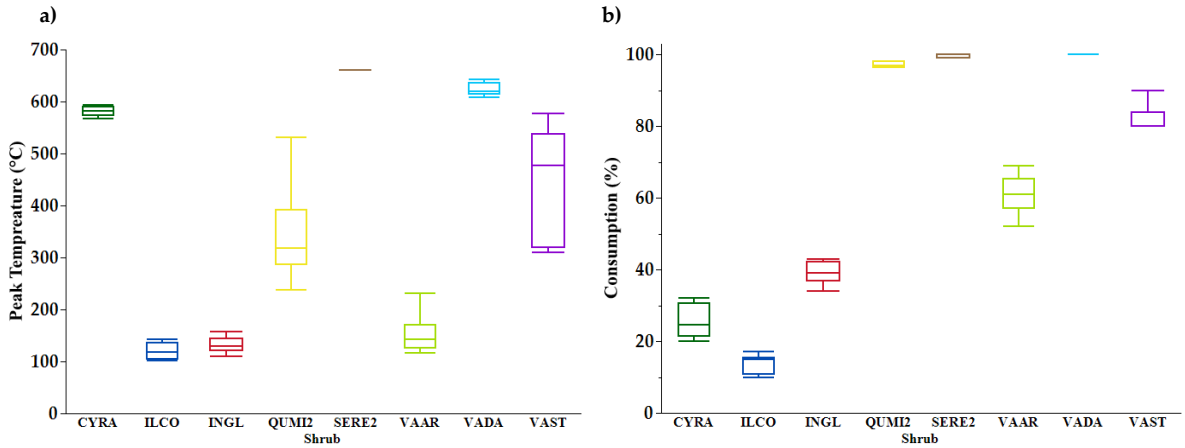

Figure 7. a) Boxplot of eight species' maximum temperature ranges during experimental burns for shrub replicas. b) Boxplot of percentage consumption per species from the six replicates.

2.3.3 *Architectural traits linked to flammability*

PLS results for T_{PEAK} using only TLS traits explained 73.85% of the variation for the first two factors and 68.88% for only the QSM-derived traits. The combined results for T_{PEAK} increased the total explained variation for the first two factors to 76.52%. The fitted parameters of two factors for T_{PEAK} had R^2Y of 0.75, 0.71, and 0.77 for TLS, QSM and Combined traits, respectively. R^2Y in PLS analysis is equivalent to adjusted R^2. Similarly, looking at the PLS results for % Con, we noted that with only TLS traits, 71.85% of the variation was explained for the first two factors and 70.72% when using the QSM-derived traits. The combined results for % Con explained 82.45% of the total variation. Our results showed an R^2Y of 0.84 when using all the architectural traits to predict the percentage of consumption. Whereas using only QSM (R^2Y = 0.81) or TLS (R^2Y = 0.78) traits had slightly lower R^2Y values.

Furthermore, we used the variable importance plot (VIP) and scaled and centered model coefficients to determine which predictor variables (shrub traits) are most predictive of T_{PEAK} and % Con for the combined PLS models. A variable is considered 'important' if its VIP value is greater than 0.8 (Olah et al., 2004; Pertille et al., 2022; H. Yu et al., 2010). The VIP results highlight the importance of the kurtosis statistic, CW:H and CD:H ratio's as TLS variables in predicting both T_{PEAK} and % Con (Figure 8). The VIP index results (Figure 8b) for most QSM traits (BA, Volume, BC, BOH, and average diameters) for predicting T_{PEAK} are smaller than 0.8, while six of the nine QSM traits had a significant contribution for predicting % Con.

Figure 9 shows a significant association between the first components of the flammability metrics and architectural metrics. The left side of the x-axis is characterized by large CD:H ratio's, larger branching angles and smaller CW:H ratios. Conversely the right side of the x-axis represents wider, flatter shrubs with closer to the ground having a small CD:H ratio and high CW:H ratio. Additionally, shrubs toward the right of the x-axis have lower branching angles and larger overall volumes. The y-axis represents an increase in flammability based on the first component of the flammability assessment (Figure 6). This correlation suggests that shrubs with generally have higher CD:H and lower CW:H are less flammable than shrubs (*Ilex coriacea* and *Ilex glabra*) while shrubs with lower CD:H and larger CW:H are generally more flammable (*Serenoa repens*).

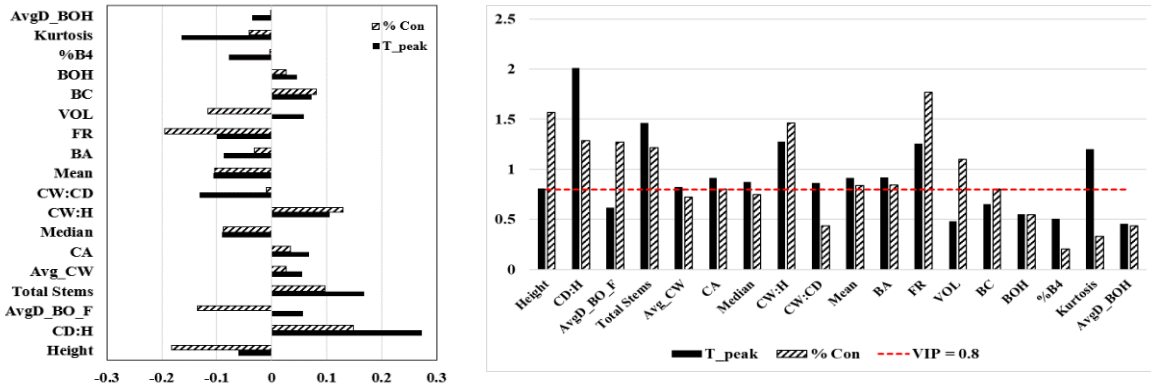

Figure 8. a) Standardized coefficient plot related to % Con and T_{PEAK} b) Variable importance plot for the PLS model for predicting % Con and T_{PEAK}, where the horizontal red dashed line is a VIP threshold of 0.8. The asterisk (*) represents QSM-derived architectural traits, and ** indicates traits attributed to both TLS and QSM.

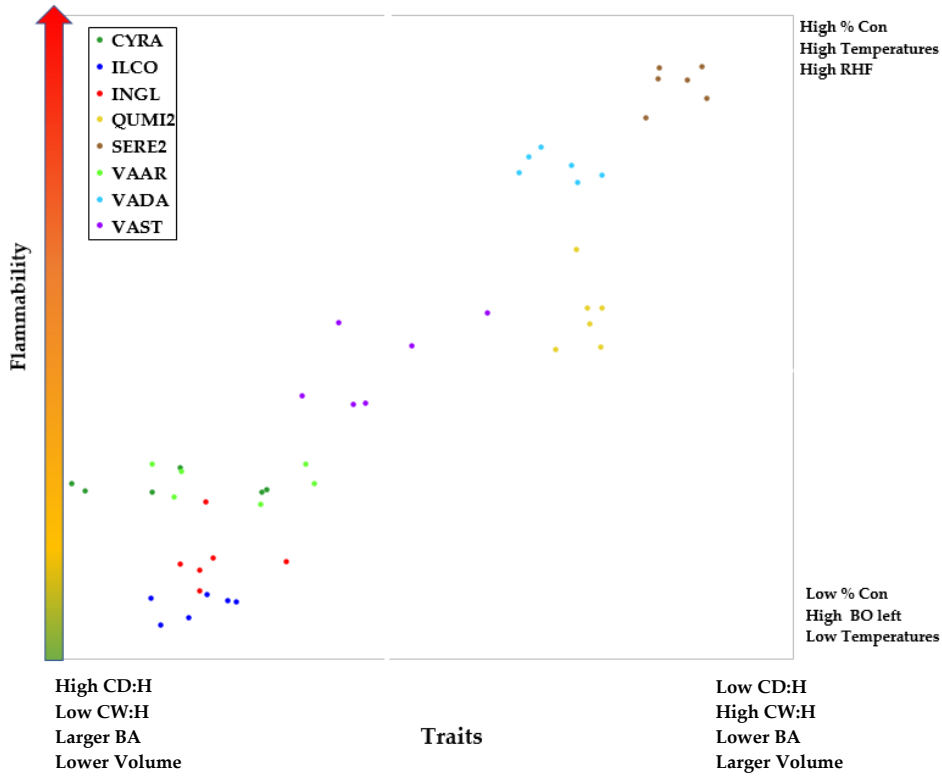

Figure 9. Flammability index of shrub species eatimated by artitectural traits using the first axis of the flammability and architectural trait PCA's.

2.4 Discussion

Our study provides one of the first methodologies incorporating TLS and QSM 3-dimensional metrics to describe shrub architectural diversity and investigate shrub flammability. The advantage of QSM is that no additional fieldwork is required as we can derive QSMs from TLS data. Furthermore, the geometric reconstruction of shrub architecture provides detailed topology measurements (i.e. branch counts, branch diameters, branch orders and angles), which cannot be extracted from the point cloud directly (M. Disney, 2019; Janoutová et al., 2021).

Using these metrics to investigate architectural diversity among species, we found a high degree of covariation among shrubs traits, with two or more traits being significantly ($p < 0.05$) correlated with each other. This is to be expected as similar selective pressures, environmental conditions, and natural growth patterns influence the evolutionary physiology of shrubs (Singhal et al., 2021; Tumino et al., 2019; Yang et al., 2022). The results of the PCA of all (TLS and QSM) shrub architectural traits indicate that various shrub species were characterized by different combinations of traits, and species in the same genus tend to be clustered (Figure 5a). For example, VADA and VAST (*Vaccinium* genus) are grouped in *q3*; ILCO and INGL are clustered in *q2* and belong to the *Ilex* genus (Figure 5a).

The results from the flammability PCA highlighted correlations between flammability components and allowed us to reduce dimensionality for further analysis. Since the first two axes explained a high percentage (79%) of the variation, with PC 1 explaining 61% of the variation and having an eigenvalue of four times larger than PC 2, it was possible to use this to deduce associations among shrub replicas and flammability components (Santacruz-García et al., 2019). As with the architectural traits, we found that shrubs of the same species had similar flammability metrics. Generally, the PCA results also indicated *Vaccinium darrowii* and *Serenoa repens* had considerably higher maximum temperatures, radiative heat fluxes and relative flame heights, suggesting that these shrubs burned at higher intensities (Loudermilk et al., 2009). These results, in conjunction with their having a higher percentage of consumption, indicated that these species were more flammable than others in our experimental burns (Alam et al., 2019; Engber & Varner, 2012). Conversely, shrubs with a higher number of branch orders left after experimental burns, and a lower percentage of consumption, temperatures, and radiative heat fluxes, are associated with less intense fires and lower overall flammability (Grootemaat et al., 2015; Varner et al., 2015). Specifically, we found that *Ilex coriacea* and *Ilex glabra* species fell in

this category. This contradicts other flammability studies on these species that found them highly flammable (Brose & Wade, 2002; Geron & Hays, 2013; Miller & Corby, 2022). We suspect our results were attributed to the fact that these shrubs had a higher height to the canopy (CD:H) and grew relatively isolated; thus, they did not have enough ladder fuels for fire to reach the canopies (Parkins et al., 2023; Warner et al., 2020). Additionally, other uncontrolled variables may have influenced their flammability since our experimental burns took place in the field and not in a laboratory setting. This further highlights the need to investigate the links between plant traits and flammability components and to conduct field-based experiments.

Numerous studies have indicated that functional traits influence flammability (Alam et al., 2019; Calitz et al., 2015; Potts et al., 2022; Tumino et al., 2019). However, these studies are often limited to small scales (leaves) or large scales (the fuel bed). In addition, research often focuses on only a few traits, and architectural traits are usually directly measured from the shrub and not derived from TLS data. As such, this study provides a new approach to linking architectural traits to flammability. The PLS models for TLS and QSM-derived traits separately and in combination, all performed well ($R^2Y > 0.7$) and highlighted drivers that promote flammability components, specifically for predicting T_{PEAK} and % Con. However, it should be noted that we did observe a slight increase in prediction accuracy when combining QSM and TLS traits. The VIP information suggested that TLS traits such as CW:H and CD:H are important drivers in fire intensity and combustibility. We found that QSM traits are not good assessors for predicting T_{PEAK}. However, for predicting consumability the QSM traits outperformed TLS traits (VIP > 0.8). Other studies found similar results from direct measurements of crown metrics (Alam et al., 2019; Burger & Bond, 2015; Long et al., 2006). Wilson et al. (2022) derived fuel structure from TLS data at a forest level and found the probability of fire severity decreased as the canopy base height increased, and the distance between the canopy base and understory increased. We did not find any supporting literature relating directly to QSM traits used to measure flammability. However, biomass, volume, and branching arrangement, which can be extracted from QSM, have been linked to various flammability components (Hogenbirk & Sarrazin-Delay, 1995; Pausas & Moreira, 2012; Schwilk, 2003). We should mention that using TLS and QSMs traits to predict flammability has some potential issues. Occlusion in the TLS data may influence the accuracy of TLS derived metrics. Additionally, as most in-field TLS collection are done leaf-on, leaves may occlude smaller branches (Calders et al. 2015; Gonzalez de Tanago et al. 2018) and uncertainties may occur when creating the QSM reconstructions (Hackenberg et al. 2015a; Momo et al. 2020; Burt et al. 2021).

2.5 Conclusions

Our study demonstrated the use of TLS and QSM-derived architectural shrub traits to investigate trait patterns and species diversity for dominant southeastern shrubs. Although TLS has been used to characterize the architecture of vegetation, we included additional novel metrics related to the topological architecture of shrubs. This allowed us to identify similarities and highlight species differences with regard to the vertical architectural structure, including shrub branch ramification, branching angle, woody volume etc. Using TLS combined with QSM opens up new approaches for studying vegetation structure and provides 3-dimensional fuel information that can be incorporated into fire models.

In addition, our field experimental burn methodology provides valuable insight into in-field flammability components of understory shrubs. Since many other studies explore the flammability of vegetation in laboratory settings or only use a proportion of the plant, our research aids in closing the gap between laboratory and field by linking shrub traits to flammability metrics at a plot scale. Overall, our analysis demonstrated a significant relationship between TLS and QSM architectural traits and field measures of flammability. Specifically, the separate TLS and QSM traits had high coefficients of determination for predicting the percentage of mass-consumed (consumability) and maximum temperatures of shrubs while burning (combustability). The QSM traits even outperformed the TLS-dervived traits in predicting consumability. Moreover, our results indicated an increased accuracy when combining the TLS and QSM traits to predict these flammability components.

These results demonstrate the potential of using QSM to provide metrics that are complementary to TLS data, potentially improve flammability predictions, and increase our understanding of the linkages between flammability and architectural traits. Furthermore, our results highlight the importance of incorporating topological vegetation structure in fire behavior studies. However, further research into optimizing QSM algorithms and extracting traits for understory vegetation is still needed, especially for complex architectures. Additionally, future research could include incorporating other flammability components or using them in combination. We will also consider scaling up from single shrub level measurements to multiple shrubs and investigating flammability for combinations of understory species in future studies.

2.6 References

Abdi, H., & Williams, L. J. (2010). Principal component analysis. *Wiley Interdisciplinary Reviews: Computational Statistics*, *2*(4), 433–459.

Abegg, M., Boesch, R., Schaepman, M. E., & Morsdorf, F. (2021). Impact of Beam Diameter and Scanning Approach on Point Cloud Quality of Terrestrial Laser Scanning in Forests. *IEEE Transactions on Geoscience and Remote Sensing*, *59*(10), 8153–8167. https://doi.org/10.1109/TGRS.2020.3037763

admin_stanpro. (2018, May 17). Reflection of light: What is specular reflection. *Stanpro*. https://www.standardpro.com/what-is-specular-reflection/

Åkerblom, M., Raumonen, P., Mäkipää, R., & Kaasalainen, M. (2017). Automatic tree species recognition with quantitative structure models. *Remote Sensing of Environment*, *191*, 1–12. https://doi.org/10.1016/j.rse.2016.12.002

Alam, M. A., Wyse, S. V., Buckley, H. L., Perry, G. L. W., Sullivan, J. J., Mason, N. W. H., Buxton, R., Richardson, S. J., & Curran, T. J. (2019). Shoot flammability is decoupled from leaf flammability, but controlled by leaf functional traits. *Journal of Ecology*, *n/a*(n/a). https://doi.org/10.1111/1365-2745.13289

Alonso-Benito, A., Arroyo, L., Arbelo, M., & Hernández-Leal, P. (2016). Fusion of WorldView-2 and LiDAR data to map fuel types in the Canary Islands. *Remote Sensing*, *8*(8), 669.

Andersen, H.-E., McGaughey, R. J., & Reutebuch, S. E. (2005). Estimating forest canopy fuel parameters using LIDAR data. *Remote Sensing of Environment*, *94*(4), 441–449. https://doi.org/10.1016/j.rse.2004.10.013

Aravanopoulos, F. A. (Phil). (2016). Conservation and Monitoring of Tree Genetic Resources in Temperate Forests. *Current Forestry Reports*, *2*(2), 119–129. https://doi.org/10.1007/s40725-016-0038-8

Arseniou, G., MacFarlane, D. W., & Seidel, D. (2021). Woody Surface Area Measurements with Terrestrial Laser Scanning Relate to the Anatomical and Structural Complexity of Urban Trees. *Remote Sensing*, *13*(16), 3153.

Atkins, J. W., Bohrer, G., Fahey, R. T., Hardiman, B. S., Morin, T. H., Stovall, A. E. L., Zimmerman, N., & Gough, C. M. (2018). Quantifying vegetation and canopy structural complexity from terrestrial LiDAR data using the forestr r package. *Methods in Ecology and Evolution*, *9*(10), 2057–2066. https://doi.org/10.1111/2041-210X.13061

Badillo, P. D., & Parfenov, V. A. (2022). *Accuracy of Alignment Procedures Used for the Creation of 3D Models*. 1103–1106.

Bailey, A. D., Mickler, R., & Frost, C. (2007). *Presettlement fire regime and vegetation mapping in southeastern coastal plain forest ecosystems*. *46*.

Banerjee, T., Heilman, W., Goodrick, S., Hiers, K., & Linn, R. (2019). *Effects of canopy midstory management and fuel moisture on wildfire behavior*. OSF Preprints. https://doi.org/10.31219/osf.io/4p57h

Barber, C. B. (2020). *Qhull manual*. http://www.qhull.org/html/index.htm#authors

Beland, M., Parker, G., Sparrow, B., Harding, D., Chasmer, L., Phinn, S., Antonarakis, A., & Strahler, A. (2019). On promoting the use of lidar systems in forest ecosystem research. *Forest Ecology and Management*, *450*, 117484. https://doi.org/10.1016/j.foreco.2019.117484

Belgiu, M., & Drăguţ, L. (2016). Random forest in remote sensing: A review of applications and future directions. *ISPRS Journal of Photogrammetry and Remote Sensing*, *114*, 24–31.

BMesh Module (bmesh)—Blender Python API. (n.d.). Retrieved 10 November 2022, from https://docs.blender.org/api/current/bmesh.html

Borchert, R., & Slade, N. A. (1981). Bifurcation ratios and the adaptive geometry of trees. *Botanical Gazette*, *142*(3), 394–401.

Bright, B. C., Loudermilk, E. L., Pokswinski, S. M., Hudak, A. T., & O'Brien, J. J. (2016). Introducing Close-Range Photogrammetry for Characterizing Forest Understory Plant Diversity and Surface Fuel Structure at Fine Scales. *Canadian Journal of Remote Sensing*, *42*(5), 460–472. https://doi.org/10.1080/07038992.2016.1229598

Brose, P., & Wade, D. (2002). Potential fire behavior in pine flatwood forests following three different fuel reduction techniques. *Forest Ecology and Management*, *163*(1–3), 71–84.

Burger, N., & Bond, W. J. (2015). Flammability traits of Cape shrubland species with different post-fire recruitment strategies. *South African Journal of Botany*, *101*, 40–48. https://doi.org/10.1016/j.sajb.2015.05.026

Burt, A., Disney, M., & Calders, K. (2018). Extracting individual trees from lidar point clouds using treeseg. *Methods in Ecology and Evolution*, *0*(0). https://doi.org/10.1111/2041-210X.13121

Calders, K., Adams, J., Armston, J., Bartholomeus, H., Bauwens, S., Bentley, L. P., Chave, J., Danson, F. M., Demol, M., Disney, M., Gaulton, R., Krishna Moorthy, S. M., Levick, S. R., Saarinen, N., Schaaf, C., Stovall, A., Terryn, L., Wilkes, P., & Verbeeck, H. (2020). Terrestrial laser scanning in forest ecology: Expanding the horizon. *Remote Sensing of Environment*, *251*, 112102. https://doi.org/10.1016/j.rse.2020.112102

Calders, K., Newnham, G., Burt, A., Murphy, S., Raumonen, P., Herold, M., Culvenor, D., Avitabile, V., Disney, M., Armston, J., & Kaasalainen, M. (2015). Nondestructive estimates of above-ground biomass using terrestrial laser scanning. *Methods in Ecology and Evolution*, *6*(2), 198–208. https://doi.org/10.1111/2041-210X.12301

Calders, K., Origo, N., Burt, A., Disney, M., Nightingale, J., Raumonen, P., Åkerblom, M., Malhi, Y., & Lewis, P. (2018). Realistic Forest Stand Reconstruction from Terrestrial LiDAR for Radiative Transfer Modelling. *Remote Sensing*, *10*(6), 933. https://doi.org/10.3390/rs10060933

Calitz, W., Potts, A. J., & Cowling, R. M. (2015). Investigating species-level flammability across five biomes in the Eastern Cape, South Africa. *Biome Boundaries in South Africa*, *101*, 32–39. https://doi.org/10.1016/j.sajb.2015.07.005

Campbell, M. J., Dennison, P. E., Hudak, A. T., Parham, L. M., & Butler, B. W. (2018). Quantifying understory vegetation density using small-footprint airborne lidar. *Remote Sensing of Environment*, *215*, 330–342. https://doi.org/10.1016/j.rse.2018.06.023

Castro, F. X., Tudela, A., & Sebastià, M. T. (2003). Modeling moisture content in shrubs to predict fire risk in Catalonia (Spain). *Agricultural and Forest Meteorology*, *116*(1), 49–59. https://doi.org/10.1016/S0168-1923(02)00248-4

Chiodi, A. M., Larkin, N. K., Varner, J. M., Hiers, J. K., Chiodi, A. M., Larkin, N. K., Varner, J. M., & Hiers, J. K. (2019). Sensitivity of prescribed burn weather windows to atmospheric dispersion parameters over southeastern USA. *International Journal of Wildland Fire*, *28*(8), 589–600. https://doi.org/10.1071/WF18209

Clark, M. L., Clark, D. B., & Roberts, D. A. (2004). Small-footprint lidar estimation of sub-canopy elevation and tree height in a tropical rain forest landscape. *Remote Sensing of Environment*, *91*(1), 68–89.

Clawges, R., Vierling, K., Vierling, L., & Rowell, E. (2008). The use of airborne lidar to assess avian species diversity, density, and occurrence in a pine/aspen forest. *Remote Sensing of Environment*, *112*(5), 2064–2073. https://doi.org/10.1016/j.rse.2007.08.023

Contreras, M. A., Staats, W., Yiang, J., & Parrott, D. (2017). Quantifying the Accuracy of LiDAR-Derived DEM in Deciduous Eastern Forests of the Cumberland Plateau. *Journal of Geographic Information System*, *9*(3), Article 3. https://doi.org/10.4236/jgis.2017.93021

Coops, N. C., Tompalski, P., Goodbody, T. R., Queinnec, M., Luther, J. E., Bolton, D. K., White, J. C., Wulder, M. A., van Lier, O. R., & Hermosilla, T. (2021). Modelling lidar-derived estimates of forest attributes over space and time: A review of approaches and future trends. *Remote Sensing of Environment*, *260*, 112477.

Demol, M., Wilkes, P., Raumonen, P., Krishna Moorthy, S., Calders, K., Gielen, B., & Verbeeck, H. (2022). Volumetric overestimation of small branches in 3D reconstructions of *Fraxinus excelsior*. *Silva Fennica*, *56*(1). https://doi.org/10.14214/sf.10550

Dent, J. M., Buckley, H. L., Lustig, A., & Curran, T. J. (2019). Flame Temperatures Saturate with Increasing Dead Material in Ulex europaeus, but Flame Duration, Fuel Consumption and Overall Flammability Continue to Increase. *Fire*, *2*(1), 6.

Disney, M. (2019). Terrestrial LiDAR: A three-dimensional revolution in how we look at trees. *New Phytologist*, *222*(4), 1736–1741. https://doi.org/10.1111/nph.15517

Disney, M. I., Boni Vicari, M., Burt, A., Calders, K., Lewis, S. L., Raumonen, P., & Wilkes, P. (2018). Weighing trees with lasers: Advances, challenges and opportunities. *Interface Focus*, *8*(2). https://doi.org/10.1098/rsfs.2017.0048

Disney, M. I., Kalogirou, V., Lewis, P., Prieto-Blanco, A., Hancock, S., & Pfeifer, M. (2010). Simulating the impact of discrete-return lidar system and survey characteristics over young conifer and broadleaf forests. *Remote Sensing of Environment*, *114*(7), 1546–1560. https://doi.org/10.1016/j.rse.2010.02.009

Disney, M., Lewis, P., & North, P. (2000). Monte Carlo ray tracing in optical canopy reflectance modelling. *Remote Sensing Reviews*, *18*(2–4), 163–196.

Du, S., Lindenbergh, R., Ledoux, H., Stoter, J., & Nan, L. (2019). AdTree: Accurate, Detailed, and Automatic Modelling of Laser-Scanned Trees. *Remote Sensing*, *11*(18). https://doi.org/10.3390/rs11182074

Duda, R. O., & Hart, P. E. (2006). *Pattern classification*. John Wiley & Sons.

Engber, E. A., & Varner, J. M. (2012). Patterns of flammability of the California oaks: The role of leaf traits. *Canadian Journal of Forest Research*, *42*(11), 1965–1975. https://doi.org/10.1139/x2012-138

Estornell, J., Ruiz, L. A., Velázquez-Martí, B., & Hermosilla, T. (2011). Analysis of the factors affecting LiDAR DTM accuracy in a steep shrub area. *International Journal of Digital Earth*, *4*(6), 521–538. https://doi.org/10.1080/17538947.2010.533201

Fan, G., Nan, L., Chen, F., Dong, Y., Wang, Z., Li, H., & Chen, D. (2020). A New Quantitative Approach to Tree Attributes Estimation Based on LiDAR Point Clouds. *Remote Sensing*, *12*(11), Article 11. https://doi.org/10.3390/rs12111779

FARO® Knowledge Base. (2021, January 20). *Laser Scanner Best Practices*. FARO® Knowledge Base. https://knowledge.faro.com/Hardware/3D_Scanners/Focus/Laser_Scanner_Best_Practices

Fassnacht, F. E., Latifi, H., & Hartig, F. (2018). Using synthetic data to evaluate the benefits of large field plots for forest biomass estimation with LiDAR. *Remote Sensing of Environment*, *213*, 115–128. https://doi.org/10.1016/j.rse.2018.05.007

Fei, S., & Yang, P. (2011). *Forest composition change in the eastern United States*.

Fletcher, T. (2009). Support vector machines explained. *Tutorial Paper*, 1–19.

Frazer, G. W., Magnussen, S., Wulder, M. A., & Niemann, K. O. (2011). Simulated impact of sample plot size and co-registration error on the accuracy and uncertainty of LiDAR-derived estimates of forest stand biomass. *Remote Sensing of Environment*, *115*(2), 636–649. https://doi.org/10.1016/j.rse.2010.10.008

(FWC) Florida Fish and Wildlife Conservation Commission. (2016). *A Management Plan for Aucilla Wildlife Management Area 2016—2026* [Management Plan]. http://floridanaturecoast.org/Img.aspx?url=/ManagementPlans/AucillaWMAManagementPlan.pdf

Gale, M. G., Cary, G. J., Van Dijk, A. I. J. M., & Yebra, M. (2021). Forest fire fuel through the lens of remote sensing: Review of approaches, challenges and future directions in the remote sensing of biotic determinants of fire behaviour. *Remote Sensing of Environment*, *255*, 112282. https://doi.org/10.1016/j.rse.2020.112282

Ganteaume, A., Jappiot, M., Curt, T., Lampin, C., & Borgniet, L. (2014). Flammability of litter sampled according to two different methods: Comparison of results in laboratory experiments. *International Journal of Wildland Fire*, *23*(8), 1061–1075. https://doi.org/10.1071/WF13045

Gao, T., Gao, Z., Sun, B., Qin, P., Li, Y., & Yan, Z. (2022). An Integrated Method for Estimating Forest-Canopy Closure Based on UAV LiDAR Data. *Remote Sensing*, *14*(17), 4317.

García, M., Saatchi, S., Casas, A., Koltunov, A., Ustin, S. L., Ramirez, C., & Balzter, H. (2017). Extrapolating Forest Canopy Fuel Properties in the California Rim Fire by Combining Airborne LiDAR and Landsat OLI Data. *Remote Sensing*, *9*(4), 394. https://doi.org/10.3390/rs9040394

Geron, C., & Hays, M. (2013). Air emissions from organic soil burning on the coastal plain of North Carolina. *Atmospheric Environment*, *64*, 192–199.

Girardeau-Montaut, D. (2016). CloudCompare. *France: EDF R&D Telecom ParisTech*, *11*.

Gonsalves, M. O. (2010). *A comprehensive uncertainty analysis and method of geometric calibration for a circular scanning airborne lidar*. The University of Southern Mississippi.

Gonzalez, P., Asner, G. P., Battles, J. J., Lefsky, M. A., Waring, K. M., & Palace, M. (2010). Forest carbon densities and uncertainties from Lidar, QuickBird, and field measurements in California. *Remote Sensing of Environment*, *114*(7), 1561–1575.

Goodwin, N., Coops, N., & Culvenor, D. (2007). Development of a simulation model to predict LiDAR interception in forested environments. *Remote Sensing of Environment*, *111*(4), 481–492.

Grootemaat, S., Wright, I. J., van Bodegom, P. M., Cornelissen, J. H. C., & Cornwell, W. K. (2015). Burn or rot: Leaf traits explain why flammability and decomposability are decoupled across species. *Functional Ecology*, *29*(11), 1486–1497. https://doi.org/10.1111/1365-2435.12449

Gusmão, G. F., Barbosa, C. R. H., Raposo, A. B., & de Oliveira, R. C. (2021). A LiDAR System Simulator Using Parallel Raytracing and Validated by Comparison with a Real Sensor. *Journal of Physics: Conference Series*, *1826*(1), 012002. https://doi.org/10.1088/1742-6596/1826/1/012002

Hackenberg, J., Wassenberg, M., Spiecker, H., & Sun, D. (2015). Non Destructive Method for Biomass Prediction Combining TLS Derived Tree Volume and Wood Density. *Forests*, *6*(4), Article 4. https://doi.org/10.3390/f6041274

Halpern, C. B., & Antos, J. A. (2022). Burn severity and pre-fire seral state interact to shape vegetation responses to fire in a young, western Cascade Range forest. *Forest Ecology and Management*, *507*, 120028.

Hamilton, D., Pacheco, R., Myers, B., & Peltzer, B. (2020). kNN vs. SVM: A comparison of algorithms. *In: Hood, Sharon M.; Drury, Stacy; Steelman, Toddi; Steffens, Ron, [Eds.]. Proceedings of the Fire Continuum-Preparing for the Future of Wildland Fire; 2018 May 21-24; Missoula, MT. Proceedings RMRS-P-78. Fort Collins, CO: U.S. Department of Agriculture, Forest Service, Rocky Mountain Research Station. p. 95-109.*, *78*, 95–109.

Harris, M. S., & Pannell, J. R. (2010). Canopy seed storage is associated with sexual dimorphism in the woody dioecious genus Leucadendron. *Journal of Ecology*, *98*(2), 509–515. https://doi.org/10.1111/j.1365-2745.2009.01623.x

Hartley, F. M., Maxwell, A. E., Landenberger, R. E., & Bortolot, Z. J. (2022). Forest Type Differentiation Using GLAD Phenology Metrics, Land Surface Parameters, and Machine Learning. *Geographies*, *2*(3), 491–515.

Hernandez-Santin, L., Rudge, M. L., Bartolo, R. E., & Erskine, P. D. (2019). Identifying Species and Monitoring Understorey from UAS-Derived Data: A Literature Review and Future Directions. *Drones*, *3*(1), 9. https://doi.org/10.3390/drones3010009

Hernando, A., Sobrini, I., Velázquez, J., & García-Abril, A. (2022). The importance of protected habitats and LiDAR data availability for assessing scenarios of land uses in forest areas. *Land Use Policy*, *112*, 105859. https://doi.org/10.1016/j.landusepol.2021.105859

Hillman, S., Wallace, L., Reinke, K., Hally, B., Jones, S., & Saldias, D. S. (2019). A Method for Validating the Structural Completeness of Understory Vegetation Models Captured with 3D Remote Sensing. *Remote Sensing*, *11*(18), Article 18. https://doi.org/10.3390/rs11182118

Hogenbirk, J., & Sarrazin-Delay, C. (1995). Using fuel characteristics to estimate plant ignitability for fire hazard reduction. In *Boreal Forests and Global Change* (pp. 161–170). Springer.

Hu, T., Sun, Y., Jia, W., Li, D., Zou, M., & Zhang, M. (2021). Study on the Estimation of Forest Volume Based on Multi-Source Data. *Sensors*, *21*(23), Article 23. https://doi.org/10.3390/s21237796

Huang, H., Li, Z., Gong, P., Cheng, X., Clinton, N., Cao, C., Ni, W., & Wang, L. (2011a, March). *Automated Methods for Measuring DBH and Tree Heights with a Commercial Scanning Lidar* [Text]. https://doi.org/info:doi/10.14358/PERS.77.3.219

Huang, H., Li, Z., Gong, P., Cheng, X., Clinton, N., Cao, C., Ni, W., & Wang, L. (2011b). Automated Methods for Measuring DBH and Tree Heights with a Commercial Scanning Lidar. *Photogrammetric Engineering & Remote Sensing*, *77*(3), 219–227. https://doi.org/10.14358/PERS.77.3.219

Hudak, A. T., Crookston, N. L., Evans, J. S., Hall, D. E., & Falkowski, M. J. (2008). Nearest neighbor imputation of species-level, plot-scale forest structure attributes from LiDAR data. *Remote Sensing of Environment*, *112*(5), 2232–2245.

Hyyppä, J., Hyyppä, H., Leckie, D., Gougeon, F., Yu, X., & Maltamo, M. (2008). Review of methods of small-footprint airborne laser scanning for extracting forest inventory data in boreal forests. *International Journal of Remote Sensing*, *29*(5), 1339–1366. https://doi.org/10.1080/01431160701736489

Janoutová, R., Homolová, L., Novotný, J., Navrátilová, B., Pikl, M., & Malenovský, Z. (2021). Detailed reconstruction of trees from terrestrial laser scans for remote sensing and radiative transfer modelling applications. *In Silico Plants*, *3*(2), diab026. https://doi.org/10.1093/insilicoplants/diab026

Jensen, J. R. (2013). *Remote Sensing of the Environment: An Earth Resource Perspective*. Pearson.

Jiang, Y., Li, C., Takeda, F., Kramer, E. A., Ashrafi, H., & Hunter, J. (2019). 3D point cloud data to quantitatively characterize size and shape of shrub crops. *Horticulture Research*, *6*, 43. https://doi.org/10.1038/s41438-019-0123-9

JMP Pro ® statistical software (Version 16). (2021). SAS Institute Inc. https://www.jmp.com/en_us/home.html

Karatzoglou, A., Smola, A., Hornik, K., Karatzoglou, M. A., SparseM, S., & Yes, L. (2007). The kernlab package. *Kernel-Based Machine Learning Lab. R Package Version 0.9.-22. Available Online: Https://Cran. r-Project. Org/Web/Packages/Kernlab (Accessed on 4 November 2015)*.

Krix, D. W., & Murray, B. R. (2018). Landscape variation in plant leaf flammability is driven by leaf traits responding to environmental gradients. *Ecosphere*, *9*(2), e02093. https://doi.org/10.1002/ecs2.2093

Krooks, A., Kaasalainen, S., Kankare, V., Joensuu, M., Raumonen, P., & Kaasalainen, M. (2014). Predicting tree structure from tree height using terrestrial laser scanning and quantitative structure models. *Silva Fenn*, *48*, 1125.

Kuhn, M. (2021). *caret: Classification and Regression Training*. https://CRAN.R-project.org/package=caret

Kuhn, M., & Vaughan, D. (2021). *yardstick: Tidy Characterizations of Model Performance*. https://CRAN.R-project.org/package=yardstick

Kumazaki, R., & Kunii, Y. (2020). Application of 3d Tree Modeling Using Point Cloud Data by Terrestrial Laser Scanner. *The International Archives of Photogrammetry, Remote Sensing and Spatial Information Sciences*, *43*, 995–1000.

Kutnar, L., Nagel, T. A., & Kermavnar, J. (2019). Effects of Disturbance on Understory Vegetation across Slovenian Forest Ecosystems. *Forests*, *10*(11), Article 11. https://doi.org/10.3390/f10111048

Lary, D. J., Alavi, A. H., Gandomi, A. H., & Walker, A. L. (2016). Machine learning in geosciences and remote sensing. *Geoscience Frontiers*, *7*(1), 3–10.

Lau, A., Bentley, L. P., Martius, C., Shenkin, A., Bartholomeus, H., Raumonen, P., Malhi, Y., Jackson, T., & Herold, M. (2018). Quantifying branch architecture of tropical trees using terrestrial LiDAR and 3D modelling. *Trees*, *32*(5), 1219–1231. https://doi.org/10.1007/s00468-018-1704-1

Lear, D. H. V., & Harlow, R. F. (2002). Fire in the eastern United States: Influence on wildlife habitat. *In: Ford, W. Mark; Russell, Kevin R.; Moorman, Christopher E., Eds. Proceedings: The Role of Fire for Nongame Wildlife Management and Community Restoration: Traditional Uses and New Directions. Gen. Tech. Rep. NE-288. Newtown Square, PA: U.S. Dept. of Agriculture, Forest Service, Northeastern Research Station. 2-10.*, *288*. https://www.fs.usda.gov/treesearch/pubs/19090

Lenard, E. (2008). Habits of trees and shrubs in landscape design. *Architecture Civil Engineering Environment*, *4*, 13–20.

Li, L., Chen, J., Mu, X., Li, W., Yan, G., Xie, D., & Zhang, W. (2020). Quantifying Understory and Overstory Vegetation Cover Using UAV-Based RGB Imagery in Forest Plantation. *Remote Sensing*, *12*(2), Article 2. https://doi.org/10.3390/rs12020298

Liang, X., & Hyyppä, J. (2013). Automatic Stem Mapping by Merging Several Terrestrial Laser Scans at the Feature and Decision Levels. *Sensors*, *13*(2), 1614–1634. https://doi.org/10.3390/s130201614

Liao, K., Li, Y., Zou, B., Li, D., & Lu, D. (2022). Examining the Role of UAV Lidar Data in Improving Tree Volume Calculation Accuracy. *Remote Sensing*, *14*(17), Article 17. https://doi.org/10.3390/rs14174410

Lingfors, D., Bright, J. M., Engerer, N. A., Ahlberg, J., Killinger, S., & Widén, J. (2017). Comparing the capability of low- and high-resolution LiDAR data with application to solar resource assessment, roof type classification and shading analysis. *Applied Energy*, *205*, 1216–1230. https://doi.org/10.1016/j.apenergy.2017.08.045

Linn, R., Reisner, J., Colman, J. J., & Winterkamp, J. (2002). Studying wildfire behavior using FIRETEC. *International Journal of Wildland Fire*, *11*(4), 233–246. https://doi.org/10.1071/wf02007

Lio, F. X. S., & Dewi, M. P. S. (2018). Karst vegetation in the natural habitat of sandalwood (Santalum album) at various altitude places in Timor Island, Indonesia. *Biodiversitas Journal of Biological Diversity*, *19*(5), 1703–1713. https://doi.org/10.13057/biodiv/d190516

Loidi Arregui, J. J., & Marcenò, C. (2022). *The Temperate Deciduous Forests of the Northern Hemisphere. A review*.

Long, A. J., Behm, A., Zipperer, W. C., Hermansen, A., Maranghides, A., & Mell, W. (2006). *Quantifying and ranking the flammability of ornamental shrubs in the southern United States*. 13–17.

López-López, S. F., Martínez-Trinidad, T., Benavides-Meza, H., Garcia-Nieto, M., & de los Santos-Posadas, H. M. (2017). Non-destructive method for above-ground biomass estimation of Fraxinus uhdei (Wenz.) Lingelsh in an urban forest. *Urban Forestry & Urban Greening*, *24*, 62–70. https://doi.org/10.1016/j.ufug.2017.03.025

Loudermilk, E. L., Hiers, J. K., O'Brien, J. J., Mitchell, R. J., Singhania, A., Fernandez, J. C., Cropper, W. P., & Slatton, K. C. (2009). Ground-based LIDAR: a novel approach to quantify fine-scale fuelbed characteristics. *International Journal of Wildland Fire*, *18*(6), 676–685.

Loudermilk, E. L., O'Brien, J. J., Goodrick, S. L., Linn, R. R., Skowronski, N. S., & Hiers, J. K. (2022). Vegetation's influence on fire behavior goes beyond just being fuel. *Fire Ecology*, *18*(1), 9. https://doi.org/10.1186/s42408-022-00132-9

Loudermilk, E. L., O'Brien, J. J., Mitchell, R. J., Cropper, W. P., Hiers, J. K., Grunwald, S., Grego, J., Fernandez-Diaz, J. C., Loudermilk, E. L., O'Brien, J. J., Mitchell, R. J., Cropper, W. P., Hiers, J. K., Grunwald, S., Grego, J., & Fernandez-Diaz, J. C. (2012). Linking complex forest fuel structure and fire behaviour at fine scales. *International Journal of Wildland Fire*, *21*(7), 882–893. https://doi.org/10.1071/WF10116

Lovell, J., Jupp, D., Newnham, G., Coops, N., & Culvenor, D. (2005). Simulation study for finding optimal lidar acquisition parameters for forest height retrieval. *Forest Ecology and Management*, *214*(1–3), 398–412.

Magalhães, S. V. G., Franklin, W. R., & Andrade, M. V. A. (2017). Fast exact parallel 3D mesh intersection algorithm using only orientation predicates. *Proceedings of the 25th ACM SIGSPATIAL International Conference on Advances in Geographic Information Systems*, 1–10. https://doi.org/10.1145/3139958.3140001

Malambo, L., Popescu, S. C., Horne, D. W., Pugh, N. A., & Rooney, W. L. (2019). Automated detection and measurement of individual sorghum panicles using density-based clustering of terrestrial lidar data. *ISPRS Journal of Photogrammetry and Remote Sensing*, *149*, 1–13. https://doi.org/10.1016/j.isprsjprs.2018.12.015

Malhi, Y., Jackson, T., Patrick Bentley, L., Lau, A., Shenkin, A., Herold, M., Calders, K., Bartholomeus, H., & Disney, M. I. (2018). New perspectives on the ecology of tree structure and tree communities through terrestrial laser scanning. *Interface Focus*, *8*(2). https://doi.org/10.1098/rsfs.2017.0052

Martin-Ducup, O., Ploton, P., Barbier, N., Momo Takoudjou, S., Mofack II, G., Kamdem, N. G., Fourcaud, T., Sonké, B., Couteron, P., & Pélissier, R. (2020). Terrestrial laser scanning reveals convergence of tree architecture with increasingly dominant crown canopy position. *Functional Ecology*, *34*(12), 2442–2452. https://doi.org/10.1111/1365-2435.13678

MATLAB. (2018). *MATLAB 9.7.0.1190202 (R2019b)*. The MathWorks Inc.

Maxwell, A. E., Warner, T. A., & Fang, F. (2018). Implementation of machine-learning classification in remote sensing: An applied review. *International Journal of Remote Sensing*, *39*(9), 2784–2817.

Mayamanikandan, T., Reddy, R. S., & Jha, C. (2019). *Non-destructive tree volume estimation using terrestrial lidar data in teak dominated Central Indian forests*. 100–103.

Melvin, M. (2021). *2020 National Prescribed Fire Use Report*. Coalition of Prescribed Fire Councils, Inc.

Meng, R., Wu, J., Zhao, F., Cook, B. D., Hanavan, R. P., & Serbin, S. P. (2018). Measuring short-term post-fire forest recovery across a burn severity gradient in a mixed pine-oak forest using multi-sensor remote sensing techniques. *Remote Sensing of Environment*, *210*, 282–296. https://doi.org/10.1016/j.rse.2018.03.019

Miller, S. R., & Corby, M. K. (2022). Fire in pines of the Southeastern US. *Global Application of Prescribed Fire*, 95.

Mohammadi, M., Rashidi, M., Mousavi, V., Karami, A., Yu, Y., & Samali, B. (2021). Quality Evaluation of Digital Twins Generated Based on UAV Photogrammetry and TLS: Bridge Case Study. *Remote Sensing*, *13*(17), Article 17. https://doi.org/10.3390/rs13173499

Moore, P. T. M. T., Miegroet, H. V. M. V., & Nicholas, N. S. N. S. (2008). Relative role of understory and overstory in carbon and nitrogen cycling in a southern Appalachian spruce–fir forestAES

Publication 7863. Utah Agricultural Experiment Station, Utah State University, Logan, Utah. *Canadian Journal of Forest Research*. https://doi.org/10.1139/X07-115

Moorthy, I., Miller, J. R., Berni, J. A. J., Zarco-Tejada, P., Hu, B., & Chen, J. (2011). Field characterization of olive (Olea europaea L.) tree crown architecture using terrestrial laser scanning data. *Agricultural and Forest Meteorology*, *151*(2), 204–214. https://doi.org/10.1016/j.agrformet.2010.10.005

Morandini, F., Santoni, P. A., Tramoni, J. B., & Mell, W. E. (2019). Experimental investigation of flammability and numerical study of combustion of shrub of rockrose under severe drought conditions. *Fire Safety Journal*, *108*, 102836. https://doi.org/10.1016/j.firesaf.2019.102836

Morsdorf, F., Mårell, A., Koetz, B., Cassagne, N., Pimont, F., Rigolot, E., & Allgöwer, B. (2010). Discrimination of vegetation strata in a multi-layered Mediterranean forest ecosystem using height and intensity information derived from airborne laser scanning. *Remote Sensing of Environment*, *114*(7), 1403–1415. https://doi.org/10.1016/j.rse.2010.01.023

Moskal, L. M., & Zheng, G. (2012). Retrieving Forest Inventory Variables with Terrestrial Laser Scanning (TLS) in Urban Heterogeneous Forest. *Remote Sensing*, *4*(1), Article 1. https://doi.org/10.3390/rs4010001

Mutanga, O., Adam, E., & Cho, M. A. (2012). High density biomass estimation for wetland vegetation using WorldView-2 imagery and random forest regression algorithm. *International Journal of Applied Earth Observation and Geoinformation*, *18*, 399–406. https://doi.org/10.1016/j.jag.2012.03.012

Noss, R. F. (2018). *Fire Ecology of Florida and the Southeastern Coastal Plain*. University Press of Florida. http://ebookcentral.proquest.com/lib/wvu/detail.action?docID=5394340

Olah, M., Bologa, C., & Oprea, T. I. (2004). An automated PLS search for biologically relevant QSAR descriptors. *Journal of Computer-Aided Molecular Design*, *18*(7), 437–449. https://doi.org/10.1007/s10822-004-4060-8

Olson, D. M., & Dinerstein, E. (2002). The Global 200: Priority ecoregions for global conservation. *Annals of the Missouri Botanical Garden*, 199–224.

Orozco-Aguilar, L., Livesley, S. J., Brack, C., & Johnstone, D. (2019). Standing volume yield, canopy structure and allometric relationships of dominant urban trees in Melbourne, Australia. *Urban Forestry & Urban Greening*, *43*, 126363. https://doi.org/10.1016/j.ufug.2019.06.006

Parker, G. G., Harding, D. J., & Berger, M. L. (2004). A portable LIDAR system for rapid determination of forest canopy structure. *Journal of Applied Ecology*, *41*(4), 755–767. https://doi.org/10.1111/j.0021-8901.2004.00925.x

Parkins, K., Cawson, J., Pickering, B., & Penman, T. (2023). Mitigation Strategies for Wildfires. In *Handbook of Fire and the Environment* (pp. 395–420). Springer.

Parsons, R. A., Linn, R. R., Pimont, F., Hoffman, C., Sauer, J., Winterkamp, J., Sieg, C. H., & Jolly, W. M. (2017). Numerical Investigation of Aggregated Fuel Spatial Pattern Impacts on Fire Behavior. *Land*, *6*(2), Article 2. https://doi.org/10.3390/land6020043

Pausas, J. G., & Bond, W. J. (2020). On the three major recycling pathways in terrestrial ecosystems. *Trends in Ecology & Evolution*, *35*(9), 767–775.

Pausas, J. G., & Moreira, B. (2012). Flammability as a biological concept. *New Phytologist*, *194*(3), 610–613. https://doi.org/10.1111/j.1469-8137.2012.04132.x

Paynter, I., Genest, D., Saenz, E., Peri, F., Li, Z., Strahler, A., & Schaaf, C. (2018). Quality Assessment of Terrestrial Laser Scanner Ecosystem Observations Using Pulse Trajectories. *IEEE Transactions on Geoscience and Remote Sensing*, *56*(11), 6324–6333. https://doi.org/10.1109/TGRS.2018.2836947

Peet, R. K., Platt, W. J., & Costanza, J. K. (2018). Fire-Maintained Pine Savannas and Woodlands of the Southeastern United States Coastal Plain. In A. M. Barton & W. S. Keeton (Eds.), *Ecology and Recovery of Eastern Old-Growth Forests* (pp. 39–62). Island Press/Center for Resource Economics. https://doi.org/10.5822/978-1-61091-891-6_3

Pérez-Harguindeguy, N., Díaz, S., Garnier, E., Lavorel, S., Poorter, H., Jaureguiberry, P., Bret-Harte, M. S., Cornwell, W. K., Craine, J. M., Gurvich, D. E., Urcelay, C., Veneklaas, E. J., Reich, P. B., Poorter, L., Wright, I. J., Ray, P., Enrico, L., Pausas, J. G., de Vos, A. C., … Cornelissen, J. H. C. (2013). New handbook for standardised measurement of plant functional traits worldwide. *Australian Journal of Botany*, *61*(3), 167. https://doi.org/10.1071/BT12225

Pertille, R. H., Citadin, I., Oliveira, L. de S. de, Broch, J. de C., Kvitschal, M. V., & Araujo, L. (2022). The influence of temperature on the phenology of apple trees grown in mild winter regions of Brazil, based on long-term records. *Scientia Horticulturae*, *305*, 111354. https://doi.org/10.1016/j.scienta.2022.111354

Poirier-Quinot, D., Noisternig, M., & Katz, B. F. (2017). *EVERTims: Open source framework for real-time auralization in VR*. 1–5.

Pokswinski, S., Gallagher, M. R., Skowronski, N. S., Loudermilk, E. L., Hawley, C., Wallace, D., Everland, A., Wallace, J., & Hiers, J. K. (2021). A simplified and affordable approach to forest monitoring using single terrestrial laser scans and transect sampling. *MethodsX*, *8*, 101484. https://doi.org/10.1016/j.mex.2021.101484

Potts, E., Tng, D., Apgaua, D., Curran, T. J., Engert, J., & Laurance, S. G. (2022). Growth form and functional traits influence the shoot flammability of tropical rainforest species. *Forest Ecology and Management*, *522*, 120485.

Primer, A. (2016). *Wildfires in the United States*.

R Core Team. (2020). *R: A Language and Environment for Statistical Computing*. R Foundation for Statistical Computing. https://www.R-project.org/

Raumonen, P. (2020). *InverseTampere/TreeQSM Manual* (2.4.0) [MATLAB]. https://github.com/InverseTampere/TreeQSM

Raumonen, P., Kaasalainen, M., Åkerblom, M., Kaasalainen, S., Kaartinen, H., Vastaranta, M., Holopainen, M., Disney, M., & Lewis, P. (2013). Fast Automatic Precision Tree Models from Terrestrial Laser Scanner Data. *Remote Sensing*, *5*(2), 491–520. https://doi.org/10.3390/rs5020491

Reich, K. F., Kunz, M., & von Oheimb, G. (2021). A new index of forest structural heterogeneity using tree architectural attributes measured by terrestrial laser scanning. *Ecological Indicators*, *133*, 108412. https://doi.org/10.1016/j.ecolind.2021.108412

Reitmann, S., Neumann, L., & Jung, B. (2021). BLAINDER—a blender AI add-on for generation of semantically labeled depth-sensing data. *Sensors*, *21*(6), 2144.

Riley, K., & Thompson, M. (2016). An Uncertainty Analysis of Wildfire Modeling. In K. Riley, P. Webley, & M. Thompson (Eds.), *Geophysical Monograph Series* (pp. 191–213). John Wiley & Sons, Inc. http://doi.wiley.com/10.1002/9781119028116.ch13

Roddy, A. B., van Blerk, J. J., Midgley, J. J., & West, A. G. (2019). Ramification has little impact on shoot hydraulic efficiency in the sexually dimorphic genus Leucadendron (Proteaceae). *PeerJ*, *7*, e6835. https://doi.org/10.7717/peerj.6835

Roussel, J.-R., attributes), F. D. B. (Enable the support of lax file and extra byte, libraries), M. I. (Is the author of the Las. and Las., documentation), D. A. (Reviewed the, R), P. M. (Helped to compile Las. code in, & method), T. de C. (Implemented the-thin_with_voxel filter. (2022). *rlas: Read and Write 'las' and 'laz' Binary File Formats Used for Remote Sensing Data* (1.6.1). https://CRAN.R-project.org/package=rlas

Roussel, J.-R., & Auty, D. (2021). *Airborne LiDAR Data Manipulation and Visualization for Forestry Applications. R package version 3.1. 2*.

Roussel, J.-R., Auty, D., Coops, N. C., Tompalski, P., Goodbody, T. R., Meador, A. S., Bourdon, J.-F., De Boissieu, F., & Achim, A. (2020). LidR: An R package for analysis of Airborne Laser Scanning (ALS) data. *Remote Sensing of Environment*, *251*, 112061.

Rowell, E., Loudermilk, E. L., Hawley, C., Pokswinski, S., Seielstad, C., Queen, Ll., O'Brien, J. J., Hudak, A. T., Goodrick, S., & Hiers, J. K. (2020a). Coupling terrestrial laser scanning with 3D fuel biomass sampling for advancing wildland fuels characterization. *Forest Ecology and Management*, *462*, 117945. https://doi.org/10.1016/j.foreco.2020.117945

Rowell, E., Loudermilk, E. L., Hawley, C., Pokswinski, S., Seielstad, C., Queen, Ll., O'Brien, J. J., Hudak, A. T., Goodrick, S., & Hiers, J. K. (2020b). Coupling terrestrial laser scanning with 3D fuel biomass sampling for advancing wildland fuels characterization. *Forest Ecology and Management*, *462*, 117945. https://doi.org/10.1016/j.foreco.2020.117945

Rowell, E., Loudermilk, E. L., Seielstad, C., & O'Brien, J. J. (2016). Using Simulated 3D Surface Fuelbeds and Terrestrial Laser Scan Data to Develop Inputs to Fire Behavior Models. *Canadian Journal of Remote Sensing*, *42*(5), 443–459. https://doi.org/10.1080/07038992.2016.1220827

Rowell, E. M., Seielstad, C. A., & Ottmar, R. D. (2016). Development and validation of fuel height models for terrestrial lidar – RxCADRE 2012. *International Journal of Wildland Fire*, *25*(1), 38. https://doi.org/10.1071/WF14170

Rowell, E. M., Seielstad, C. A., Ottmar, R. D., Rowell, E. M., Seielstad, C. A., & Ottmar, R. D. (2015). Development and validation of fuel height models for terrestrial lidar – RxCADRE 2012. *International Journal of Wildland Fire*, *25*(1), 38–47. https://doi.org/10.1071/WF14170

Saarinen, N., Kankare, V., Vastaranta, M., Luoma, V., Pyörälä, J., Tanhuanpää, T., Liang, X., Kaartinen, H., Kukko, A., Jaakkola, A., Yu, X., Holopainen, M., & Hyyppä, J. (2017). Feasibility of Terrestrial laser scanning for collecting stem volume information from single trees. *ISPRS Journal of Photogrammetry and Remote Sensing*, *123*, 140–158. https://doi.org/10.1016/j.isprsjprs.2016.11.012

Santacruz-García, A. C., Bravo, S., Corro, F. del, & Ojeda, F. (2019). A comparative assessment of plant flammability through a functional approach: The case of woody species from Argentine Chaco region. *Austral Ecology*, *44*(8), 1416–1429. https://doi.org/10.1111/aec.12815

Schwilk, D. W. (2003). Flammability Is a Niche Construction Trait: Canopy Architecture Affects Fire Intensity. *The American Naturalist*, *162*(6), 725–733. https://doi.org/10.1086/379351

Scratchpixel. (2022). *An Overview of the Ray-Tracing Rendering Technique*. https://www.scratchapixel.com/lessons/3d-basic-rendering/ray-tracing-overview/ray-tracing-rendering-technique-overview

Shi, Y., Skidmore, A. K., Wang, T., Holzwarth, S., Heiden, U., Pinnel, N., Zhu, X., & Heurich, M. (2018). Tree species classification using plant functional traits from LiDAR and hyperspectral data. *International Journal of Applied Earth Observation and Geoinformation*, *73*, 207–219. https://doi.org/10.1016/j.jag.2018.06.018

Silva, A. G. P., Görgens, E. B., Campoe, O. C., Alvares, C. A., Stape, J. L., & Rodriguez, L. C. E. (2015). Assessing biomass based on canopy height profiles using airborne laser scanning data in eucalypt plantations. *Scientia Agricola*, *72*, 504–512. https://doi.org/10.1590/0103-9016-2015-0070

Singhal, S., Roddy, A. B., DiVittorio, C., Sanchez-Amaya, A., Henriquez, C. L., Brodersen, C. R., Fehlberg, S., & Zapata, F. (2021). Diversification, disparification and hybridization in the desert shrubs Encelia. *New Phytologist*, *230*(3), 1228–1241. https://doi.org/10.1111/nph.17212

Skowronski, N., Clark, K., Nelson, R., Hom, J., & Patterson, M. (2007). Remotely sensed measurements of forest structure and fuel loads in the Pinelands of New Jersey. *Remote Sensing of Environment*, *108*(2), 123–129. https://doi.org/10.1016/j.rse.2006.09.032

Skowronski, N. S., Clark, K. L., Duveneck, M., & Hom, J. (2011a). Three-dimensional canopy fuel loading predicted using upward and downward sensing LiDAR systems. *Remote Sensing of Environment*, *115*(2), 703–714. https://doi.org/10.1016/j.rse.2010.10.012

Skowronski, N. S., Clark, K. L., Duveneck, M., & Hom, J. (2011b). Three-dimensional canopy fuel loading predicted using upward and downward sensing LiDAR systems. *Remote Sensing of Environment*, *115*(2), 703–714. https://doi.org/10.1016/j.rse.2010.10.012

Skowronski, N. S., Gallagher, M. R., & Warner, T. A. (2020). Decomposing the interactions between fire severity and canopy fuel structure using multi-temporal, active, and passive remote sensing approaches. *Fire*, *3*(1), 7.

Srinivasan, S., Popescu, S. C., Eriksson, M., Sheridan, R. D., & Ku, N.-W. (2015). Terrestrial Laser Scanning as an Effective Tool to Retrieve Tree Level Height, Crown Width, and Stem Diameter. *Remote Sensing*, *7*(2), 1877–1896. https://doi.org/10.3390/rs70201877

Su, W., Zhu, D., Huang, J., & Guo, H. (2018). Estimation of the vertical leaf area profile of corn (Zea mays) plants using terrestrial laser scanning (TLS). *Computers and Electronics in Agriculture*, *150*, 5–13. https://doi.org/10.1016/j.compag.2018.03.037

Su, X., Wang, M., Huang, Z., Fu, S., & Chen, H. Y. (2019). Forest Understorey Vegetation: Colonization and the Availability and Heterogeneity of Resources. *Forests*, *10*(11), 944.

Sun, G., & Ranson, K. J. (2000). Modeling lidar returns from forest canopies. *IEEE Transactions on Geoscience and Remote Sensing*, *38*(6), 2617–2626. https://doi.org/10.1109/36.885208

Tachajapong, W., Lozano, J., Mahalingam, S., Zhou, X., & Weise, D. R. (2008). An investigation of crown fuel bulk density effects on the dynamics of crown fire initiation in shrublands. *Combustion Science and Technology*, *180*(4), 593–615.

Tao, S., Labrière, N., Calders, K., Fischer, F. J., Rau, E.-P., Plaisance, L., & Chave, J. (2021). Mapping tropical forest trees across large areas with lightweight cost-effective terrestrial laser scanning. *Annals of Forest Science*, *78*(4), 103. https://doi.org/10.1007/s13595-021-01113-9

Team, R. C. (2013). R Core Team: A language and environment for statistical computing R Foundation for Statistical Computing. *Vienna, Austria*.

Tomșa, V. R., Curtu, A. L., & Niță, M. D. (2021). Tree Shape Variability in a Mixed Oak Forest Using Terrestrial Laser Technology: Implications for Mating System Analysis. *Forests*, *12*(2), Article 2. https://doi.org/10.3390/f12020253

Torresan, C., Chiavetta, U., & Hackenberg, J. (2018). Applying quantitative structure models to plot-based terrestrial laser data to assess dendrometric parameters in dense mixed forests. *Forest Systems*, *27*(1), 004. https://doi.org/10.5424/fs/2018271-12658

Tumino, B. J., Duff, T. J., Goodger, J. Q., & Cawson, J. G. (2019). Plant traits linked to field-scale flammability metrics in prescribed burns in Eucalyptus forest. *PloS One*, *14*(8). https://doi.org/10.1371/journal.pone.0221403

U.S. National Park Service. (n.d.). *Eastern Deciduous Forest* [NPS.gov]. National Capital Inventory and Monitoring Network. Retrieved 29 October 2022, from https://www.nps.gov/im/ncrn/eastern-deciduous-forest.htm

Vagizov, M., Istomin, E., Miheev, V., & Potapov, A. (2021). Visual Digital Forest Model Based on a Remote Sensing Data and Forest Inventory Data. *Remote Sensing*, *13*(20), 4092.

van der Walt, L. (2021, May 12). *What are Meshes in 3D Modeling?* Webdesignvirtual.Com. http://wedesignvirtual.com/what-are-meshes-in-3d-modeling/

Vandendaele, B., Martin-Ducup, O., Fournier, R. A., & Pelletier, G. (n.d.). Mobile and terrestrial laser scanning for tree volume estimation in temperate hardwood forests.

Varner, J. M., Kane, J. M., Kreye, J. K., & Engber, E. (2015). The Flammability of Forest and Woodland Litter: A Synthesis. *Current Forestry Reports*, *1*(2), 91–99. https://doi.org/10.1007/s40725-015-0012-x

Vicari, M. B., Disney, M., Wilkes, P., Burt, A., Calders, K., & Woodgate, W. (2019). Leaf and wood classification framework for terrestrial LiDAR point clouds. *Methods in Ecology and Evolution*, *10*(5), 680–694. https://doi.org/10.1111/2041-210X.13144

Wagers, S., Castilla, G., Filiatrault, M., & Sanchez-Azofeifa, G. A. (2021). Using TLS-Measured Tree Attributes to Estimate Aboveground Biomass in Small Black Spruce Trees. *Forests*, *12*(11), Article 11. https://doi.org/10.3390/f12111521

Walter, J. A., Stovall, A. E. L., & Atkins, J. W. (2021). Vegetation structural complexity and biodiversity in the Great Smoky Mountains. *Ecosphere*, *12*(3), e03390. https://doi.org/10.1002/ecs2.3390

Wang, D., Brunner, J., Ma, Z., Lu, H., Hollaus, M., Pang, Y., & Pfeifer, N. (2018). Separating Tree Photosynthetic and Non-Photosynthetic Components from Point Cloud Data Using Dynamic Segment Merging. *Forests*, *9*(5), Article 5. https://doi.org/10.3390/f9050252

Wang, D., Momo Takoudjou, S., & Casella, E. (2020). LeWoS: A universal leaf-wood classification method to facilitate the 3D modelling of large tropical trees using terrestrial LiDAR. *Methods in Ecology and Evolution*, *11*(3), 376–389. https://doi.org/10.1111/2041-210X.13342

Wang, L., Birt, A. G., Lafon, C. W., Cairns, D. M., Coulson, R. N., Tchakerian, M. D., Xi, W., Popescu, S. C., & Guldin, J. M. (2013). Computer-based synthetic data to assess the tree delineation algorithm from airborne LiDAR survey. *GeoInformatica*, *17*(1), 35–61. https://doi.org/10.1007/s10707-011-0148-1

Wang, L., Zhou, X., Zhu, X., Dong, Z., & Guo, W. (2016). Estimation of biomass in wheat using random forest regression algorithm and remote sensing data. *The Crop Journal*, *4*(3), 212–219. https://doi.org/10.1016/j.cj.2016.01.008

Warner, T. A., Skowronski, N. S., & La Puma, I. (2020). The influence of prescribed burning and wildfire on lidar-estimated forest structure of the New Jersey Pinelands National Reserve. *International Journal of Wildland Fire*, *29*(12), 1100. https://doi.org/10.1071/WF20037

Waser, L. T., Fischer, C., Wang, Z., & Ginzler, C. (2015). Wall-to-Wall Forest Mapping Based on Digital Surface Models from Image-Based Point Clouds and a NFI Forest Definition. *Forests*, *6*(12), Article 12. https://doi.org/10.3390/f6124386

Watt, P. J., & Donoghue, D. N. M. (2005). Measuring forest structure with terrestrial laser scanning. *International Journal of Remote Sensing*, *26*(7), 1437–1446. https://doi.org/10.1080/01431160512331337961

Weiser, F., Sauer, A., Gettueva, D., Field, R., Irl, S. D. H., Vetaas, O., Chiarucci, A., Hoffmann, S., Fernández-Palacios, J. M., Otto, R., Jentsch, A., Provenzale, A., & Beierkuhnlein, C. (2021).

Impacts of Forest Fire on Understory Species Diversity in Canary Pine Ecosystems on the Island of La Palma. *Forests*, *12*(12), Article 12. https://doi.org/10.3390/f12121638

Westfall, J. A., & Woodall, C. W. (2007). Measurement repeatability of a large-scale inventory of forest fuels. *Forest Ecology and Management*, *253*(1), 171–176. https://doi.org/10.1016/j.foreco.2007.07.014

White, J. C., Coops, N. C., Wulder, M. A., Vastaranta, M., Hilker, T., & Tompalski, P. (2016). Remote Sensing Technologies for Enhancing Forest Inventories: A Review. *Canadian Journal of Remote Sensing*, *42*(5), 619–641. https://doi.org/10.1080/07038992.2016.1207484

White, R. H., & Zipperer, W. C. (2010). Testing and classification of individual plants for fire behaviour: Plant selection for the wildland–urban interface. *International Journal of Wildland Fire*, *19*(2), 213–227.

Wilkes, P., Lau, A., Disney, M., Calders, K., Burt, A., Gonzalez de Tanago, J., Bartholomeus, H., Brede, B., & Herold, M. (2017). Data acquisition considerations for Terrestrial Laser Scanning of forest plots. *Remote Sensing of Environment*, *196*, 140–153. https://doi.org/10.1016/j.rse.2017.04.030

Wilkes, P., Shenkin, A., Disney, M., Malhi, Y., Bentley, L. P., & Vicari, M. B. (2021). Terrestrial laser scanning to reconstruct branch architecture from harvested branches. *Methods in Ecology and Evolution*, *12*(12), 2487–2500. https://doi.org/10.1111/2041-210X.13709

Wilson, N., Bradstock, R., & Bedward, M. (2022). Influence of fuel structure derived from terrestrial laser scanning (TLS) on wildfire severity in logged forests. *Journal of Environmental Management*, *302*, 114011. https://doi.org/10.1016/j.jenvman.2021.114011

Wright, M. N., & Ziegler, A. (2017). ranger: A Fast Implementation of Random Forests for High Dimensional Data in C++ and R. *Journal of Statistical Software*, *77*(1), 1–17. https://doi.org/10.18637/jss.v077.i01

Wu, B., Zheng, G., Chen, Y., & Yu, D. (2021). Assessing inclination angles of tree branches from terrestrial laser scan data using a skeleton extraction method. *International Journal of Applied Earth Observation and Geoinformation*, *104*, 102589. https://doi.org/10.1016/j.jag.2021.102589

Wyse, S. V., O'Connell, D. M., Holland, P. S., Wright, M. J., Hosted, C. L., Whitelock, S. L., Geary, I. J., Maurin, K. J. L., & Curran, T. J. (2016). A quantitative assessment of shoot flammability for 60 tree and shrub species supports rankings based on expert opinion. *International Journal of Wildland Fire*, *25*(4), 466. https://doi.org/10.1071/WF15047

Xu, D., Wang, H., Xu, W., Luan, Z., & Xu, X. (2021). *LiDAR applications to estimate forest biomass at individual tree scale: Opportunities, challenges and future perspectives. Forests. 2021; 12 (5): 1-19*.

Yan, Z., Liu, R., Cheng, L., Zhou, X., Ruan, X., & Xiao, Y. (2019). A concave hull methodology for calculating the crown volume of individual trees based on vehicle-borne LiDAR data. *Remote Sensing*, *11*(6), 623.

Yang, S., Shi, Z., Sun, Y., Wang, X., Yang, W., Gao, J., & Wang, X. (2022). Stoichiometric Ratios of Carbon, Nitrogen and Phosphorus of Shrub Organs Vary with Mycorrhizal Type. *Agriculture*, *12*(7), Article 7. https://doi.org/10.3390/agriculture12071061

Young, A. L., & Koerner, S. E. (2022). Understory dynamics in North Carolina longleaf pine savannas: Biodiversity, dominance, and biomass. *Journal of Vegetation Science*, *33*(2), e13126. https://doi.org/10.1111/jvs.13126

Yu, H., Luedeling, E., & Xu, J. (2010). Winter and spring warming result in delayed spring phenology on the Tibetan Plateau. *Proceedings of the National Academy of Sciences*, *107*(51), 22151–22156. https://doi.org/10.1073/pnas.1012490107

Yu, P. (2022). Research and Prediction of Ecological Footprint Using Machine Learning: A Case Study of China. *2022 International Conference on Big Data, Information and Computer Network (BDICN)*, 112–116. https://doi.org/10.1109/BDICN55575.2022.00029

Yun, T., Cao, L., An, F., Chen, B., Xue, L., Li, W., Pincebourde, S., Smith, M. J., & Eichhorn, M. P. (2019). Simulation of multi-platform LiDAR for assessing total leaf area in tree crowns. *Agricultural and Forest Meteorology*, *276*, 107610.

Zhang, S., Liu, G., Cui, Q., Huang, Z., Ye, X., & Cornelissen, J. H. C. (2021). New field wind manipulation methodology reveals adaptive responses of steppe plants to increased and reduced wind speed. *Plant Methods*, *17*(1), 5. https://doi.org/10.1186/s13007-020-00705-2

Zhang, Z., Li, X., & Liu, H. (2022). Biophysical feedback of forest canopy height on land surface temperature over contiguous United States. *Environmental Research Letters*, *17*(3), 034002. https://doi.org/10.1088/1748-9326/ac4657

Zheng, J., Tarin, M. W. K., Jiang, D., Li, M., Zhang, M., Chen, L., He, T., Hong, X., & Zheng, Y. (2021a). Various distances and orientations influenced the branching traits of Dendrocalamus minor var. Amoenus in Dongshan Island, China. *Global Ecology and Conservation*, *26*, e01468. https://doi.org/10.1016/j.gecco.2021.e01468

Zheng, J., Tarin, M. W. K., Jiang, D., Li, M., Zhang, M., Chen, L., He, T., Hong, X., & Zheng, Y. (2021b). Various distances and orientations influenced the branching traits of Dendrocalamus minor var. Amoenus in Dongshan Island, China. *Global Ecology and Conservation*, *26*, e01468. https://doi.org/10.1016/j.gecco.2021.e01468

Zhou, G., Lucas-Borja, M. E., Eisenhauer, N., Eldridge, D. J., Liu, S., & Delgado-Baquerizo, M. (2022). Understorey biodiversity supports multiple ecosystem services in mature Mediterranean forests. *Soil Biology and Biochemistry*, *172*, 108774. https://doi.org/10.1016/j.soilbio.2022.108774

Zhou, Q., Grinspun, E., Zorin, D., & Jacobson, A. (2016). Mesh arrangements for solid geometry. *ACM Transactions on Graphics*, *35*(4), 39:1-39:15. https://doi.org/10.1145/2897824.2925901

Zhu, Z., Kleinn, C., & Nölke, N. (2020). Towards Tree Green Crown Volume: A Methodological Approach Using Terrestrial Laser Scanning. *Remote Sensing*, *12*(11), Article 11. https://doi.org/10.3390/rs12111841

Zinnert, J. C., Shiflett, S. A., Vick, J. K., & Young, D. R. (2013). Plant functional traits of a shrub invader relative to sympatric native shrubs. *Ecosphere*, *4*(10), 1–11.

3. CHAPTER THREE

Plot-level volume estimations from synthetic point cloud using machine learning algorithms

Michelle S. Bester [1]*, Aaron E. Maxwell[1], Michael R. Gallagher [2], Nicholas S. Skowronski [3]

[1] Department of Geology and Geography, West Virginia University, Morgantown, WV, 26505, USA

[2] USDA Forest Service, Northern Research Station, New Lisbon, NJ 08064, USA

[3] USDA Forest Service, Northern Research Station, 180 Canfield Street, Morgantown, WV 26505, USA

* Corresponding author

Abstract:

In this study, we assessed the 3D architectural drivers of understory flammability by evaluating the use of architectural metrics derived from the TLS point cloud and 3D reconstructions of the shrubs. The study area was located in a fire-prone longleaf pine forest ecosystem using eight species based on their representativeness in the understory. We found that the same shrubs species were clustered together, and each species was associated with a unique combination of flammability and architectural traits. The final correlation results suggest that higher crown depth-to-height (CD:H) and lower crown width-to-height (CW:H) ratios are less flammable. In contrast, shrubs with lower CD:H and larger CW:H are generally more flammable. These results demonstrate the potential of using QSM to provide metrics that are complementary to TLS data, potentially improve flammability predictions, and increase our understanding of the linkages between flammability and architectural traits. Furthermore, this study represents the first effort comparing flammability obtained through TLS-derived architectural trait analysis, including novel shrub topology metrics.

Keywords: Terrestrial light detection and ranging; Quantitative Structure Models (QSM); architectural traits; woody shrubs

3.1 Introduction

Forests are one of the most biologically diverse terrestrial ecosystems globally. Consequently, they play a vital role in ecosystem processes, support numerous biological communities, offer primary production resources, and mitigate climate change through carbon sequestration and storage (Aravanopoulos, 2016; Hu et al., 2021; Waser et al., 2015). As such, there is a need for accurate information for quantifying forest resources and monitoring their dynamics (Liao et al., 2022; Vagizov et al., 2021). With recent advancements in remote sensing technologies, there have been considerable improvements in retrieving forest parameters. In particular, lidar (light detection and ranging) systems can capture the three-dimensional structure of forests and provide estimations of forest parameters (Andersen et al., 2005; Hu et al., 2021; Skowronski et al., 2011b).

Previous studies have implemented lidar to derive height, aboveground biomass, volume, density, basal area, and canopy attributes at a plot or individual tree level (Coops et al., 2021; Gao et al., 2022; Hu et al., 2021; Xu et al., 2021). For example, Silva et al. used canopy height profile statistics from airborne laser scanning (ALS) to map stem biomass of even-aged eucalyptus plantations in Brazil (Silva et al., 2015). Using TLS-based variables, Mayamanikandan et al.'s study illustrated that volume estimations can be derived with relatively low (5.13%) bias relative to manual, field-based measurements (Mayamanikandan et al., 2019). Saarinen et al. investigated the feasibility of using terrestrial laser scanning (TLS) for estimating tree volume at a single-tree level. They found that volume estimation accuracy increased as the number of scans increased and that accuracy depended on the distance of the TLS from the tree (Saarinen et al., 2017). Skowronski et al. also noted the value of using downward scanning aerial lidar in conjunction with upward sensing profiling lidar to better characterize the three-dimensional (3D) tree canopy structure in comparison to only using aerial data (Skowronski et al., 2011a). Since individual tree characteristics and stand-level canopy and subcanopy densities, volumes, and biomass are valuable inputs to many ecological algorithms and remote sensing models, prior studies have aimed to develop and/or assess technologies and methods to obtain forest parameters as efficiently and accurately as possible. Moreover, the associated accuracy assessment typically involves comparing the lidar-derived variables to sampled in-situ measurements using empirical modeling techniques. This poses challenges for larger study areas where extensive ground reference data are needed and in situations where the variable of interest is difficult to actually measure or estimate using field methods.

Comprehensive field data collections are expensive, laborious, and time-consuming, and inconsistencies in collection methods may arise (Fassnacht et al., 2018; Parker et al., 2004; Vandendaele et al., 2022; Xu et al., 2021). According to Westfall and Woodal, there were inconsistencies for more than half of the measured forest fuel attributes in a large-scale sampling effort conducted as part of the Forest Inventory and Analysis (FIA) program of the United States Department of Agriculture (USDA) Forest Service (Westfall & Woodall, 2007).

Furthermore, lidar-based measurements are also subject to some uncertainty. Uncertainties propagate from errors in the sensor position due to incorrect global positioning system (GPS) information, interference from the atmosphere, instrument effects such as afterpulse (noise induced from laser firing), returns per pulse, or sensor calibration (Gonsalves, 2010; Gonzalez et al., 2010; Vicari et al., 2019). Inherent complexity of forest stands at both the plot- and individual-tree levels, as well as terrain variability, affect lidar acquisition accuracy (Andersen et al., 2005; Moorthy et al., 2011). For example, Clark et al.'s study documented that higher vegetation densities reduced the probability of detecting the ground surface and limited the ability to discriminate sub-canopy returns (Clark et al., 2004). Lidar-based estimations are further influenced by the point density, sensing distance, and angle of transmission of the TLS laser pulses. Specifically, lidar pulses that reach the uppermost part of the canopy have a larger footprint due to the beam divergence inherent to a specific instrument (M. Disney, 2019). Further, the number of single location scans that are collected and subsequently merged to characterize a plot impacts the point-cloud's spatial resolution and, consequently, the amount of occlusion of and by vegetation structure (Malambo et al., 2019). Numerous studies have tried to minimize the impact of occlusion (e.g., Loudermilk et al. (2012), Abegg et al. (2021) and Rowell et al. (2016, 2020b; Rowell et al., (2015)) through characterizing stands by obtaining scans from multiple scan positions. However, these studies still noted limitations; artifacts and errors are induced by external factors, such as weather conditions (wind, fog, or precipitation) and by mixed effects caused by laser pulses intersecting multiple small branches or compact, dense vegetation [9,25-29]. Finally, the processing procedure from raw point clouds to lidar-estimated models or summary metrics further confounds uncertainties. This includes georeferencing, co-registration and merging, segmentation, subsetting, and classifying the point cloud data (Alonso-Benito et al., 2016; Calders et al., 2020). Tao et al. (2021) noted geolocation errors of up to 6 m for TLS-derived stem positions. Frazer et al. (2011) investigated the uncertainty between plot size and co-registration. They found that the impact of co-registration errors was more

pronounced in spatially heterogenous plots with taller vegetation in comparison to plots with more homogeneity. These studies highlight the complexity of lidar acquisition and processing, along with the need to investigate it under unbiased conditions.

To overcome the abovementioned study limitations, we propose using synthetic data and simulated lidar datasets to investigate the accuracy of lidar-derived estimations of stand-level characteristics and the effect of occlusion within forest plots of varying complexity (i.e., tree and shrub density and configuration). These datasets are quantitatively similar to lidar datasets created within the "real" world, with the added advantage of having no positional noise within the point cloud, the ability to register multiple scans without any co-registration error, and ability to model against known stand-level metrics as opposed to those estimated using field methods (Fassnacht et al., 2018; Wang et al., 2013). This allows for comparisons between methods for estimating stand characteristics, means to summarize three-dimensinal point distributions, and techniques and workflows to empirically estimate metrics of interest without having the confounding variables of noise, errors, and lack of accurate ground measurements to model against. There is also the added advantage of testing multiple configurations with little to no added expenseIn a review on enhancing forest inventories using remote sensing, White et al. commented that synthetic data could vastly improve our understanding of the relationship between forest structure and lidar attributes (White et al., 2016). Goodwin et al. further emphasized the potential of synthetic data for testing forest metrics calculated from lidar data (Goodwin et al., 2007). We argue that such simulated studies can inform best practices for designing field collection protocols and comparing methods for empirically estimating stand-level metrics. We further argue that exploring these problems in a synthetic space can inform expected accuracies and outcomes when using TLS to characterize real forest stands when model against real ground data. Further, this experimental framework can be expanded to explore other research questions, such as the impact of noise, co-registration error, field data uncertainty or abundance, and varying means to summarize the point cloud into a set of metrics for incorporation into empirical modeling.

A few prior studies have proposed simulating lidar data of forest stands using simplified ray-tracing methods. Sun and Ranson (2000) developed a full waveform lidar simulator that captured the horizontal and vertical structure of geometrically simple (elliptical and conical) forest stands. Similarly, Wang et al. used simple geometric shapes to generate artificial forest stands and simulate aerial lidar (ALS) sampling. However, they filtered out the understory and

interpolated the canopy to a 2-dimensional raster to calculate forest metrics (L. Wang et al., 2013). Disney et al. made use of more detailed tree models and ray-tracing canopy scattering methods to simulate lidar responses. They investigated canopy height retrieval under a range of conditions (different scan angles and sampling density). They found that the simulated lidar height generally underestimated 'real' canopy height; however, their research did not include any understory vegetation and they noted that their methodology needs further validation and testing as exact parameters were not known (Disney et al., 2010).

In this study, we present a practical workflow to create realistic trees and shrubs, and forest stands with varying densities, which are subsequently scanned with simulated discrete-return terrestrial lidar. Using these synthetic datasets, our main objectives were to (1) evaluate the impact of scan density and occlusion for modeling forest parameters, (2) to quantify how scanner location patterns influence TLS acquisitions in forests, and (3) compare the prediction accuracy of empirical ML algorithms (random forests (RF), *k*-nearest neighbor (kNN), and support vector machines (SVM)) for estimating total tree and shrub volume and surface areas using metrics derived from the TLS data and the plot-level volume and surface area measurements. We argue that this experimental framework can be expanded to explore other research questions, such as the impact of noise, co-registration error, field data uncertainty, and varying means to summarize the point cloud into a set of metrics (i.e., feature space) for incorporation into empirical modeling.

3.2 **Methods**

3.2.1 Synthetic Plot Generation

Real-world forest stands are complex terrestrial biomes, comprising diverse vegetation that frequently overlap and/or grow intertwined and can occur on rugged, variable terrain and contain varying levels of litter and downed woody debris. However, since we are trying to demonstrate the validity of this method and predict forest parameters accurately, we decided to simplify our forest stand but still keep it representative of a natural forest plot. Since, mixed evergreen-deciduous forests are one of the most abundant forest types in the Northern Hemisphere (Loidi Arregui & Marcenò, 2022), we decided to imitate this natural forest for our study. Specifically, in North America, these forest ecosystems expand over a large portion of the eastern United States and southern Canada. Eastern United States mixed forests are dominated

by evergreen conifers (eastern white pine (*Pinus strobus)* and Hemlock (*Tsuga canadensis*)) and broadleaf deciduous trees, including various oak *(Quercus),* maple (*Acer*) and hickory (*Carya*) species (Fei & Yang, 2011; Hartley et al., 2022; U.S. National Park Service, 2022; Zhang et al., 2022). Moreover, these forests form part of the World Wildlife Fund's (WWF) global priority ecoregions for conservation due to their high levels of biodiversity of both fauna and flora (Olson & Dinerstein, 2002).

We developed our forest plots within the Blender™ version 3.10. (http://www.blender.org) open source 3D model creation software. The generation of these forest plots is a multi-step process. First, we constructed a 20 m x 20 m filled planar mesh as our forest floor (hereafter referred to as the ground plane). A mesh is a collection of faces, edges, and vertices that make up a 3D shape (van der Walt, 2021). Our plots had flat terrain as slope and ruggedness would induce uncertainty and influence our accuracy assessment (Campbell et al., 2018; Contreras et al., 2017; Estornell et al., 2011). Blender uses a Cartesian coordinate system (X,Y,Z); as such our plane center was located at (0,0,0). The initial tree models were imported from the 'Tree Vegetation Pro V5' (VegPro) add-on tool created by Bproduction (https://bproduction-3d.com/). VegPro contains an extensive 3D model library of diverse and varied trees, shrubs, tropical plants, tree hedges, and ornamental plants, all optimized for Blender™. We used two generic evergreen pine models and two broadleaf deciduous trees (maple and oak) models for our artificial overstory. We also included one woody shrub model with two stems for the understory.

In order to automatize the plot creation process, we used the embedded Python application programming interface (API). The plot generation started by randomizing (with predefined constraints) the number and placement of each tree/shrub model within the 20 m by 20 m ground plane. We set a distance condition on the randomization in such a manner that no tree or shrub trunks or crowns overlap. Although this type of distribution is unrealistic, it ensures discrimination between models and allows for accurate calculations of forest parameters such as surface area and volume. Additionally, we customized each tree/shrub model by randomizing the scale, rotation, and crown size. These customizations change the orientation, minimum and maximum height, and scale the model crowns and trunk diameters by a percentage of the initial model (M_i) (original from VegPro). We set thresholds on the customization parameters to ensure model sizes are comparable to their real-world counterparts. The structural parameter thresholds for these models are summarised in Table 1.

Table 1. Initial model dimensions and randomization thresholds of 3D models placed within a forest plot.

Model	M_i Height (Z)	M_i Crown Dimensions (X, Y)	Randomization Threshold (min, max)	Random Rotation (X, Y, Z)
Pine 1	15.0 m	5.0 m, 6.0 m	60%, 130%	(±4°, ±4°, 360°)
Pine 2	10.0 m	4.0 m, 4.5 m	60%, 130%	(±4°, ±4°, 360°)
Oak	12.0 m	5.0 m, 6.0m	60%, 130%	(±4°, ±4°, 360°)
Maple	8.0 m	3.8 m, 3.8 m	50%, 150%	(±4°, ±4°, 360°)
Shrub	1.5 m	2.2 m, 1.8 m	40%, 150%	(±4°, ±4°, 360°)

*M_i is the initial model dimensions before randomization

Once a plot has been generated, we ensure all trunks and leaves are assigned "materials." The materials function describes the surface properties of the model, which defines how the model will appear when rendered and how the lidar simulator will interact with it. For example, the type of material (reflective or diffuse) will impact the intensity of the reflected beam; while the opacity of the model surface will determine the travel distance of the laser beam (i.e., for translucent objects, rays will continue past a model intersection point to simulate transmission). We assigned the same material properties to all models except the base color, where a slightly darker green hue was used for deciduous tree leaves. Our stem/trunk material was opaque, and we used the default VegPro stem/trunk surface parameters. The specular (brightness), roughness, and metallic parameters were 1.0, 0.55, and 0, respectively, on a scale from 0 to 1.0. Similarly, we used a default VegPro leaf material. However, we set it to have a hatched transparency, allowing light to disperse through the canopy. A specular reflection parameter value of 1.0 would have a high intensity, and the angle of incidence would be reflected in a single outgoing direction. Surface roughness and metallic values of 0 would represent a glossy object that is not metallic (admin_stanpro, 2018; Poirier-Quinot et al., 2017). It should be noted that no spectral reflectance metrics were calculated from the TLS point cloud, so these color metrics were primarily used for visualization and not used to generate predictor variables as input to the ML modeling workflow.

We executed the script within a loop to create 200 randomized plots. After each iteration, we calculated each tree and shrub volume and surface area (see section 2.3), saved the blender file, and removed all tree and shrub models in the scene before initializing the next model

iteration and subsequent plot generation. We illustrate an example of one densely packed and one sparse mixed-forest plot model in Figure 1 below.

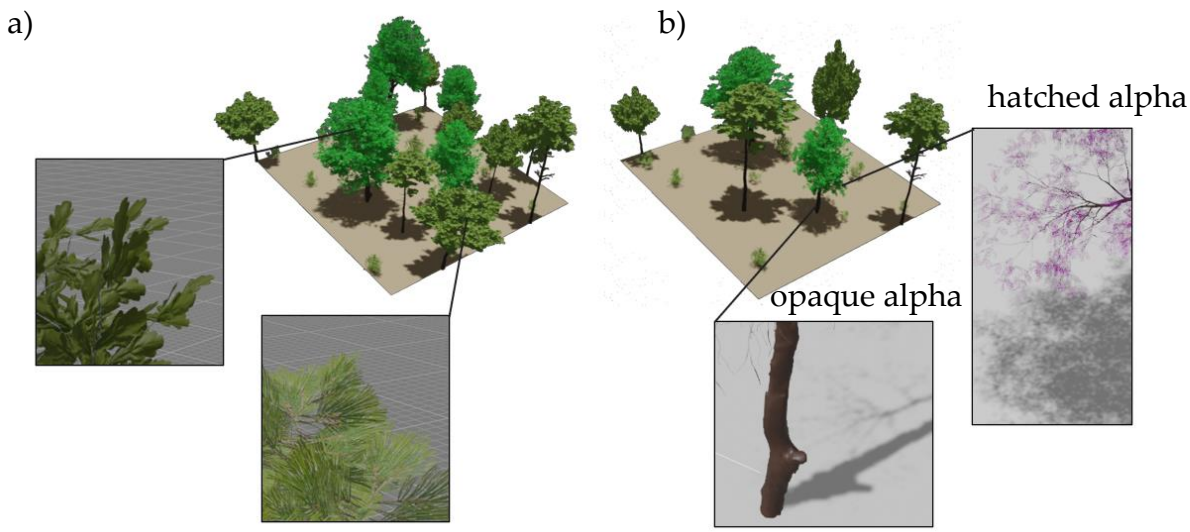

Figure 1. a) Example of a densely populated forest plot with zoomed insets of oak and pine leaf structure. **b)** Example of a sparsely populated forest plot with zoomed insets illustrating opaque trunk and hatched transparency for canopy

3.2.2 Simulated lidar

To simulate the TLS scans, we used a range scanner simulation add-on in Blender called Blainder (Reitmann et al., 2021), developed by Lorenzo Neumann and freely available from github (https://github.com/ln-12/blainder-range-scanner). We implemented that add-on using its Python API within Blender. The lidar functionality of the range scanner is based on a ray tracing approach. Ray tracing is a global illumination algorithm based on the emission of rays to determine the visibility of three-dimensional objects from a certain point (Gusmão et al., 2021; Scratchpixel, 2022; Yun et al., 2019). Previous works from Disney et al. (2000; 2010) provide a detailed review of ray tracing for remote sensing and the latter specifically for forests. Briefly, the algorithm traces the beam path from the center of the scanner (camera) for each pixel on the

screen, until it collides with an object in the virtual scene. When the collision occurs, the distance is calculated, and object attributes are recorded. Diffuse sampling beams are generated at an intersection with a scene object, sending further beams on possible routes by which they diffuse (scatterer) based on the object's material properties. After each measurement, the direction of the beam is adjusted horizontally and/or vertically according to the sensor configuration (Disney et al., 2000; Goodwin et al., 2007; Reitmann et al., 2021).

In our study, we used a rotating sensor type with a horizontal and vertical field of view of 360°, with a step size of 0.2° in both the X and Y direction. This gave us a total of 3.24 Million points per scan. The step size determines the resolution of the sensor; step sizes closer to zero would have higher resolutions. This approach assumes that there is no beam divergence and that the beam width is constant. We simulated one scan from the center (SC = 0,0,0) of the forest plot at a height of 2 m (0,0,2) and a scan from each corner of the plot (CS 1-4) (Figure 2, triangles). For the corner plot scans, we placed the virtual camera (origin of the scanner) 2 m away from the ground plane, the coordinates (X,Y,Z) relative to the plot center are as follows: CS 1 = (12,12, 2), CS 2 = (12,-12, 2), CS 3 = (-12,12,2) and finally CS 4 = (-12,12,2). We did not set a maximum distance limit that the beam could travel; instead, we enclosed our plot in a 30 x 30 x 30 m box (6 planes) with an opaque material (Figure 2, blue planes). This acted as a wall and allowed us to capture all pulses that would otherwise have no associated return. Having these points are helpful for determining occlusion and accounting for all transmitted laser pulses in subsequent calculations. We visualize the top and side view of our plot and camera setup in Figure 2. The final step was to save these scans in .laz format for further analysis. Similar to the plot generation, we automated the lidar simulation process using the Python API and ran it for the 200 synthetic plots.

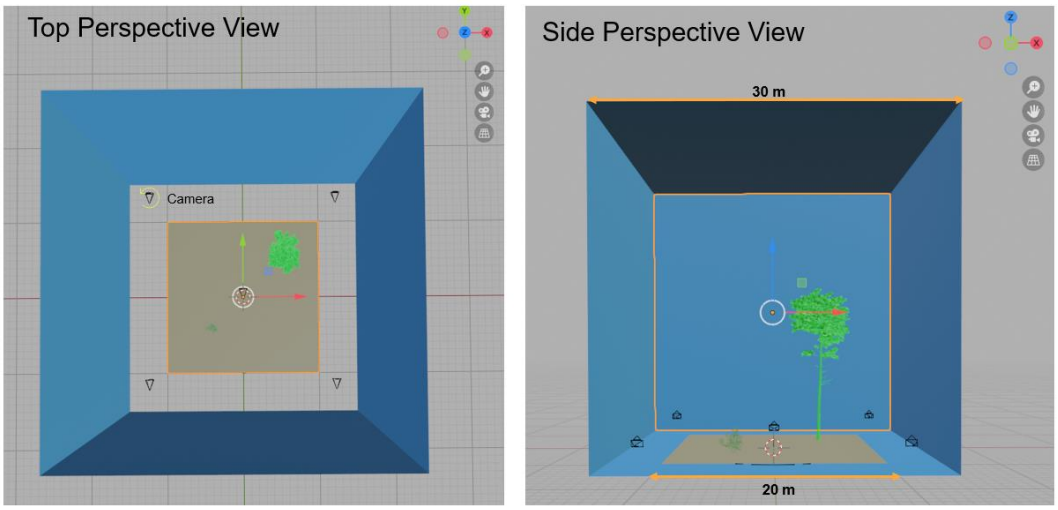

Figure 2. Scanner location configuration within the virtual plot (light brown square) with 30 m square box (blue planes). For visualization purposes, the top view excludes the top and bottom sides of box, while the side view excludes the front plane.

3.2.3 Measured metrics

To assess the impact of density and location of hypothetical lidar on forest parameter estimates, we calculated various summary metrics from the point cloud data. We calculated metrics based on only the center scan as well as the aggregation of all scans (center and four corners). Our analysis was performed on imported .las files within the R open-source data science environment and language (R Core Team, 2020). We only used the Z-values for our metric calculations; the true color (RGB) and intensity values would not be realistic since we assigned the same materials to all objects.

The calculated point cloud metrics are summarized in Table 2. First, we calculated the total number of returned points and the number of points intersecting the box. This allows for a calculation of the percent of points striking the box, which would indirectly correlate with the area and volume of trees and shrubs within the plot. Next, the box was clipped out, leaving only the returns within each forest plot. We performed point cloud manipulation (filter, clipping, etc.) using the lidR (Roussel et al., 2020; Roussel & Auty, 2021) and rlas (Roussel et al., 2022) packages. Next, we summarized the data relative to height strata. We filtered the point cloud

data into height bins of 0.0-2.0 m, 2.0-4.0 m, 4.0-6.0 m, 6.0 8.0 m, and > 8.0 m. We chose these height bins based on typical shrub and canopy heights within mixed deciduous forests. Within each height bin, we calculated the metrics summarized in Table 2. We summarized all point returns within our 20 m x 20 m plot, non-ground returns within the 20 m x 20 m plot, and returns within each of the five height strata. This resulted in a total of 54 variables for each of the 200 plots.

Table 2. Summary metrics generated from point cloud data.

Subset	Variable	Count
Entire point cloud (including box)	% of returns from only box	1
20 m x 20 plot	Ground count	1
	% of returns in plot that were ground	1
	Not ground count	1
	% of returns in plot that were not ground	1
Not ground in plot	Height quantiles (10% through 90% by 10%)	9
	Height mn, md, std, skew, and kurt	5
By height strata	Not ground count in strata	5
	% of not ground returns in plot from within strata	5
	Height mn, med, std, skew, and kurt	25

mn = mean, md = median, std = standard deviation; skew = skewness; kurt = kurtosis

3.2.4 Modeling and Validation

We calculated the volume and surface area of the individual virtual trees and shrubs within the Blender Python API using the 'bMesh Module'(*BMesh Module (Bmesh) — Blender Python API*, n.d.). These data were exported and summed per plot for modeling purposes. To assess how well the simulated point cloud metrics estimate the known measurements, we employed three machine learning algorithms, namely RF, *k*NN, and SVM. These models were trained using the simulated lidar metrics as the predictor variables and the known volume and surface area from the 3D plots as the dependent variables.

In the last decade, machine learning-based algorithms have gained significant attention, especially in the field of remote sensing (Hamilton et al., 2020; Hartley et al., 2022; Lary et al., 2016; Maxwell et al., 2018; Yu, 2022). Since our study's purpose was to predict volume and surface area from a large set (30+) of predictor variables, we decided that machine learning algorithms would be better suited than statistical regression approaches for this study.

Furthermore, these models could account for complex variable interactions, correlated predictor variables, and non-linear relationships.

SVM is a supervised learning algorithm that attempts to find the optimal hyperplane, defined as the boundary that provides the largest margin or separating distance between classes or groups, in *n*-dimensional space. When classes cannot be separated using a linear hyperplane, the data can be projected to a higher dimensional space, a process known as the kernel trick, in which the separating boundary may be more linear (Fletcher, 2009; Hamilton et al., 2020). kNN is a non-parametric model that uses similarity (based on distance functions) to predict new data points; specifically, new samples are compared to the *k* closest samples from the training set within the multidimensional feature space (Duda & Hart, 2006). Ensemble learning, methods that generate many classifiers and aggregate their results, has recently gained much interest. RF regression models, developed by Breiman, are ensemble decision tree algorithms where the tree is 'grown' with some randomization (Wright & Ziegler, 2017). Decision trees use recursive binary partitioning to split the data into more homogeneous subsets and generate rulesets to perform classification or regression. Within RF specifically, each tree in the ensemble uses a subset of the training samples, which are selected using bootstrapping (i.e., random sampling with replacement). Also, only a subset of the predictor variables is available for splitting at each decision node. The goal of using a subset of the training data and variables is to reduce the correlation between trees and minimize overfitting. In other words, a set of weak classifiers are collectively strong and generalize well due to reduced overfitting.

Our models for predicting surface area and volume were trained in R (R Core Team, 2020) using the caret package (Kuhn, 2021). RF was implemented through caret using the ranger package (Wright & Ziegler, 2017) while SVM was implemented using the kernlab package (Karatzoglou et al., 2007). We included a center and scale pre-processing transformation for all our models since kNN and SVM make use of distance-based calculations and require all predictor variables to be consistently scaled. For RF, the number of random predictor variables available for splitting at each node hyperparameter (*mtry*) was uniquely optimized for each model or feature space using ten-fold cross-validation and a grid search to test ten values. The *ntree* parameter (number of trees to grow) was set to 500. In a review article by Belgiu et al. on RF algorithms for remote sensing applications, they noted that a *ntree* of 500 provides stable predictions and satisfactory results (Belgiu & Drăguţ, 2016). For kNN and SVM algorithms, the

k and *cost* parameters were optimized, and the best hyperparameter was selected based on the lowest RMSE.

To obtain multiple results and to characterize the variability in model performance, we trained and assessed 50 model replicates using different training and testing partitions, selected using a bootstrapping method in which a random set of 75% of the samples (150 plots) was used to train a model, and the remaining 25% (50 plots) were withheld for model validation. It should be noted that hyperparameter optimization was performed separately for each replicate so as not to induce data leakage by using the withheld samples for a specific run to perform the hyperparameter optimization or center and scaling. Using the withheld data, we calculated the R-squared and root mean square error (RMSE) metrics using the yardstick (Kuhn & Vaughan, 2021) package in R (R Core Team, 2020) for model validation.

3.3 Results

We aimed to create randomized forest plots with varying densities. Table 3 provides descriptive statistics highlighting volume and surface area variability across our 200 synthetic plots. Figure 3 shows the distribution of surface area (a) and volume (b), as represented using violin and boxplots for all plots, as well as a histogram showing variability within individual plots. The mean volume and surface area across all plots were 711.80 m^3 and 4,778.62 m^2, respectively. The least dense plot (plot 181) had a volume of 8.15 m^3 while the densest plot (plot 140) had a volume of 2,625.12 m^3. Plot 181 only consisted of two pine trees and six small shrubs. In contrast, plot 140 consisted of 11 shrubs, six pine trees, and nine deciduous trees.

Table 3. Descriptive statistics of known volume and surface area across the 200 synthetic plots.

Descriptive Statistic	Volume (m^3)	Surface Area (m^2)
Minimum	8.10	292.073
Maximum	2625.12	10281.53
1st Quartile	357.93	2564.77
Median	611.91	4694.18
3rd Quartile	1010.69	6925.20
Mean	711.80	4778.62
Standard deviation	499.38	2504.90
Interquartile range (IQR)	483.89	3232.39

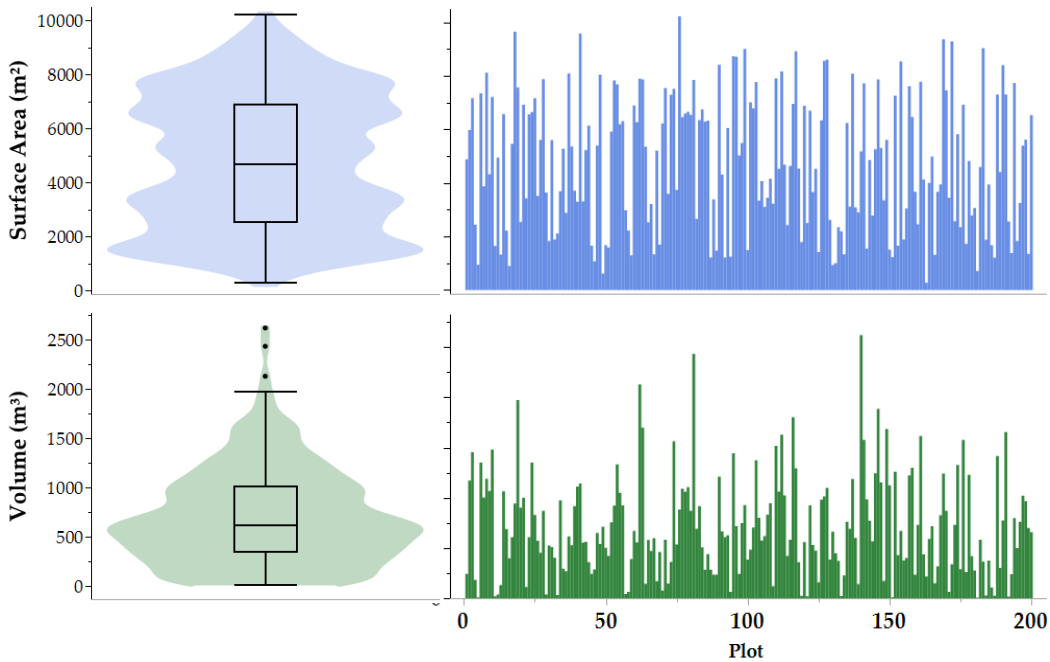

Figure 3. Distribution of known forest metrics. (a) Violin plot of the distribution of surface area across the 200 plots and histogram of individual plot surface areas. (b) Violin plot of the distribution of volume across all 200 plots with a histogram of individual plot volumes

Table 4 provides descriptive statistics highlighting the amount of occlusion as a percentage across the 200 synthetic plots. We calculated occlusion from the 'holes' on the box that enclosed our plot. Ideally, if there were no occlusion, the box walls would be completely covered by the maximum amount of points produced by the scan. If there is an object between the wall and the scanner, beam from the scanner would intersect with the object and not reach the wall. In Figure 4, we use a stacked bargraph to illustrate the difference in the amount of occlusion in the plots when using only one scan versus using multiple scan locations (i.e., center scan and four corners). When using multiple scans the mean percentage of occlusion across all plots decreased nearly 2-fold, from 10.53% to only 5.14%. Moreover, there is a large difference in the occlusion variance (33.21%) across plots when using only one scan. This suggests that density within the plot affects the occlusion from the center scan.

Table 4. Descriptive statistics of the percentage of occlusion across all sites and surface area across the 200 synthetic plots.

Descriptive Statistic	Middle Scan Only	All Scans
Minimum	0.838	0.680
Maximum	25.837	13.261
Mean	10.526	5.138
Variance	33.212	6.145
Standard deviation	5.763	2.479

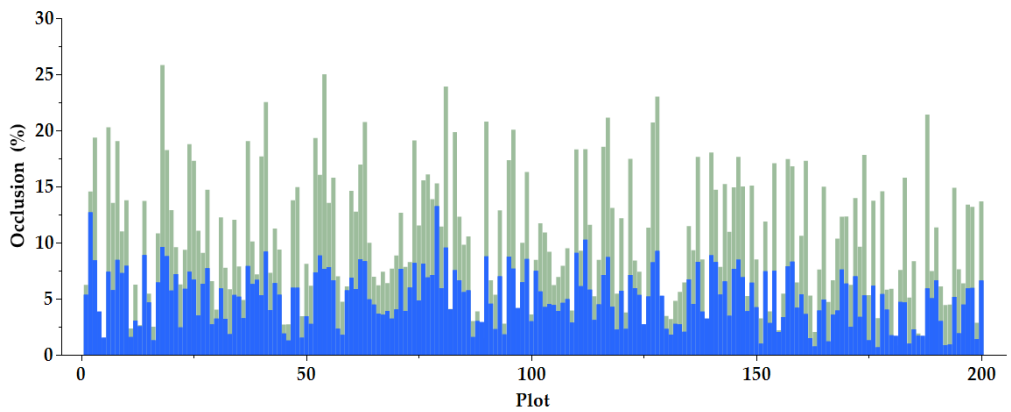

Figure 4. Bargraph depicting the percentage of occlusion for all scans (blue) and only the middle scan (green) per plot

Figure 5 shows the distribution of RMSE, calculated by predicting the withheld 50 validation plots based on 50 model replicates using different training and testing partitions with the results differentiated by scan density, ML algorithm, and the metric being predicted. The RMSE is in the units of the predicted metrics (i.e. cubic m for volume and square m for surface area). Figure 6 presents the same results relative to the R-squared metric. For the surface area results as assessed with the RMSE metric (Figure 5a), we see that the middle scan generally had higher RMSE values across all algorithms, suggesting poorer performance in comparison to using all scan locations. Similarly, the volume predictions using the RMSE metric also had higher error values across all algorithms when only using the middle scan for predictions. Overall, the algorithms had smaller interquartile ranges for using all scans except for the SVM area metric as compared to only the middle scan. When making area predictions using metrics

generated from all scans, the mean RMSEs were 1,258.12 m^2, 1,520.07 m^2, and 1,323.19 m^2 for the RF, kNN, and SVM algorithms, respectively. The volume predictions using the RMSE metric also had variability across the algorithms and scan density, the mean RF RMSEs were 307.10 m^3 and 381.61 m^3, mean kNN RMSEs were 363.77 m^3 and 414.14 m^3, and SVM mean RMSEs were 289.22 m^3 and 393.26 m^3, for all scans and middle, respectively.

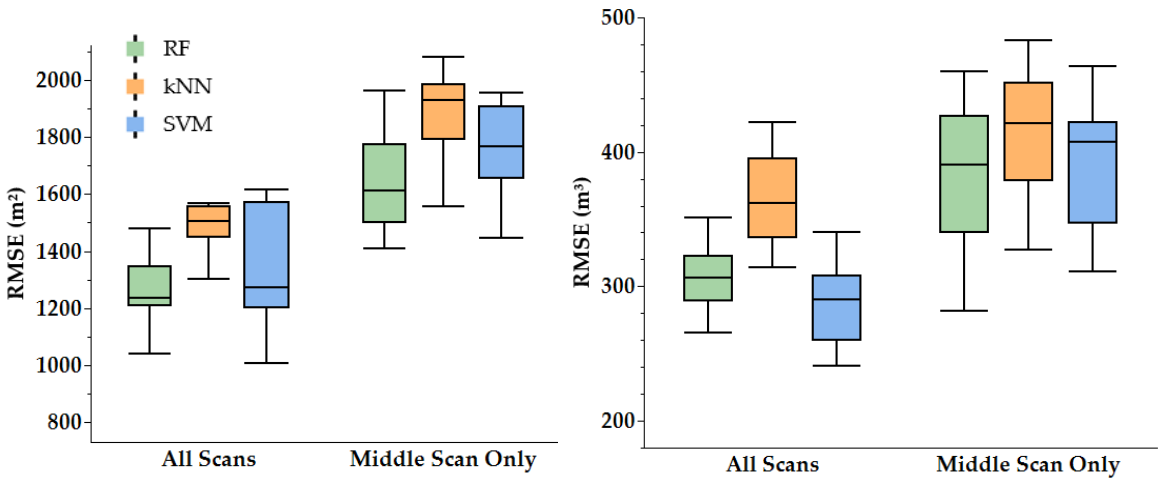

Figure 5. Distribution of RMSE results for RF,kNN, and SVM across 200 plots. (a) For area prediction for all scans and middle scans only. (b) For volume prediction for all scans and middle scan only.

Performance and correlation for the volume predictions were generally poorer than those for the surface area predictions. We hypothesize that this is due to the occlusion of internal structure by modeled leaves and dimensionality, meaning predictions for the surface area is only in 2 dimensions, whereas volume predictions are in 3 dimensions. This adds another level of complexity for prediction. Overall, we found high R^2 values when predictions were made from metrics calculated from multiple scans, especially for surface area with a mean R^2 value of 0.76, 0.63, and 0.68, for RF, kNN, and SVM, respectively. The RF algorithm had the highest overall R^2 value (0.86) for area prediction, while SVM had the highest R^2 value (0.78) for volume prediction. For the single scan predictions, RF had the highest R^2 values for both area and volume predictions. The interquartile range was relatively consistent for all predictions across all the algorithms, with a difference of just 0.035 between the largest and smallest interquartile ranges.

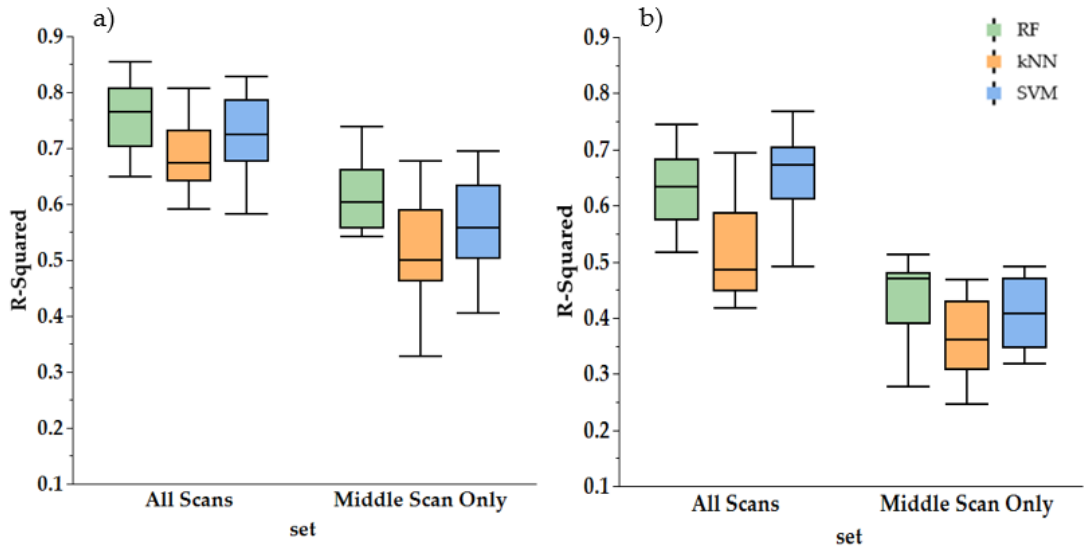

Figure 6. Distribution of R^2 results for RF,kNN, and SVM across 200 plots. (a) Area prediction for all scans and middle scans only. (b) Volume prediction for all scans and middle scan only.

3.4 Discussion and Future work

Applications relying on point cloud data, either directly or using information from them for sustainable forest management, have increased over the last decade (Contreras et al., 2017; Hernando et al., 2022; Hudak et al., 2008; White et al., 2016). Thus, understanding how plot scale forest structure and TLS scan location configuration influence the accuracy of forest metrics would be valuable for optimizing lidar acquisition for forest monitoring and remote sensing applications. Our study provides a replicable semi-automated approach for creating synthetic forest plots and simulating lidar point clouds. Furthermore, due to the benefit of known forest parameters, with set characteristics (materials, illumination source) and no noise within the simulated point cloud, it is possible to evaluate the impact of occlusion and performance of various methods and the errors associated with predictions.

Results from this study demonstrated that the lidar scan location affected prediction accuracy. In particular, occlusion is strongly related to the sampling density and plot complexity. For a single scan from the middle, the average R^2 across all models and predictions was 0.49, whereas the average R^2 across all models and predictions increased to 0.67 when using

the four corners and a center scan. Moreover, the mean RMSE for the multiple scan location for surface area and volume was smaller than the RMSE from just the center scan location. We argue that this is because the multi-scan configuration captures the plot structure from multiple angles and more laser beams enter the tree crown through gaps, which minimizes objects' occlusion within the plot. The point cloud density is also increased to optimize the detection and variable prediction of vegetation elements. These results are similar to findings from studies based on real-world data (Calders et al., 2020; Hyyppä et al., 2008; Saarinen et al., 2017; Watt & Donoghue, 2005). For example, Wilkes et al. (2017) investigated TLS sampling configurations for deriving forest plot scale structure metrics and concluded that increasing the number of scan locations will always improve accuracy, regardless of scanner specifications or sampling approach. More similar to our approach, Yun et al. (2019) adopted a computer simulation methodology to investigate virtual scanning patterns for estimating total leaf area. Their results found that only 25–38% of leaf area was retrieved and occlusion occurred on leaves distal to the scanner when the target tree was scanned from a single position. However, when three virtual scans were performed around a tree, the accuracy of leaf area recovery reached approximately 60–72%, and occlusion was restricted to just the crown center.

We further assessed modeling algorithms and errors associated with forest parameter estimations. When comparing RF, kNN, and SVM machine-learning algorithms, we noted that RF using the R^2 metric for parameter optimization performed slightly better than kNN and SVM for forest parameter (surface area and volume) predictions with a mean R^2 of 0.62,0.52 and 0.58 for RF, kNN and SVM respectively. We hypothesize that RF performs better overall as it has the capability to deal with complex relationships between large amounts of data. Moreover, RF models use an ensemble of trees to improve robustness. Wang et al. (2016) noted that RF is regarded as one of the most precise prediction methods for regression-type modeling. RF has also been widely applied in remote sensing and has been publicized as reliable (Belgiu & Drăguţ, 2016; Mutanga et al., 2012; Wang et al., 2016).

We need predictor variables as inputs for these models to estimate forest parameters from the lidar. This is often in the form of metrics derived from the point cloud; in our study, these are the metrics derived in Table 2. We used these metrics to predict surface area and volume, while research using synthetic data for biomass estimations by Fassnacht et al. (2018) did not consider any metrics derived from the point cloud, but instead restricted their analysis to metrics derived from canopy height models (only using the upper portion of lidar). Consequently,

although they employed RF for predictions, a comparison between these two studies is difficult. Other studies have also utilized synthetic data to understand uncertainty and error propagation. Lovell et al. (2005) modeled trees using simple geometric shapes (cones, ellipsoids, and cylinders), creating plantation stands and simulated small footprint lidar data to determine the optimal acquisition parameters for measuring tree height. Disney et al. (2010) used five experiments to quantify the impact of pulse density, scan angle, footprint size, and canopy structure for estimating canopy height and gave a detailed conclusion on each of these variables' impact on canopy height estimation accuracy. However, different techniques were employed in both these studies to evaluate uncertainties. Therefore, comparisons between studies pose a challenge and highlights the need for a replicable method for evaluating lidar uncertainty.

Since we used this as a feasibility study for evaluating simulated lidar, some simplifications were made. This included using a limited number of vegetation species and having no overlapping trees and shrubs in the stand. In addition, all species had uniform foliage density and were assigned the same material characteristics, and we had flat ground terrain and a constant laser pulse. Future studies could develop more realistic forest stands and investigate multifarious lidar-related aspects from acquisition to prediction. This could include investigating the effect of added noise to the point, for example, by simulating wind or beam divergence. The impact of distance from the scanner on prediction accuracy or how scan density affects other forest parameters besides volume and surface area. It would also be useful to evaluate other metrics and algorithms for prediction. The focus of our future work will be to incorporate real-world objects, such as trees or shrubs modeled by quantitative structure models into the virtual space for further analysis.

3.5 Conclusion

In this study, we present a semi-automated approach for creating forest stands and simulating lidar. We further investigate the impact of scan location for modeling forest parameters. Using the simulated lidar-derived metrics, we found that the number of scan positions and forest complexity influences the amount of occlusion and subsequently prediction accuracy. Therefore, choosing an optimized scanning strategy can minimize the effect of occlusion and increase data quality.

Furthermore, we highlight the potential for using synthetic remote-sensing datasets to examine the lidar acquisition and scanning characteristics under controlled parameter sets that can be implemented across different forest stand complexities. This research allows us to reexamine existing methods and optimize workflows, data collection, and algorithm selection. Additionally, deep learning models are being incorporated into remote sensing applications and the need for large datasets for training models is increasing, as such synthetic datasets can provide a potential solution to this challenge as large realistic datasets can be generated in a precise, timely, and cost-effective manner. Finally, it should be noted that the approach is not just limited to creating forest plots, but has a wider application in remote sensing as well as other fields.

References

Abegg, Meinrad, Ruedi Boesch, Michael E. Schaepman, and Felix Morsdorf. 2021. 'Impact of Beam Diameter and Scanning Approach on Point Cloud Quality of Terrestrial Laser Scanning in Forests'. *IEEE Transactions on Geoscience and Remote Sensing* 59 (10): 8153–67. https://doi.org/10.1109/TGRS.2020.3037763.

Alonso-Rego, Cecilia, Stéfano Arellano-Pérez, Carlos Cabo, Celestino Ordoñez, Juan Gabriel Álvarez-González, Ramón Alberto Díaz-Varela, and Ana Daría Ruiz-González. 2020. 'Estimating Fuel Loads and Structural Characteristics of Shrub Communities by Using Terrestrial Laser Scanning'. *Remote Sensing* 12 (22): 3704. https://doi.org/10.3390/rs12223704.

Alonso-Rego, Cecilia, Stéfano Arellano-Pérez, Juan Guerra-Hernández, Juan Alberto Molina-Valero, Adela Martínez-Calvo, César Pérez-Cruzado, Fernando Castedo-Dorado, Eduardo González-Ferreiro, Juan Gabriel Álvarez-González, and Ana Daría Ruiz-González. 2021. 'Estimating Stand and Fire-Related Surface and Canopy Fuel Variables in Pine Stands Using Low-Density Airborne and Single-Scan Terrestrial Laser Scanning Data'. *Remote Sensing* 13 (24): 5170. https://doi.org/10.3390/rs13245170.

Andersen, Hans-Erik, Robert J. McGaughey, and Stephen E. Reutebuch. 2005. 'Estimating Forest Canopy Fuel Parameters Using LIDAR Data'. *Remote Sensing of Environment* 94 (4): 441–49. https://doi.org/10.1016/j.rse.2004.10.013.

Aravanopoulos, Filippos A. (Phil). 2016. 'Conservation and Monitoring of Tree Genetic Resources in Temperate Forests'. *Current Forestry Reports* 2 (2): 119–29. https://doi.org/10.1007/s40725-016-0038-8.

Arroyo, Lara A., Cristina Pascual, and José A. Manzanera. 2008. 'Fire Models and Methods to Map Fuel Types: The Role of Remote Sensing'. *Forest Ecology and Management* 256 (6): 1239–52. https://doi.org/10.1016/j.foreco.2008.06.048.

Breiman, Leo. 2001. 'Random Forests'. *Machine Learning* 45 (1): 5–32.

Brown, James K. 1981. 'Bulk Densities of Nonuniform Surface Fuels and Their Application to Fire Modeling'. *Forest Science* 27 (4): 667–83. https://doi.org/10.1093/forestscience/27.4.667.

Brown, James K. n.d. 'Handbook for Inventorying Downed Woody Material', 32.

Calders, Kim, Glenn Newnham, Andrew Burt, Simon Murphy, Pasi Raumonen, Martin Herold, Darius Culvenor, et al. 2015. 'Nondestructive Estimates of Above-Ground Biomass Using Terrestrial Laser Scanning'. *Methods in Ecology and Evolution* 6 (2): 198–208. https://doi.org/10.1111/2041-210X.12301.

Chen, Yang, Xuan Zhu, Marta Yebra, Sarah Harris, and Nigel Tapper. 2016. 'Strata-Based Forest Fuel Classification for Wild Fire Hazard Assessment Using Terrestrial LiDAR'. *Journal of Applied Remote Sensing* 10 (4): 046025. https://doi.org/10.1117/1.JRS.10.046025.

Conto, Tiago de, Kenneth Olofsson, Eric Bastos Görgens, Luiz Carlos Estraviz Rodriguez, and Gustavo Almeida. 2017. 'Performance of Stem Denoising and Stem Modelling Algorithms on Single Tree Point Clouds from Terrestrial Laser Scanning'. *Computers and Electronics in Agriculture* 143 (December): 165–76. https://doi.org/10.1016/j.compag.2017.10.019.

Cooper, Sam D., David P. Roy, Crystal B. Schaaf, and Ian Paynter. 2017. 'Examination of the Potential of Terrestrial Laser Scanning and Structure-from-Motion Photogrammetry for Rapid Nondestructive Field Measurement of Grass Biomass'. *Remote Sensing* 9 (6): 531. https://doi.org/10.3390/rs9060531.

Coops, Nicholas C, Piotr Tompalski, Tristan RH Goodbody, Martin Queinnec, Joan E Luther, Douglas K Bolton, Joanne C White, Michael A Wulder, Oliver R van Lier, and Txomin Hermosilla. 2021. 'Modelling Lidar-Derived Estimates of Forest Attributes over Space and Time: A Review of Approaches and Future Trends'. *Remote Sensing of Environment* 260: 112477.

Disney, Mathias. 2019. 'Terrestrial LiDAR: A Three-Dimensional Revolution in How We Look at Trees'. *New Phytologist* 222 (4): 1736–41. https://doi.org/10.1111/nph.15517.

Erdody, Todd L., and L. Monika Moskal. 2010. 'Fusion of LiDAR and Imagery for Estimating Forest Canopy Fuels'. *Remote Sensing of Environment* 114 (4): 725–37. https://doi.org/10.1016/j.rse.2009.11.002.

Falkowski, Michael J., Paul E. Gessler, Penelope Morgan, Andrew T. Hudak, and Alistair M. S. Smith. 2005. 'Characterizing and Mapping Forest Fire Fuels Using ASTER Imagery and Gradient Modeling'. *Forest Ecology and Management* 217 (2): 129–46. https://doi.org/10.1016/j.foreco.2005.06.013.

Fassnacht, Fabian Ewald, Hooman Latifi, and Florian Hartig. 2018. 'Using Synthetic Data to Evaluate the Benefits of Large Field Plots for Forest Biomass Estimation with LiDAR'. *Remote Sensing of Environment* 213 (August): 115–28. https://doi.org/10.1016/j.rse.2018.05.007.

Finney, Mark A, Sara S McAllister, Jason M Forthofer, and Torben P Grumstrup. 2021. *Wildland Fire Behaviour: Dynamics, Principles and Processes*. CSIRO PUBLISHING.

'Francis Marion and Sumter National Forests - Home'. n.d. Accessed 22 July 2022. https://www.fs.usda.gov/scnfs/.

Gale, Matthew G., Geoffrey J. Cary, Albert I. J. M. Van Dijk, and Marta Yebra. 2021. 'Forest Fire Fuel through the Lens of Remote Sensing: Review of Approaches, Challenges and Future Directions in the Remote Sensing of Biotic Determinants of Fire Behaviour'. *Remote Sensing of Environment* 255 (March): 112282. https://doi.org/10.1016/j.rse.2020.112282.

Gallagher, Michael R., Aaron E. Maxwell, Luis Andrés Guillén, Alexis Everland, E. Louise Loudermilk, and Nicholas S. Skowronski. 2021. 'Estimation of Plot-Level Burn Severity Using Terrestrial Laser Scanning'. *Remote Sensing* 13 (20): 4168. https://doi.org/10.3390/rs13204168.

Gao, Ting, Zhihai Gao, Bin Sun, Pengyao Qin, Yifu Li, and Ziyu Yan. 2022. 'An Integrated Method for Estimating Forest-Canopy Closure Based on UAV LiDAR Data'. *Remote Sensing* 14 (17): 4317.

García, Mariano, F. Mark Danson, David Riaño, Emilio Chuvieco, F. Alberto Ramirez, and Vishal Bandugula. 2011. 'Terrestrial Laser Scanning to Estimate Plot-Level Forest Canopy Fuel Properties'. *International Journal of Applied Earth Observation and Geoinformation* 13 (4): 636–45. https://doi.org/10.1016/j.jag.2011.03.006.

García, Mariano, David Riaño, Emilio Chuvieco, Javier Salas, and F. Mark Danson. 2011. 'Multispectral and LiDAR Data Fusion for Fuel Type Mapping Using Support Vector Machine and Decision Rules'. *Remote Sensing of Environment* 115 (6): 1369–79. https://doi.org/10.1016/j.rse.2011.01.017.

Girardeau-Montaut, Daniel. 2016. 'CloudCompare'. *France: EDF R&D Telecom ParisTech* 11.

Gonsalves, Michael Oliver. 2010. *A Comprehensive Uncertainty Analysis and Method of Geometric Calibration for a Circular Scanning Airborne Lidar*. The University of Southern Mississippi.

Gonzalez, Patrick, Gregory P Asner, John J Battles, Michael A Lefsky, Kristen M Waring, and Michael Palace. 2010. 'Forest Carbon Densities and Uncertainties from Lidar, QuickBird, and Field Measurements in California'. *Remote Sensing of Environment* 114 (7): 1561–75.

Han, Tao, and Gerardo Arturo Sánchez-Azofeifa. 2022. 'A Deep Learning Time Series Approach for Leaf and Wood Classification from Terrestrial LiDAR Point Clouds'. *Remote Sensing* 14 (13): 3157. https://doi.org/10.3390/rs14133157.

Hiers, J. Kevin, Joseph J. O'Brien, R. J. Mitchell, John M. Grego, E. Louise Loudermilk, J. Kevin Hiers, Joseph J. O'Brien, R. J. Mitchell, John M. Grego, and E. Louise Loudermilk. 2009. 'The Wildland Fuel Cell Concept: An Approach to Characterize Fine-Scale Variation in Fuels and Fire in Frequently Burned Longleaf Pine Forests'. *International Journal of Wildland Fire* 18 (3): 315–25. https://doi.org/10.1071/WF08084.

Hiers, J. Kevin, Joseph J. O'Brien, J. Morgan Varner, Bret W. Butler, Matthew Dickinson, James Furman, Michael Gallagher, et al. 2020. 'Prescribed Fire Science: The Case for a Refined Research Agenda'. *Fire Ecology* 16 (1): 11. https://doi.org/10.1186/s42408-020-0070-8.

Hiers, Quinn A., E. Louise Loudermilk, Christie M. Hawley, J. Kevin Hiers, Scott Pokswinski, Chad M. Hoffman, and Joseph J. O'Brien. 2021. 'Non-Destructive Fuel Volume Measurements Can Estimate Fine-Scale Biomass across Surface Fuel Types in a Frequently Burned Ecosystem'. *Fire* 4 (3): 36. https://doi.org/10.3390/fire4030036.

Hillman, Samuel, Luke Wallace, Arko Lucieer, Karin Reinke, Darren Turner, and Simon Jones. 2021. 'A Comparison of Terrestrial and UAS Sensors for Measuring Fuel Hazard in a Dry Sclerophyll Forest'. *International Journal of Applied Earth Observation and Geoinformation* 95 (March): 102261. https://doi.org/10.1016/j.jag.2020.102261.

Hillman, Samuel, Luke Wallace, Karin Reinke, Bryan Hally, Simon Jones, and Daisy S. Saldias. 2019. 'A Method for Validating the Structural Completeness of Understory Vegetation Models Captured with 3D Remote Sensing'. *Remote Sensing* 11 (18): 2118. https://doi.org/10.3390/rs11182118.

Hines, Francis, Francis Hines, Kevin G Tolhurst, Andrew AG Wilson, and Gregory J McCarthy. 2010. *Overall Fuel Hazard Assessment Guide*. Victorian Government, Department of Sustainability and Environment Melbourne.

Hu, Tao, Yuman Sun, Weiwei Jia, Dandan Li, Maosheng Zou, and Mengku Zhang. 2021. 'Study on the Estimation of Forest Volume Based on Multi-Source Data'. *Sensors* 21 (23): 7796. https://doi.org/10.3390/s21237796.

Hudak, Andrew T, Akira Kato, Benjamin C Bright, E Louise Loudermilk, Christie Hawley, Joseph C Restaino, Roger D Ottmar, et al. 2020. 'Towards Spatially Explicit Quantification of Pre- and Postfire Fuels and Fuel Consumption from Traditional and Point Cloud Measurements'. *Forest Science* 66 (4): 428–42. https://doi.org/10.1093/forsci/fxz085.

Jia, Gensuo J., Ingrid C. Burke, Alexander F. H. Goetz, Merrill R. Kaufmann, and Bruce C. Kindel. 2006. 'Assessing Spatial Patterns of Forest Fuel Using AVIRIS Data'. *Remote Sensing of Environment* 102 (3): 318–27. https://doi.org/10.1016/j.rse.2006.02.025.

Keane, Robert E., Kathy Gray, Robert E. Keane, and Kathy Gray. 2013. 'Comparing Three Sampling Techniques for Estimating Fine Woody down Dead Biomass'. *International Journal of Wildland Fire* 22 (8): 1093–1107. https://doi.org/10.1071/WF13038.

Kessell, Stephen R., Meredith W. Potter, Collin D. Bevins, Larry Bradshaw, and Bruhe W. Jeske. 1978. 'Analysis and Application of Forest Fuels Data'. *Environmental Management* 2 (4): 347–63. https://doi.org/10.1007/BF01866675.

Key, Carl H, and Nathan C Benson. 2006. 'Landscape Assessment (LA)'. *In: Lutes, Duncan C.; Keane, Robert E.; Caratti, John F.; Key, Carl H.; Benson, Nathan C.; Sutherland, Steve; Gangi, Larry J. 2006. FIREMON: Fire Effects Monitoring and Inventory System. Gen. Tech. Rep. RMRS-GTR-164-CD. Fort Collins, CO: US Department of Agriculture, Forest Service, Rocky Mountain Research Station. p. LA-1-55* 164.

Kuhn, Max. 2021. *Caret: Classification and Regression Training*. https://CRAN.R-project.org/package=caret.

Kuhn, Max, and Davis Vaughan. 2021. *Yardstick: Tidy Characterizations of Model Performance*. https://CRAN.R-project.org/package=yardstick.

Lasaponara, Rosa, and Antonio Lanorte. 2007. 'Remotely Sensed Characterization of Forest Fuel Types by Using Satellite ASTER Data'. *International Journal of Applied Earth Observation and Geoinformation* 9 (3): 225–34.

'Leica BLK360 Imaging Laser Scanner'. n.d. Accessed 21 July 2022. https://leica-geosystems.com/products/laser-scanners/scanners/blk360.

Liao, Kuo, Yunhe Li, Bingzhang Zou, Dengqiu Li, and Dengsheng Lu. 2022. 'Examining the Role of UAV Lidar Data in Improving Tree Volume Calculation Accuracy'. *Remote Sensing* 14 (17): 4410. https://doi.org/10.3390/rs14174410.

Lillesand, Thomas, Ralph W Kiefer, and Jonathan Chipman. 2015. *Remote Sensing and Image Interpretation*. John Wiley & Sons.

Loudermilk, E. Louise, J. Kevin Hiers, Joseph J. O'Brien, Robert J. Mitchell, Abhinav Singhania, Juan C. Fernandez, Wendell P. Cropper, et al. 2009. 'Ground-Based LIDAR: A Novel Approach to Quantify Fine-Scale Fuelbed Characteristics'. *International Journal of Wildland Fire* 18 (6): 676–85. https://doi.org/10.1071/WF07138.

Loudermilk, E. Louise, Joseph J. O'Brien, Robert J. Mitchell, Wendell P. Cropper, J. Kevin Hiers, Sabine Grunwald, John Grego, et al. 2012. 'Linking Complex Forest Fuel Structure and Fire Behaviour at Fine Scales'. *International Journal of Wildland Fire* 21 (7): 882–93. https://doi.org/10.1071/WF10116.

Malambo, L., S. C. Popescu, D. W. Horne, N. A. Pugh, and W. L. Rooney. 2019. 'Automated Detection and Measurement of Individual Sorghum Panicles Using Density-Based Clustering of Terrestrial Lidar Data'. *ISPRS Journal of Photogrammetry and Remote Sensing* 149 (March): 1–13. https://doi.org/10.1016/j.isprsjprs.2018.12.015.

Mayamanikandan, T, R Suraj Reddy, and CS Jha. 2019. 'Non-Destructive Tree Volume Estimation Using Terrestrial Lidar Data in Teak Dominated Central Indian Forests'. In , 100–103. IEEE.

Moorthy, Inian, John R. Miller, Jose Antonio Jimenez Berni, Pablo Zarco-Tejada, Baoxin Hu, and Jing Chen. 2011. 'Field Characterization of Olive (Olea Europaea L.) Tree Crown Architecture Using Terrestrial Laser Scanning Data'. *Agricultural and Forest Meteorology* 151 (2): 204–14. https://doi.org/10.1016/j.agrformet.2010.10.005.

Mutlu, Muge, Sorin C Popescu, Curt Stripling, and Tom Spencer. 2008. 'Mapping Surface Fuel Models Using Lidar and Multispectral Data Fusion for Fire Behavior'. *Remote Sensing of Environment* 112 (1): 274–85.

Olsoy, Peter J., Nancy F. Glenn, and Patrick E. Clark. 2014. 'Estimating Sagebrush Biomass Using Terrestrial Laser Scanning'. *Rangeland Ecology & Management* 67 (2): 224–28. https://doi.org/10.2111/REM-D-12-00186.1.

Parker, Geoffrey G., David J. Harding, and Michelle L. Berger. 2004. 'A Portable LIDAR System for Rapid Determination of Forest Canopy Structure'. *Journal of Applied Ecology* 41 (4): 755–67. https://doi.org/10.1111/j.0021-8901.2004.00925.x.

Parsons, Russell A., Rodman R. Linn, Francois Pimont, Chad Hoffman, Jeremy Sauer, Judith Winterkamp, Carolyn H. Sieg, and W. Matt Jolly. 2017. 'Numerical Investigation of Aggregated Fuel Spatial Pattern Impacts on Fire Behavior'. *Land* 6 (2): 43. https://doi.org/10.3390/land6020043.

Parsons, Russell A., William E. Mell, and Peter McCauley. 2011. 'Linking 3D Spatial Models of Fuels and Fire: Effects of Spatial Heterogeneity on Fire Behavior'. *Ecological Modelling* 222 (3): 679–91. https://doi.org/10.1016/j.ecolmodel.2010.10.023.

Parsons, Russell, W Matt Jolly, Chad Hoffman, and Roger Ottmar. 2016. 'The Role of Fuels in Extreme Fire Behavior'. *Synthesis of Knowledge of Extreme Fire Behavior*, 55.

Peterson, Birgit, Kurtis J. Nelson, Carl Seielstad, Jason Stoker, W. Matt Jolly, and Russell Parsons. 2015. 'Automated Integration of Lidar into the LANDFIRE Product Suite'. *Remote Sensing Letters* 6 (3): 247–56. https://doi.org/10.1080/2150704X.2015.1029086.

'Piedmont National Wildlife Refuge'. n.d. FWS.Gov. Accessed 22 July 2022. https://www.fws.gov/refuge/piedmont.

Pimont, François, Russell Parsons, Eric Rigolot, François de Coligny, Jean-Luc Dupuy, Philippe Dreyfus, and Rodman R. Linn. 2016. 'Modeling Fuels and Fire Effects in 3D: Model Description and Applications'. *Environmental Modelling & Software* 80 (June): 225–44. https://doi.org/10.1016/j.envsoft.2016.03.003.

Pokswinski, Scott, Michael R. Gallagher, Nicholas S. Skowronski, E. Louise Loudermilk, Christie Hawley, Derek Wallace, Alexis Everland, Jon Wallace, and J. Kevin Hiers. 2021. 'A Simplified

and Affordable Approach to Forest Monitoring Using Single Terrestrial Laser Scans and Transect Sampling'. *MethodsX* 8 (January): 101484. https://doi.org/10.1016/j.mex.2021.101484.

Prichard, Susan J, David V Sandberg, Roger D Ottmar, Ellen Eberhardt, Anne Andreu, Paige Eagle, and Kjell Swedin. 2013. 'Fuel Characteristic Classification System Version 3.0: Technical Documentation'. *Gen. Tech. Rep. PNW-GTR-887. Portland, OR: US Department of Agriculture, Forest Service, Pacific Northwest Research Station. 79 p.* 887.

R Core Team. 2020. *R: A Language and Environment for Statistical Computing*. Vienna, Austria: R Foundation for Statistical Computing. https://www.R-project.org/.

Reeves, Matthew C., Kevin C. Ryan, Matthew G. Rollins, Thomas G. Thompson, Matthew C. Reeves, Kevin C. Ryan, Matthew G. Rollins, and Thomas G. Thompson. 2009. 'Spatial Fuel Data Products of the LANDFIRE Project'. *International Journal of Wildland Fire* 18 (3): 250–67. https://doi.org/10.1071/WF08086.

Rodríguez-Lozano, Borja, Emilio Rodríguez-Caballero, Lisa Maggioli, and Yolanda Cantón. 2021. 'Non-Destructive Biomass Estimation in Mediterranean Alpha Steppes: Improving Traditional Methods for Measuring Dry and Green Fractions by Combining Proximal Remote Sensing Tools'. *Remote Sensing* 13 (15): 2970. https://doi.org/10.3390/rs13152970.

Rollins, Matthew G. 2009. 'LANDFIRE: A Nationally Consistent Vegetation, Wildland Fire, and Fuel Assessment'. *International Journal of Wildland Fire* 18 (3): 235–49. https://doi.org/10.1071/WF08088.

Ross, C. Wade, E. Louise Loudermilk, Nicholas Skowronski, Scott Pokswinski, J. Kevin Hiers, and Joseph O'Brien. 2022. 'LiDAR Voxel-Size Optimization for Canopy Gap Estimation'. *Remote Sensing* 14 (5): 1054. https://doi.org/10.3390/rs14051054.

Roussel, Jean-Romain, and David Auty. 2021. 'Airborne LiDAR Data Manipulation and Visualization for Forestry Applications. R Package Version 3.1. 2'.

Roussel, Jean-Romain, David Auty, Nicholas C Coops, Piotr Tompalski, Tristan RH Goodbody, Andrew Sánchez Meador, Jean-François Bourdon, Florian De Boissieu, and Alexis Achim. 2020. 'LidR: An R Package for Analysis of Airborne Laser Scanning (ALS) Data'. *Remote Sensing of Environment* 251: 112061.

Roussel, Jean-Romain, and Jianbo Qi. 2020. *RCSF: Airborne LiDAR Filtering Method Based on Cloth Simulation*. https://CRAN.R-project.org/package=RCSF.

Rowell, Eric, E. Louise Loudermilk, Christie Hawley, Scott Pokswinski, Carl Seielstad, LLoyd Queen, Joseph J. O'Brien, Andrew T. Hudak, Scott Goodrick, and J. Kevin Hiers. 2020. 'Coupling Terrestrial Laser Scanning with 3D Fuel Biomass Sampling for Advancing Wildland Fuels Characterization'. *Forest Ecology and Management* 462 (April): 117945. https://doi.org/10.1016/j.foreco.2020.117945.

Rowell, Eric, E. Louise Loudermilk, Carl Seielstad, and Joseph J. O'Brien. 2016. 'Using Simulated 3D Surface Fuelbeds and Terrestrial Laser Scan Data to Develop Inputs to Fire Behavior Models'. *Canadian Journal of Remote Sensing* 42 (5): 443–59. https://doi.org/10.1080/07038992.2016.1220827.

Rowell, Eric M., Carl A. Seielstad, Roger D. Ottmar, Eric M. Rowell, Carl A. Seielstad, and Roger D. Ottmar. 2015. 'Development and Validation of Fuel Height Models for Terrestrial Lidar – RxCADRE 2012'. *International Journal of Wildland Fire* 25 (1): 38–47. https://doi.org/10.1071/WF14170.

Saarinen, Ninni, Ville Kankare, Mikko Vastaranta, Ville Luoma, Jiri Pyörälä, Topi Tanhuanpää, Xinlian Liang, et al. 2017. 'Feasibility of Terrestrial Laser Scanning for Collecting Stem Volume Information from Single Trees'. *ISPRS Journal of Photogrammetry and Remote Sensing* 123 (January): 140–58. https://doi.org/10.1016/j.isprsjprs.2016.11.012.

Sandberg, David V., Roger D. Ottmar, and Geoffrey H. Cushon. 2001. 'Characterizing Fuels in the 21st Century'. *International Journal of Wildland Fire* 10 (4): 381–87. https://doi.org/10.1071/wf01036.

Seielstad, Carl, Crystal Stonesifer, Eric Rowell, and Lloyd Queen. 2011. 'Deriving Fuel Mass by Size Class in Douglas-Fir (Pseudotsuga Menziesii) Using Terrestrial Laser Scanning'. *Remote Sensing* 3 (8): 1691–1709. https://doi.org/10.3390/rs3081691.

Sikkink, Pamela G., Robert E. Keane, Pamela G. Sikkink, and Robert E. Keane. 2008. 'A Comparison of Five Sampling Techniques to Estimate Surface Fuel Loading in Montane Forests*'. *International Journal of Wildland Fire* 17 (3): 363–79. https://doi.org/10.1071/WF07003.

Silva, André Gracioso Peres, Eric Bastos Görgens, Otávio Camargo Campoe, Clayton Alcarde Alvares, José Luiz Stape, and Luiz Carlos Estraviz Rodriguez. 2015. 'Assessing Biomass Based on Canopy Height Profiles Using Airborne Laser Scanning Data in Eucalypt Plantations'. *Scientia Agricola* 72 (December): 504–12. https://doi.org/10.1590/0103-9016-2015-0070.

Skowronski, Nicholas, Kenneth Clark, Ross Nelson, John Hom, and Matt Patterson. 2007. 'Remotely Sensed Measurements of Forest Structure and Fuel Loads in the Pinelands of New Jersey'. *Remote Sensing of Environment*, The Application of Remote Sensing to Fire Research in the Eastern United States, 108 (2): 123–29. https://doi.org/10.1016/j.rse.2006.09.032.

Skowronski, Nicholas S., Kenneth L. Clark, Matthew Duveneck, and John Hom. 2011a. 'Three-Dimensional Canopy Fuel Loading Predicted Using Upward and Downward Sensing LiDAR Systems'. *Remote Sensing of Environment* 115 (2): 703–14. https://doi.org/10.1016/j.rse.2010.10.012.

———. 2011b. 'Three-Dimensional Canopy Fuel Loading Predicted Using Upward and Downward Sensing LiDAR Systems'. *Remote Sensing of Environment* 115 (2): 703–14. https://doi.org/10.1016/j.rse.2010.10.012.

Skowronski, Nicholas S., Michael R. Gallagher, and Timothy A. Warner. 2020. 'Decomposing the Interactions between Fire Severity and Canopy Fuel Structure Using Multi-Temporal, Active, and Passive Remote Sensing Approaches'. *Fire* 3 (1): 7. https://doi.org/10.3390/fire3010007.

Skowronski, Nicholas S., Scott Haag, Jim Trimble, Kenneth L. Clark, Michael R. Gallagher, Richard G. Lathrop, Nicholas S. Skowronski, et al. 2015. 'Structure-Level Fuel Load Assessment in the Wildland–Urban Interface: A Fusion of Airborne Laser Scanning and Spectral Remote-Sensing Methodologies'. *International Journal of Wildland Fire* 25 (5): 547–57. https://doi.org/10.1071/WF14078.

'St. Marks National Wildlife Refuge'. n.d. FWS.Gov. Accessed 22 July 2022. https://www.fws.gov/refuge/st-marks.

Stovall, Atticus E. L., and Jeff W. Atkins. 2021. 'Assessing Low-Cost Terrestrial Laser Scanners for Deriving Forest Structure Parameters', July. https://doi.org/10.20944/preprints202107.0690.v1.

Vagizov, Marsel, Eugenie Istomin, Valerie Miheev, and Artem Potapov. 2021. 'Visual Digital Forest Model Based on a Remote Sensing Data and Forest Inventory Data'. *Remote Sensing* 13 (20): 4092.

Vandendaele, Bastien, Olivier Martin-Ducup, Richard A Fournier, and Gaëtan Pelletier. 2022. 'mobile and terrestrial laser scanning for tree volume estimation in temperate hardwood forests'.

Varga, Timothy A., and Gregory P. Asner. 2008. 'Hyperspectral and Lidar Remote Sensing of Fire Fuels in Hawaii Volcanoes National Park'. *Ecological Applications* 18 (3): 613–23. https://doi.org/10.1890/07-1280.1.

Vicari, Matheus B., Mathias Disney, Phil Wilkes, Andrew Burt, Kim Calders, and William Woodgate. 2019. 'Leaf and Wood Classification Framework for Terrestrial LiDAR Point Clouds'. *Methods in Ecology and Evolution* 10 (5): 680–94. https://doi.org/10.1111/2041-210X.13144.

Wallace, Luke, Samuel Hillman, Bryan Hally, Ritu Taneja, Andrew White, and James McGlade. 2022. 'Terrestrial Laser Scanning: An Operational Tool for Fuel Hazard Mapping?' *Fire* 5 (4): 85. https://doi.org/10.3390/fire5040085.

Waser, Lars T., Christoph Fischer, Zuyuan Wang, and Christian Ginzler. 2015. 'Wall-to-Wall Forest Mapping Based on Digital Surface Models from Image-Based Point Clouds and a NFI Forest Definition'. *Forests* 6 (12): 4510–28. https://doi.org/10.3390/f6124386.

Westfall, J. A., and C. W. Woodall. 2007. 'Measurement Repeatability of a Large-Scale Inventory of Forest Fuels'. *Forest Ecology and Management* 253 (1): 171–76. https://doi.org/10.1016/j.foreco.2007.07.014.

Wright, Marvin N., and Andreas Ziegler. 2017. 'Ranger: A Fast Implementation of Random Forests for High Dimensional Data in C++ and R'. *Journal of Statistical Software* 77 (1): 1–17. https://doi.org/10.18637/jss.v077.i01.

Xu, D, H Wang, W Xu, Z Luan, and X Xu. 2021. 'LiDAR Applications to Estimate Forest Biomass at Individual Tree Scale: Opportunities, Challenges and Future Perspectives. Forests. 2021; 12 (5): 1-19'.

OVERALL CONCLUSION

The paucity of understory research, specifically relating to characterizing architectural traits and their relationship with flammability, was the motivation for this dissertation research. Chapter one presents a workflow for reconstructing and characterizing the architectural structure of woody shrubs using a TLS-based QSM approach. Metrics derived from the modeled shrubs were correlated with manual measurements, demonstrating that the models successfully characterized shrub architecture. We noted, however, that shrub complexity, point cloud density, and uncertainty affected model accuracy.

In chapter two, we further adapted and tested the TLS-based QSM for understory shrubs by applying the methodology to shrubs from fire-dependent pine forest ecosystems. Here, we incorporate TLS and QSM 3D metrics to investigate shrub flammability. To measure shrub flammability, we conducted experimental burns, and recorded flammability traits. Overall, our analysis demonstrated a significant relationship between TLS and QSM architectural traits and field measures of flammability. Moreover, our results indicated an increased accuracy when combining the TLS and QSM traits to predict these flammability components. The ability to accurately characterize the 3D structure of fuels allows for more realistic fire behavior modeling scenarios and improvement in forest monitoring applications.

Techniques that utilize TLS have demonstrated to be robust and accurate in estimating forest structure parameters (Moskal & Zheng, 2012; Wilson et al., 2022). However, there is still some degree of uncertainty. In order to evaluate modeling accuracies, we needed a 'perfect' dataset. As no data in the real world is without uncertainty, in the final chapter of this dissertation, we developed semi-automated computer-modeled synthetic forest plots and simulated TLS. This allowed us to evaluate the impact of scan location and plot complexity on occlusion as well as accurately compare machine learning algorithms for predicting 'known' forest parameters. The results from this research allow us to re-examine existing methods and optimize workflows, data collection, and algorithm selection. Additionally, as remote sensing applications lean towards deep learning methodologies, the need for large datasets for training models is increasing. Since large realistic datasets can be generated cost-effective and accurately, we see synthetic datasets as a potential solution to this challenge

In conclusion, the TLS and QSM provide a range of novel measurement approaches that is useful for characterizing understory vegetation structure in 3D.

APPENDIX

Due to the nature of this work using large data files, all data, scripts and models can be accessed by email request through dropbox.

A list of available folders are listed below:

Appendix A:

TLS and QSM data for ten architecturally different shrubs (Manuscript 1)

Appendix B:

TLS and QSM data for all understory vegetation used in manuscript 2

Raw flammability results from FLIR data

Script for calculating metrics

Appendix C:

Synthetic plots (blender software files)

Synthetic plots simulated LiDAR scans (.laz)

Scripts for calculating metrics

Scripts for machine learning predictions